International Atomic Energy Agency

INDC(BLR)-007
Distr. G

INDC INTERNATIONAL NUCLEAR DATA COMMITTEE

EVALUATION OF NEUTRON DATA FOR AMERICIUM-242m

V.M. Maslov, E.Sh. Sukhovitskij, Yu.V. Porodzinskij,
G.B. Morogovskij

Radiation Physics & Chemistry Problems Institute
220109, Minsk-Sosny, Belarus

January 1997

IAEA NUCLEAR DATA SECTION, WAGRAMERSTRASSE 5, A-1400 VIENNA

Reproduced by the IAEA in Austria
January 1997

INDC(BLR)-007
Distr. G

EVALUATION OF NEUTRON DATA FOR AMERICIUM-242m

V.M. Maslov, E.Sh. Sukhovitskij, Yu.V. Porodzinskij,
G.B. Morogovskij

Radiation Physics & Chemistry Problems Institute
220109, Minsk-Sosny, Belarus

Abstract

The evaluation of neutron data for ^{242m}Am is made in the energy region from 10^{-5} eV up to 20 MeV. The results of the evaluation are compiled in the ENDF/B-VI format.

This work is performed under the Project Agreement CIS-03-95 with the International Science and Technology Center (Moscow). The Financing Party for the Project is Japan. The evaluation was requested by Y. Kikuchi (JAERI).

Date of Manuscript: December 19, 1996

Contents

1 Introduction

The advanced nuclear fuel cycle studies request the nuclear data of transplutonium isotopes.[1] The neutron data for americium isotopes are especially important in this respect. Recently we have evaluated the data for ^{243}Cm, ^{245}Cm, ^{246}Cm, ^{241}Am and ^{243}Am. In this work the evaluation of ^{242m}Am neutron data is performed. Neutron capture on ^{241}Am produces ^{242}Am nuclides in metastable state. The fission cross section of ^{242m}Am is of paramount importance, because it defines the yield of higher actinides, which might be produced by successive neutron captures. The next isotope, which neutron data would be evaluated is ^{242g}Am, the short-lived ground state of ^{242}Am. The curium and americium isotopes data to be evaluated were requested by the former General Manager of Japan Nuclear data Center Dr. Y. Kikuchi. The quantities evaluated are resolved and unresolved resonance parameters, total, elastic and inelastic scattering, fission, capture, (n,2n) and (n,3n) reaction cross sections, angular and energy distributions of secondary neutrons, including partial (n,xn) and (n,xnf) reaction spectra, fission spectra and number of neutrons per fission. The incident neutron energy range covered is from 10^{-5} eV up to 20 MeV. The evaluated quantities are compared with ENDF/B-VI[2] , JEF-2.2[3] and JENDL-3[4] evaluations.

2 Resolved resonance region

The measured data base is rather incomplete, since basically there are only fission data. Specifically, there are two rather old data sets by Bowman et al.[5] and Seeger et al.[6] and two more recent data sets by Browne et al.[7] and Dabbs et al.[8], which are systematically discrepant. Generally, two former data sets support the measurement by Browne et al.[7]

2.1 Previous evaluations of resolved resonance parameters

The evaluated resonance parameters of ENDF/B-VI are based on 6 resonance parameters E_r , Γ_n , Γ_γ , Γ_f by Bowman et al.[5] up to 3.50 eV. In JENDL-3 and JEF-2.2 evaluations the resonance parameters by Browne et al.[7] up to 20 eV are adopted.

Thermal fission σ_f and capture σ_γ cross sections of ENDF/B-VI, JEF-2.2 and JENDL-3.2 are rather discrepant. In ENDF/B-VI thermal fission cross section σ_f value is based on the estimate by Bowman et al.[5], which is a weighted average of data values by Hulet et al.[9] and Wolfsberg et al.[10] In JENDL-3 estimate of thermal fission cross section is based on measurement

by Browne et al.[7] The thermal fission cross section adopted in JEF-2.2 is due to Ihle et al.[11] This rather high value is fitted with the aid of negative resonance.

2.2 Measured data fitting

The purpose of current resonance parameter evaluation is to extract resolved resonance parameters up to 43.5 eV by analysis of fission cross section data by Browne et al.[7] The specific feature of this odd-odd target neutron resonances is large symmetric 0.178-eV resonance, which defines the thermal cross section values and small, if any, influence of negative resonances on neutron cross sections.

The multi-level Breit-Wigner formalism is employed. This is almost totally correct procedure, since due to exceptionally high number of fission channels there is no resonance-resonance interference. The assigning of resonance spins was done as follows. Two assumptions were adopted: the number of resonances with spin J is proportional to $(2J+1)$, reduced neutron width distribution should obey that of Porter-Thomas, neutron resonance spacing distribution should obey that of Wigner.

2.2.1 Thermal cross sections

The following measured data on thermal fission cross section are available:

1) value by Hulet et al.[9] for $\sigma_f = 6390 \pm 500$ b, measured relative to ^{239}Pu fission cross section of 806 barns for neutrons with a Maxwellian energy distribution;

2) value for $\sigma_f = 6830 \pm 300$ b by Wolfsberg et al.[10], measured relative to ^{235}U;

3) value for $\sigma_f = 6328 \pm 320$ b by Browne et al.[7];

4) value for $\sigma_f = 7600 \pm 300$ b by Wolfsberg et al.[12];

5) value for $\sigma_f = 6080 \pm 500$ b by Zhuravlev et al.[13];

6) value for $\sigma_f = 6950 \pm 250$ b by Dabbs et al.[8];

The following measured data on thermal capture cross section are available:

1) value for $\sigma_\gamma = 2260 \pm 200$ b by Zhuravlev et al.[13];

2) value for $\sigma_\gamma = 2000 \pm 300$ b by Street et al.[14];

We employed the value of thermal cross sections $\sigma_f = 6328 \pm 320$ b, defined by Browne et al.[7]

2.2.2 Fission cross section

We employ the fission data of Browne et al.[7] up to 43.5 eV. Measured data of Seeger et al.[6] and Bowman et al.[5] are compatible with the former data only below 0.46 eV and above 50 eV. They are used to extract additional

information as regards the number and positions of resonances. Since the total width and level spacing values are close, while energy resolution seem to be rather poor, radiative width could be fixed at 50 meV for all resonances. Resonance parameters $g\Gamma_n$ and Γ_f and E_r above 19.7 eV were obtained for 107 resonances. Thermal cross section values are presented in Table 2.1. The total number of resonances amounts to 155, as compared with 48 resonances up to 19.7 eV employed in previous evaluations. Generally speaking, the added resonances above 19.7 eV should be perceived as clusters of resonances. However, the extracted resonance parameters fit the data by Browne et al.[7] up to 43.5 eV.

2.2.3 Resonance parameter analysis

We have got 155 resonance parameters up to 43.5 eV. The average resonance parameters, thermal cross sections and resonance integrals are presented in Table 2.1. Figures 2.1- 2.10 demonstrate the available fission data fit below 43.5 eV. The present resonance parameters fit the measured data by Browne et al.[7] above 19.7 eV with the same accuracy as below 19.7 eV. Average resonance parameters of present evaluation and original parameters by Browne et al.[7] are quite compatible. The same is true as compared with JEF-2.2 evaluated resonance parameters, with the exception of average reduced neutron width $\langle\Gamma_n^0\rangle$ value. Large Γ_n^0 value of negative resonance increases appreciably $\langle\Gamma_n^0\rangle$ value. The values of average fission width $\langle\Gamma_f\rangle$ and resonance spacing $\langle D\rangle$ for present resonance parameters and those by Browne et al.[7] almost coincide. The main differences between specific resonance parameters are fission width values of weak resonances. This results in some improvement of distribution of fission widths description with chi-squared distribution (see Fig. 2.11). The present estimate of the number of degrees of freedom for fission width distribution $\nu_f = 6.3$ and the estimate of the effective number of fission channels $N_f = 2\pi\langle\Gamma_f\rangle/\langle D\rangle = 5.4$ are rather close to each other. Table 2.1 shows that calculated thermal fission cross section of present evaluation is fairly compatible with measured data. The resonance missing as well as average reduced neutron width $\langle\Gamma_n^0\rangle$ and neutron resonance spacing $\langle D\rangle$ distributions are discussed below.

Resonance integrals, calculated for various libraries, shown in Table 2.1, are compatible. Present estimate of capture resonance integral I_γ is smaller than that of ENDF/B-VI and JENDL-3. The calculated fission resonance integral $I_f = 1544.01$ b is compatible with $I_f = 1570\pm110$ b, estimated by Bowman et al.[5], but is significantly lower than $I_f = 1800\pm65$ b, obtained by Dabbs et al.[8]

Table 2.1

	ENDF/B-VI	JEF-2.2	JENDL-3	This evaluation
$\langle\Gamma_n^0\rangle$, meV	0.2682	0.1434	0.1093	0.1050
$\langle\Gamma_f\rangle$, meV	0.1349	0.3555	0.3626	0.3730
$\langle\Gamma_\gamma\rangle$, meV	50	49	50	50
$\langle D\rangle$, eV	0.6154	0.4235	0.4154	0.4107
$S_0 \times 10^4$	2.6148	1.8861	1.3438	1.2835
σ_t , barn	7968.08	8694.62	7668.53	7624.69
σ_γ , barn	1342.46	1806.25	1253.53	1229.23
σ_f , barn	6619.78	6874.65	6409.34	6390.21
σ_n , barn	5.8426	13.716	5.6670	5.2526
g_γ	1.1107	1.06805	1.10610	1.10268
g_f	1.1048	1.09845	1.10097	1.09777
I_γ , barn	285.366	262.472	245.831	239.610
I_f , barn	1885.6	1641.60	1560.96	1543.91

The average resonance parameters, thermal total σ_t, capture σ_γ, fission σ_f and scattering σ_n cross sections, $g_\gamma-$, and g_f-factors, as well as resonance integrals $I\gamma$ and I_f values are calculated with codes PSYCHE and INTER.[15] In case of present evaluation the multi-level Breit-Wigner formalism was used, while for of JENDL-3 and ENDF/B-VI evaluation single-level formula was employed.

3 Unresolved resonance region

3.1 Review

Unresolved resonance region of ^{242m}Am is supposed to be from 0.043 keV up to 27.2832 keV. The lower energy is the end-point of resolved resonance region, the upper energy is the threshold energy of the fourth excited level, giving notable inelastic scattering. We suppose $s-$, $p-$ and $d-$wave neutron-nucleus interactions to be effective.

3.2 The s-wave average resonance parameter evaluation

3.2.1 Estimate of resonance level missing influence on $\langle D_{obs}\rangle$ and $\langle S_0\rangle$

The preliminary estimates of average partial widths were obtained by averaging the evaluated resolved resonance parameters up to 28.45 eV. Obtained resolved resonance parameters describe the experimental data up to 43 eV.

However resonance parameters above 28.45 eV would not be used for average parameter determination due to poor experimental resolution. Figure 3.1 shows the cumulative sum of resolved resonance levels. The averaged resolved resonance parameters are as follows:

$$\langle \Gamma_n^0 \rangle = 1.062 \times 10^{-4} \text{ (eV)}^{1/2}$$
$$\langle \Gamma_f \rangle = 0.368 \text{ eV}$$
$$\langle D_{obs} \rangle = 0.422 \text{ eV}$$
$$\langle \Gamma\gamma \rangle = 50.0 \text{ meV}$$

Note that due to missing of weak resonances below 28.45 eV these values overestimate actual average reduced neutron width $\langle g\Gamma_n^0 \rangle$ and neutron resonance spacing $\langle D_{obs} \rangle$. To get a physically justified values of $\langle g\Gamma_n^0 \rangle$ and $\langle D_{obs} \rangle$ we employ a method, which is described elsewhere.[16] Both reduced neutron width and neutron resonance spacing distributions are obtained in a unified approach. We take into account the correlation of weak resonance missing and resonance missing due to poor experimental resolution. The resolution function parameters as well as $\langle g\Gamma_n^0 \rangle$ and $\langle D_{obs} \rangle$ values are obtained by maximum likelihood method when comparing experimental distributions of reduced neutron width and resonance spacing with Porter-Thomas and Wigner distributions, modified for the resonance missing. The latter distributions are called here expected distributions.

3.2.2 Evaluation of $\langle D_{obs} \rangle$, $\langle S_0 \rangle$, $\langle \Gamma_\gamma \rangle$ and $\langle \Gamma_f \rangle$ based on the resonance parameters

To evaluate average neutron resonance spacing $\langle D_{obs} \rangle$ and s-wave neutron strength function S_0 we apply our method[16] to the resolved resonance data base. We suppose that data only up to 28.45 eV should be taken into account. The evaluated values are:

$$S_0 = (1.215 \pm 0.247) \times 10^{-4} \text{ (eV)}^{-1/2}$$
$$\langle D_{obs} \rangle = (0.271 \pm 0.024) \text{ eV}$$

Figure 3.2 shows the cumulative sum of reduced neutron widths. Figure 3.3 shows the comparison of expected and experimental reduced neutron width distributions. Figure 3.4 shows the comparison of distributions for neutron resonance spacing. The expected distributions shown on the figures 3.3 and 3.4 demonstrate the effect of resonance missing. The figures 3.3, 3.4 show also that for energy interval of 0-28.45 eV the expected distributions are consistent with the experimental data within statistical errors . That is the reason to consider the estimates of $\langle D_{obs} \rangle$ and S_0 reliable.

3.3 The s-, p- and d-wave average resonance parameter evaluation

3.3.1 Neutron width

Average neutron width is calculated as follows

$$\langle \Gamma_n^{lJ} \rangle = S_l \langle D_J \rangle E_n^{1/2} P_l,$$

where P_l is the transmission factor for the lth partial wave, which was calculated within black nucleus model. The p-wave neutron strength function $S_1 = 2.020 \times 10^{-4}$ $(\mathrm{eV})^{-1/2}$ was calculated with the optical model, using the deformed optical potential, described below. According to the results of optical model calculations S_0 was assumed to decrease linearly to the value of S_0=$1.150 \times 10^{-4} (\mathrm{eV})^{-1/2}$ for neutron energy of 27.2832keV. The d-wave neutron strength function was taken from optical model calculations: S_2 $= 1.540 \times 10^{-4}$ $(\mathrm{eV}).^{-1/2}$ Since the d-wave contribution is rather small, the impact of any reasonable approximation on calculated values is negligible.

3.3.2 Neutron resonance spacing

Neutron resonance spacing $\langle D_J \rangle$ was calculated with the phenomenological model[18], which takes into account the shell, pairing and collective effects. The main parameter of the model $\tilde{a}$ was normalized to the observed neutron resonance spacing $\langle D_{obs} \rangle$ =0.271 eV.

3.3.3 Fission width

Fission widths are calculated within a double-humped fission barrier model. Energy and angular momentum dependences of fission width are defined by the transition state spectra at inner and outer barrier humps. We constructed transition spectra by supposing the triaxiality of inner saddle and mass asymmetry at outer saddle. They will be described below. The calculated fission widths $\langle \Gamma_f^{9/2-} \rangle$ and $\langle \Gamma_f^{11/2-} \rangle$ are normalized to $\langle \Gamma_f \rangle$ =0.395 meV, which allows to describe fission measured data in unresolved resonance region. This value coincides within errors with the average resolved resonance fission width.

3.3.4 Radiative capture width

Energy and angular momentum dependences of radiative capture width are calculated within a two-cascade γ-emission model with allowance for the (n,γf) and (n,γn') reaction competition to the (n,$\gamma\gamma$) reaction. In this energy region (n,$\gamma\gamma$) reaction appears to be a radiative capture reaction. The radiative capture width was normalized to the value of $\langle \Gamma_\gamma \rangle$ =50.0 meV. (For details see Chapter IV).

3.4 Cross section evaluation in the region 0.043-27.2832 keV

3.4.1 Fitting of fission cross section structure

Experimental fission cross-sections in the unresolved resonance region are measured by Bowman et al.[5], Seeger et al.[6],Browne et al.[7] and Dabbs et al.[8] Data by Browne et al.[7] and Dabbs et al.[8] averaged over short energy intervals demonstrate similar structures, but the former data are systematically lower by $\sim$ 15% in the unresolved resonance energy region. Data by Bowman et al.[7] and Seeger et al.[6] demonstrate unreasonable energy structure. Data by Browne et al.[7] were chosen as the most reliable. Statistical model calculations reproduce the trend of data by Browne et al.[7] Measured fission data exhibit prominent structure below incident neutron energy of 1 keV (see Fig. 3.5), which can not be reproduced varying average fission width value, since the degrees of freedom number for fission width distribution ν_f $\sim$ 10, consistent with the fission barrier transition states structure. (For details see Chapter IV). Structure present in data by Browne et al.[7] was fitted by adjusting S_0 strength function values in the chosen energy intervals up to 1 keV. Above 1 keV average resonance parameters fit the measured data. Comparison of evaluated fission cross section with measured data in the unresolved resonance energy region is given on Fig. 3.5.

3.4.2 Capture cross section energy dependence

Capture cross section of ^{242m}Am have never been measured. Evaluation is based on calculated values.

3.4.3 Comparison of current, JENDL-3, JEF-2 and ENDF/B-VI evaluated data

Present evaluated fission cross section is consistent with JENDL-3 and JEF-2.2 evaluations in the unresolved resonance region since all of them are based on data by Browne et al.[7] The evaluation of ENDF/B-VI is much higher as it is based on data by Bowman et al.[6] Figure 3.6 gives the comparison of fission cross section evaluations. Similar discrepancies are noticed when comparing the (n,γ) reaction cross sections (see Fig. 3.7). Current evaluated capture cross section σ_γ is rather close to JENDL-3 evaluation, which is only $\sim$ 10% higher. Evaluated capture cross section of JENDL-3 does not expose any structure that must appear due to that, present in fission cross section. This structure in fission cross section was reproduced in JENDL-3 evaluation with smooth background file. Although average cross sections of present and JENDL-3 evaluations are consistent, average fission width values differ drastically: $\langle\Gamma_f\rangle$ = 1.28 meV in JENDL-3 value and $\langle\Gamma_f\rangle$ = 0.395 meV in present evaluation. To compensate the increase of calculated fission cross section due to large value of $\langle\Gamma_f\rangle$, the number of degrees of freedom ν_f = 1 for fission width distribution was assumed in JENDL-3 evaluation.

That assumption seems unjustified, because the number of degrees of freedom determined from the fission width data is $\nu_f = 6.5$. The estimate of ν_f based on the number of transition states corresponding to the highest (inner) fission barrier hump is also much more greater than unity for any entrance channel. This underestimation of ν_f may influence the calculated self-shielding factors. In case of ENDF/B-VI evaluation the discrepancies are due to different estimates of average neutron width value. Comparison of the evaluated fission and capture cross sections is given in Table 3.1.

Table 3.1 Comparison of the evaluated fission and capture cross sections

Energy,	σ_f, b				σ_γ, b			
keV	present	JENDL-3	JEF-2	B-VI	present	JENDL-3	JEF-2	B-VI
0.043	42.83	52.00	66.26	118.03	8.59	14.11	9.21	20.44
0.055	72.37	75.00	58.77	104.44	14.48	12.40	8.17	18.07
0.070	49.20	50.00	52.01	92.11	9.85	10.97	7.23	15.91
0.090	43.67	43.00	45.87	81.23	8.74	9.65	6.37	14.01
0.110	38.84	37.00	41.45	73.50	7.77	8.75	5.76	12.66
0.150	29.79	33.00	35.52	62.44	5.96	7.43	4.94	10.73
0.180	32.39	32.10	32.26	57.30	6.47	6.82	4.48	9.84
0.225	30.69	29.75	32.91	50.84	6.13	6.07	4.57	8.71
0.275	27.05	25.80	29.44	45.73	5.40	5.46	4.09	7.82
0.325	20.97	22.04	24.08	42.16	4.19	5.02	3.35	7.20
0.375	19.17	18.92	22.41	39.08	3.83	4.67	3.12	6.66
0.450	17.57	16.98	20.51	35.52	3.51	4.25	2.86	6.04
0.550	15.68	15.95	18.41	32.03	3.13	3.83	2.56	5.43
0.700	14.10	14.35	16.32	28.14	2.81	3.40	2.28	4.76
0.900	13.55	13.00	14.44	24.72	2.70	2.98	2.02	4.16
1.100	12.47	12.23	13.12	22.29	2.48	2.69	1.84	3.74
4.500	6.42	6.39	6.68	10.41	1.27	1.36	0.96	1.70
11.000	4.42	4.43	4.64	5.78	0.87	0.96	0.70	0.95
27.2832	3.30	3.34	3.50	3.84	0.64	0.75	0.57	0.60

4 Fast neutron cross sections

The measured neutron data in fast neutron energy region, i.e. above ~27 keV are available only for fission cross section. There is a systematic discrepancy in fission data up to 20 MeV. Basically, the most extensive data

sets by Dabbs et al.[8] and Browne et al.[7] agree both in energy calibration and overall shape, while the latter data average appear to be ~18% lower. Above emissive fission threshold there is a striking shape difference. Nonetheless, the available fission data fit would be used as a constraint for (n,n'), (n,γ), $(n,2n)$ and $(n,3n)$ reaction cross sections calculation. The average resonance fission width will be reproduced within double-humped fission barrier model. To fix fission channel parameters the systematic trends are used.

4.1 Optical potential

The deformed optical potential for n+^{242m}Am interaction is employed. The starting values for the potential parameters were those for n+^{241}Am interaction, defined in our previous evaluation[19] by slightly varying potential parameters[20] of n + ^{238}U interaction. They fit total cross section data by Phillips and Howe[21], available for n+ ^{241}Am interaction. The isotopic dependences of real and imaginary parts of the potential were calculated using the optical potential parameter systematics.[22] Previously we modified the original potential geometry parameters[20] to fit total cross section and differential scattering data for N-odd and even targets above 10 MeV. This procedure of parameter fitting is well tested in case of ^{233}U, ^{239}Pu, ^{235}U, ^{232}Th and ^{238}U targets. Three levels of the metastable 5^- state rotational band (5^-,6^-,7^-) are coupled, 5^- state is assumed to be a ground state. The deformation parameters β_2 and β_4 are obtained by fitting S_0 value of 1.215×10^{-4} $(\mathrm{eV})^{-1/2}$ determined from resolved resonance parameters and S_1 having value lower than 2.00×10^{-4} $(\mathrm{eV}).^{-1/2}$ The potential parameters are as follows:

$$V_R = 46.10 - 0.3E, MeV, r_R = 1.26\ fm, a_R = 0.615\ fm$$
$$W_D = \begin{cases} 3.53 + 0.4E, MeV, & E \leq 10 MeV, r_D = 1.24\ fm, a_D = 0.5\ fm \\ 7.53\ MeV, & E > 10\ MeV \end{cases}$$
$$V_{SO} = 6.2\ MeV, r_{SO} = 1.12\ fm, a_{SO} = 0.47\ fm, \beta_2 = 0.206, \beta_4 = 0.092$$

The s-, p-, and d-wave strength functions and potential scattering cross section, calculated with this potential parameters in a coupled channel approach at incident neutron energy of 43 eV are:

$$S_0 = 1.219 \times 10^{-4}(\mathrm{eV})^{-1/2} \quad , \quad R' = 9.1677 \text{ fm}$$

and at 27.2832 keV are:

$$S_0 = 1.150 \times 10^{-4}(\mathrm{eV})^{-1/2} \quad S_1 = 2.020 \times 10^{-4}(\mathrm{eV})^{-1/2} \quad S_2 = 1.540 \times 10^{-4}(\mathrm{eV})^{-1/2}$$

The reaction cross sections, calculated with deformed optical potential and spherical optical potential, which is used in JENDL-3 evaluation, are

compared on Fig. 4.1. The significant differences below 1 MeV and above 10 MeV would be manifested in inelastic scattering cross section and $(n, 3n)$ cross section. The total cross section seem rather different (see figs. 4.2), especially at low energies. The differences at low energies are due to rather low value of $s-$wave strength function, adopted in present evaluation.

4.2 Fission cross section

4.2.1 Status of the experimental data

A small number of measurements are available for fission cross section, unfortunately most of them are discrepant with each other either in shape and absolute values.

Fission cross section of ^{242m}Am was first measured by Seeger et al.[6] from 20 eV up to ~1 MeV at the bomb-shot. Above 10 keV ratio of fission cross sections of ^{242m}Am and ^{235}U was obtained, there is a great scatter of data points. The amount of ^{242m}Am in the target was defined by mass spectrometric ratio of ^{242m}Am/^{241}Am alongside with α-counting of ^{241}Am foil.

Fission cross section of ^{242m}Am was measured by Bowman et al.[5] from 0.02 eV up to 6 MeV at the 30-MeV linac. Fission fragments were registered with corona spark detectors. Fission foil contained only 19.8% of ^{242m}Am, the rest was composed from ^{241}Am and ^{243}Am. Below 5 eV and above 1 keV up to 6 MeV fission cross section of ^{242m}Am was measured as a ratio to fission cross section of ^{239}Pu. The data are normalized at 0.0253 eV to the value of 6600 barns measured in a reactor thermal neutron flux. Between 2.3 eV and 2.5 keV BF_3-counter was used as a flux monitor. In this energy region the data are normalized to the 3.3-eV resonance of the measurement below 5 eV. Below 300 keV no correction is applied for the ^{241}Am and ^{243}Am impurities in the sample. Above 1 keV the data are normalized in the 1.0- to 2.5-keV region. The fission cross section estimate at 2.5 MeV of 2.2±0.6 barns seem to be rather high as compared with more recent measurements.

The fission cross section was measured by Browne et al.[7] from 0.001 eV to 20 MeV using 100-MeV linac-produced neutrons. In the thermal (0.001-3 eV) and high (1 keV to 20 MeV) energy regions fission cross section ratio of ^{242m}Am and ^{235}U was obtained. The relative cross section in resonance energy region (0.5 eV to 10 keV) was normalized to the measured thermal energy cross section between 0.7 and 1.7 eV. Neutrons were produced with linac. The measurement at 14.1 MeV was made with ICT accelerator at LLNL, neutrons were produced via ^{3}H(d,n)^{4}He reaction. The isotopic purity of the sample was at least 99%. The fission chamber used minimized the alpha pileup effects. The sample mass was defined by α-counting of ^{241}Am impurity using ^{241}Am/^{242m}Am atom ratio measured by mass spectroscopy.

The data are severely discrepant with previously measured data by Dabbs et al.[8], which are up to ~18% higher, however the data shapes are quite similar.

The similar energy range covered by Dabbs et al.[8] in one measurement is from 0.005 eV to 20 MeV. They have measured cross sections ratio of ^{242m}Am and ^{235}U above 101 keV, while at lower energies ^{6}Li(n,α) cross section, normalized to ^{235}U fission cross section in the 7.8-eV to 11-eV interval served as a standard. The reduction of the effects of intense alpha-particle background was achieved with special fission ionization chamber design. Below 101 keV the data of Dabbs et al.[8] are systematically higher than previous data by Browne et al.[7] Above the emissive fission threshold the data of Dabbs et al.[8] tend to be closer to data by Browne et al.[7], i.e. above the emissive fission threshold the shapes of the data by Dabbs et al.[8] and Browne et al.[7] are drastically different.

The energy dependence of fission cross section ratio of ^{242m}Am and ^{235}U was defined by Fomushkin et al.[23] in the incident neutron energy range from 0.04 MeV to 4.5 MeV. The neutrons with energies of 0.04 - 2 MeV were produced by the underground nuclear explosion. In the incident neutron energy of 1.0 - 4.52 MeV the neutrons were produced via T(p,n) reaction. The fission events were detected with a polymer film detectors. The isotopic purity of the sample was at least 85%. The sample weight was defined by α-counting of ^{242}Cm decay. The fission cross section at incident neutron energy ~14.8 MeV was also measured. The measurement was made relative to the ^{235}U fission cross section. The neutrons were produced by the T(d,n) reaction.

The ratio of fission cross sections of ^{242m}Am and ^{239}Pu was measured in the energy range from 0.135 to 7.4 MeV by Fursov et al.[24] The neutrons were produced by the ^{7}Li(p,n)^{7}Be, T(p,n)^{3}He and D(d,n)^{3}He reactions. The energy dependence of fission ratios was defined using ionization fission chambers. The mass ratio of ^{242m}Am in the sample was defined by α-counting. The isotopic purity of the sample was 85.6%.The absolute values of fission cross section ratios were obtained using measurements with mica detectors. The absolute values of fission cross sections were obtained using ^{239}Pu fission cross section of ENDF/B-VI. The data are compatible with data by Browne et al.[7] There is strong discrepancy with data by Dabbs et al.[8]

Absolute values of the ^{242m}Am measured neutron-induced fission cross section were obtained using ^{235}U reference fission cross section of ENDF/B-VI.[3]

The problem of consistency of ^{242m}Am fission cross section data looks as follows. Appreciable discrepancies occur below ~1 MeV . The data by Seeger et al.[6] are just scattering, while the data by Bowman et al.[5] and Fomushkin et al.[23] support the data by Dabbs et al.[8] up to 0.1 MeV. Above

0.3 MeV they have rather different shapes and are discrepant with data by Dabbs et al.[8] and by Browne et al.[7](see Fig. 4.4).

In the plateau region the data by Fursov et al.[24] are compatible with the data by Browne et al.[7] up to ~4 MeV, at higher energies there is an upward trend of the former data. However, this feature is characteristic for the fission cross section measurements relative to ^{239}Pu fission cross section. The upward data trend above 4 MeV incident neutron energy seems to be slightly incorrect, which may be due to doing measurements relative to ^{239}Pu fission cross section. The data of Dabbs et al.[8] are lying systematically (up to ~18 %) higher. The data by Fomushkin et al.[23] seem to define the lowest fission cross section level (see Fig. 4.5).

At excitation energies above emissive fission threshold the discrepancy between data by Browne et al.[7] and Dabbs et al.[8] is rather large. The data of Fomushkin et al.[23] at 14.8 MeV predict more reasonable fission cross section value just above (n,2nf) fission reaction threshold (see Fig. 4.6).

4.2.2 Statistical model calculation of fission cross section

Basically, we choose to fit data by Browne et al.[7] in describing measured data base. That means the lower cross section level in the first plateau region and at lower energies as compared with data by Dabbs et al.[8] We will follow the trend of data by Browne et al.[7] and Fursov et al.[24] up to ~7.8 MeV. The comparison of calculated fission cross section with measured data is shown in figs. 4.4, 4.5 and 4.6. The statistical theory calculation of fission cross section was accomplished within the double-humped fission barrier model. The approach employed in code STAT is described in more details elsewhere.[25,26,27] The procedure of calculating fission transmission coefficients is briefly described below.

4.2.3 Fission transmission coefficient, level density and transition state spectrum

The different behavior of level densities of fissioning odd-even and residual odd-odd nuclei at low excitation energies should be taken into account.[28] The one-quasiparticle neutron states of odd-even ^{243}Am fissioning nuclide, lying below the three-quasiparticle states excitation threshold define the shape of ^{242m}Am(n,f) fission cross section below incident neutron energy of ~1 MeV. Specifically, the step-like shape of fission cross section around 0.1 - 0.4 MeV. At higher incident neutron energies three-quasiparticle states could be excited in fissioning nucleus ^{243}Am at deformations of inner fission barrier hump. They define the fission cross section shape around 1 - 2.5 MeV incident neutron energy.

We construct the discrete transition state spectra up to 200 keV, using

one-quasiparticle states of Bolsterli et al.[29] (see Table 4.1). At higher excitation energies the continuous level densities are used. Each one-quasiparticle state is assumed to have a rotational band built on it with a rotational constant, dependent upon the respective saddle deformation. These levels comprise the discrete transition spectra at both saddles. The discrete transition spectra, as well as continuous level contribution to the fission transmission coefficient are dependent upon the order of symmetry for ^{243}Am fissioning nucleus at inner and outer saddles. Due to the axial asymmetry at the inner saddle[30] we additionally assume $(2J+1)$ rotational levels for each J value. The negative parity bands $K^{\pi} = 1/2^{-}$,$3/2^{-}$, $5/2^{-}$ ... at outer saddle are assumed to be doubly degenerate due to mass asymmetry.[30] With transition state spectra thus defined (see Table 4.1) the fission barrier parameters are obtained (see Table 4.2). The fission widths $\Gamma_f^{9/2^-} = 0.435$ eV and $\Gamma_f^{11/2^-} = 0.349$ eV are calculated at incident neutron energy of 0.043 keV. These values give average fission width $\langle\Gamma_f\rangle = 0.390$ meV, which is consistent with estimate, obtained from unresolved resonance region.

The generalized pairing model provides the means of taking into account the discrete character of few-quasiparticle excitations. It was shown to be important in case of even-odd fissioning and even-even residual nuclei in ^{244}Cm(n,f) and ^{246}Cm(n,f) reactions.[28,31] The quasi-resonance structure, appearing above fission threshold in neutron-induced fission cross section is interpreted. The discrete character of few-quasiparticle excitations is virtually unimportant in case of odd-odd ^{242}Am residual nuclide. We will model the discrete few-quasiparticle excitation effects in level density of odd-even ^{243}Am fissioning nuclide in the following approximate way.[31] The level density of axially symmetric fissioning nucleus is calculated in constant temperature approximation, i.e. $\rho(U) = T_f^{-1}\exp((U-U_o)/T_f)$. The respective parameters, nuclear temperature T_f and excitation energy shift U_o are defined at the matching energy $U_c = 3.6$ MeV. At excitation energies above U_c the continuum part of the transition state spectrum is represented with the phenomenological model[18], which takes into account pairing, shell and collective effects at saddle deformations. The asymptotic value of the main parameter of the level density for fissioning nucleus ^{243}Am is assumed to be the same, as that of ^{243}Am compound nuclide. After that the effects of non-axiality and mass asymmetry are included. The detailed procedure of calculating fission transmission coefficient is described elsewhere.[25,26,27] The respective parameters: shell correction at saddles δW, pairing correlation function Δ, quadrupole deformation ε,and momentum of inertia at zero temperature $F_0/\hbar^2$ are given in Table 4.3.

The threshold energies for the excitations of few-quasiparticle states are calculated within generalized pairing model[18] using closed-form equations by Fu.[32] The procedure is described in more detail elsewhere.[33] In case of

odd-even nuclei the nuclear level density $\rho(U)$ up to the three-quasiparticle excitation threshold is virtually independent on the excitation energy, since the intrinsic state density is constant. In this excitation energy region we will model the level density as $\rho(U) = T_f^{-1}\exp((\Delta_f - U_o)/T_f)$. Above the three-quasiparticle states excitation threshold the constant temperature model is used, since the intrinsic state density here is a smooth function of excitation energy. For excitation energies below five-quasiparticle and above three-quasiparticle states excitation threshold the level density is slightly increased, as compared with constant temperature model approximation: $\rho(U) = T_f^{-1}\exp((U - U_o + \delta)/T_f), \delta$ =0.1 MeV. The one- and three-quasiparticle states level density of odd-even fissioning nucleus ^{243}Am defines the fission cross section shape at incident neutron energies below ~3 MeV. Above ~3 MeV incident neutron energy fission cross section the pre-equilibrium emission of secondary neutron is important. The parameters used for calculation of residual nuclide ^{242}Am level density for neutron emission competition are described below.

The parameters used for calculation of residual nuclide ^{242m}Am level density for neutron emission competition are described below.

Below incident neutron energy of 0.273 MeV the neutron cross sections are calculated within Hauser-Feshbach approach with a width fluctuation correction taken into account. For width fluctuation correction calculation only Porter-Thomas fluctuations are taken into account. Effective number of degrees of freedom for fission channel is defined at the higher (inner) saddle as $\nu_f^{J\pi} = \mathrm{T}_f^{J\pi}/\mathrm{T}_{f\,\mathrm{max}}^{J\pi}$, where $\mathrm{T}_{f\,\mathrm{max}}^{J\pi}$ is the maximum value of the fission transmission coefficient $\mathrm{T}_f^{J\pi}$. Above incident neutron energy of 0.273 MeV the Tepel et al.[34] approach is employed. The calculations are made with code STAT.[35]

Table 4.1

Transition spectra band-heads of ^{243}Am

inner saddle		outer saddle	
K^π	E_{K^π}, MeV	K^π	E_{K^π}, MeV
$3/2^-$	0.0	$5/2^+$	0.0
$5/2^+$	0.140	$5/2^-$	0.0
$7/2^-$	0.180	$3/2^+$	0.08
$5/2^-$	0.180	$3/2^-$	0.08
		$1/2^+$	0.04
		$1/2^-$	0.04
		$1/2^+$	0.05
		$1/2^-$	0.05

Table 4.2

Fission barrier parameters

Nucleus	Barrier	Barrier height, MeV	Curvature, MeV
^{243}Am	inner	6.4	0.8
^{243}Am	outer	4.85	0.5
^{242}Am	inner	6.315	0.6
^{242}Am	outer	5.775	0.4
^{241}Am	inner	6.000	0.8
^{241}Am	outer	5.350	0.5
^{240}Am	inner	6.100	0.6
^{240}Am	outer	6.000	0.4
^{239}Am	inner	6.000	0.8
^{239}Am	outer	5.400	0.6

Table 4.3

Level density parameters of ^{243}Am fissioning nucleus and residual nucleus ^{242}Am

Parameter	inner saddle	outer saddle	neutron channel
δW, MeV	2.5	0.6	-2.487
$\triangle$, MeV	$\triangle_0$	$\triangle_0$	$\triangle_0$
ε	0.6	0.8	0.24
$F_0/\hbar^2$, MeV^{-1}	100	200	73

4.2.4 Fission cross section above emissive fission threshold

The first chance fission cross section of ^{242m}Am(n,f) reaction above the emissive fission threshold is fixed with the level density and fission barrier parameters systematics[25] (see Tables 4.2, 4.3) and secondary neutron spectra parameterization (see Fig. 4.7). A consistent description of a complete set of measured data on (n,f), (n,2n) and (n,3n) for ^{238}U and ^{235}U targets was accomplished with the secondary neutron spectra parameterization[36], which is used here.

The fission cross section is calculated with the statistical code STAPRE[37] (see Fig.4.6). Near the emissive fission threshold the pre-equilibrium emission of first neutron is rather important due to high neutron binding energy of ^{243}Am compound nuclide. The fission barrier parameters of ^{242}Am, fissioning in (n,nf) reaction are defined by fitting[19] data on ^{241}Am neutron-induced fission in the first plateau region (see Fig. 4.7). The resulted fission

barrier parameters of ^{242m}Am does not allow fitting ^{242m}Am(n,f) data by Browne et al.[7] well above emissive fission threshold. This discrepancy is unavoidable within present model approach without appreciable variation of model parameters. To fit the data by Browne et al.[7] first-chance fission cross section should be increased appreciably by softening the first emitted neutron spectra. However, we do not think this procedure justified in this particular case, since the discrepancy of the same kind we encounter[38] in case of ^{245}Cm(n,f) data by Browne et al.[40], measured in the same environment. The peculiar feature is that the calculated fission cross section shape is similar to that of data by Dabbs et al.[8] The calculated fission cross section around (n,2nf) reaction threshold neutron energy is roughly consistent with data by Fomushkin et al.[23] at 14.8 MeV. On the other hand, the ^{243}Am compound nuclide fission barrier parameters describe the measured data on neutron-induced fission cross section of ^{243}Am target above emissive fission threshold.[40](see Fig.4.8).

The calculated fission cross section is different from JENDL-3 and ENDF/B-VI evaluated curves above (n,nf) reaction threshold (see Fig. 4.9).

4.3 Inelastic scattering cross section

The inelastic scattering cross section is calculated with the statistical codes STAT[35] and STAPRE.[37] The discrete level excitation (compound and direct), continuum excitation and pre-equilibrium emission contribute to the inelastic scattering cross section.

4.3.1 Levels of ^{242}Am

The low-lying levels of scheme of Nuclear Data Sheets[41] appears incomplete at rather low excitation energy (see Fig. 4.10). The experimental data on odd-odd ^{242}Am nuclide energy levels are supplemented by the results of the intrinsic level modelling by Sood.[42] The still unobserved doublet of two-quasiparticle bandheads $J = 6^-$ ($K^\pi = 6^-$) and $J = 1^-$ ($K^\pi = 6^-$) is predicted, the Gallagher-Moszkovski splitting energy being ~80 keV. Assuming $E^J_{K^\pi} = A[J(J+1) - K(K+1)]$, A =5.5 keV, we model a rotational level sequence. The levels in Table 4.4 are shown with respect to the metastable state J =5$^-$ of 0.04863 MeV.

4.3.2 ^{242}Am level density

The continuum level density below excitation energy U_c = 2.4 MeV is calculated with the constant temperature model

$$\rho(U) = T^{-1} \exp((U - U_o)/T),$$

here, energy shift U_0 = -1.6452 MeV, nuclear temperature T = 0.39241 MeV are the constant temperature model parameters. The cumulative number of observed levels is compared with constant temperature approximation on Fig.4.10. At higher excitation energies the phenomenological model[18] is used. The main model parameter $\tilde{a}$ for ^{242}Am residual nucleus is obtained by fitting the evaluated neutron resonance spacing of ^{241}Am target nuclide $\langle D_{obs} \rangle$ = 0.505 eV.

4.3.3 Compound inelastic scattering

The residual nucleus ^{242m}Am level density modelling, adopted in present work changes the inelastic scattering cross section below 5 MeV as compared with previous evaluations (see figs. 4.11 - 4.14). We assume that missing of levels in odd-odd nuclide ^{242}Am occurs at rather low excitation energy of ~0.27 MeV. That is the main reason of discrepancy with JENDL-3 evaluation, where discrete levels are used up to ~0.7 MeV. The estimate of ENDF/B-VI seem to be rather low due to unreasonably high estimate of fission cross section in first plateau region. Above ~1.5 MeV incident neutron energy the discrepancies are due to direct excitation of the "ground" state band $K^\pi = 5^-$ levels $J^\pi = 6^-$ and $J^\pi = 7.^-$ Above 1 MeV incident neutron energy inelastic scattering to the continuum gives a major contribution to the total inelastic scattering cross section (see Fig. 4.11). However, the continuum inelastic scattering contributions of JEF-2 and JENDL-3 evaluations seem to be distorted. Above 5 MeV incident neutron energy pre-equilibrium emission and direct inelastic scattering are the two reaction mechanisms which define inelastic scattering cross section (see Fig. 4.11). The pre-equilibrium model parameters were tested by the statistical model description of ^{238}U+n interaction secondary neutron spectra and consistent description of fission and (n,xn) reaction data for major actinides.[36] Steep decrease of continuum inelastic scattering cross section of ENDF/B-VI above 5 MeV (see Fig. 4.12) is due to missing of pre-equilibrium emission of neutrons. The evaluation of continuum inelastic scattering cross section of JEF-2.2 seem to be sharply overestimated above 5 MeV. The shape of continuum inelastic scattering cross section of JENDL-3 around 20 MeV possibly is due to reaction cross section shape, since there is no pre-equilibrium emission contribution in JENDL-3 evaluation.

4.3.4 Direct inelastic scattering

The direct inelastic scattering mechanism changes the shape of metastable band head $K^\pi = 5^-$ rotational levels $J^\pi = 6^-$ and $J^\pi = 7^-$ excitation cross sections above 1 MeV incident neutron energy (see figs. 4.13, 4.14). This mechanism defines partly the hard-energy tail in total inelastic scattering

cross section (see Fig. 4.11). The calculations were accomplished with the code COUPLE.[22]

Table 4.4
Level scheme of ^{242}Am

$E^J_{K^\pi}$, MeV	J	π	K	band	$E^J_{K^\pi}$, MeV	J	π	K	band
-0.04863	1	–	0	A	0.21447	7	-	0	A
-0.00453	0	-	0	A	0.22147	2	+		
0.0	5	-	5	B	0.22637	3	-	1	D*
0.00427	3	-	0	A	0.23467	3	+		
0.02717	2	-	0	A	0.23977	4	-	3	E
0.06537	6	-	5	B	0.24317	2	-	2	F
0.09137	6	-	6	C*	0.25637	8	-	6	C*
0.09937	5	-	0	A	0.25827	3	-		
0.10127	4	-	0	A	0.27037	4	-	1	D*
0.14137	7	-	5	B					
0.14897	3	-							
0.16837	7	-	6	C*					
0.17137	1	-	1	D*					
0.18187	2	+	1						
0.19337	2	-	1	D*					
0.19547	3	-	3	E					
0.21437	6	-	0	A					

*)added

4.3.5 ^{243}Am level density

The level density of odd-even compound nuclide ^{243}Am one needs to calculate radiative capture width and (n,γn') reaction contribution to the compound inelastic scattering cross section. The continuum level density below excitation energy U_c = 3.6 MeV is calculated with the constant temperature model, the constant temperature model parameters are: energy shift U_0 = -0.98278 MeV, nuclear temperature T = 0.39984 MeV. The cumulative number of observed levels is compared with constant temperature approximation on Fig. 4.15. At higher excitation energies the phenomenological model[18] is used. The main model parameter $\tilde{a}$ for ^{243}Am residual nucleus is obtained by fitting the evaluated neutron resonance spacing of ^{242m}Am target nuclide $\langle D_{obs} \rangle$ = 0.271 eV, the metastable state excitation energy is taken into account.

4.4 Radiative capture cross section

The radiative capture cross section is calculated within a statistical approach up to 5 MeV. Radiative capture strength function equals $S_{\gamma 0} = 759.72$. At higher incident neutron energies we assume radiative capture cross section to be constant. The radiative capture width was calculated with (n,γf) and (n,γn') reactions competition against "true" capture reaction (n,$\gamma\gamma$). Notwithstanding rather high fission threshold for ^{243}Am compound nuclide the competition of (n,γf) reaction is still stronger than that of (n,γn') reaction. The influence of (n,γn') and (n,γf) reaction competition on radiative capture cross section is illustrated on Fig. 4.16 by sharp decrease of capture cross section above 1 MeV incident neutron energy, as compared with (n,γx) reaction cross section.

4.5 Cross sections of (n,2n) and (n,3n) reactions

The current and previous evaluated (n,2n) and (n,3n) cross sections are rather different. The magnitude of (n,2n) cross section below the (n,2nf) reaction threshold is defined by (n,nf) and (n,2n) reaction competition. To calculate the (n,2n) reaction cross section we use an approach, developed for the description of ^{238}U(n,2n) reaction cross section.[36] The present and previous evaluated fission cross sections are rather different, as well as reaction cross sections above 10 MeV incident neutron energy (see Fig. 4.1). The present and previous evaluations are compared in Fig. 4.17. There is no hard-energy tail in (n,2n) reaction cross sections of ENDF/B-VI, JENDL-3 and JEF-2 evaluations. In case of (n,3n) reaction the difference in reaction cross section above 11 MeV (see Fig. 4.1) contributes essentially to the discrepancy with JENDL-3 evaluation, shown on Fig. 4.18.

5 Energy distributions of secondary neutrons

There is no measured data on secondary neutron spectra. To calculate neutron energy distributions of (n,xnγ) and (n,xnf), x=1, 2, 3 reactions we use a simple Weisscopf-Ewing evaporation model[43] taking into account fission,and gamma competition to neutron emission for appearing A+1, A, A-1, A-2 - mass nuclei. The pre-equilibrium emission of first neutron is included.

5.1 Model calculations of (n,nx) reaction spectra

The first neutron spectra for the (n,nx) reaction is the sum of evaporated and pre-equilibrium emitted neutron contributions. The pre-equilibrium emission contribution is calculated with a parameter systematics tested in case of n+^{238}U and n+^{235}U interactions.[24,35] Fission and neutron competition

and pre-equilibrium emission of first neutron is tested to be consistent with adopted in Chapter IV and give (n,nf), (n,2f), (n,3nf), (n,2n), (n,3n) and (n,nγ) cross-sections close to calculated above. The pre-equilibrium neutron emission contribution in case of ^{242m}Am target nucleous is notable for rather low neutron incident energies (see Chapter IV). We have calculated the 1st, 2nd and 3d neutron spectra for the (n,nγ), (n,2n) and (n,3n), where applicable. According to the ENDF/B-VI format we included the secondary neutron spectra in the following way. The calculated spectra were summed up and tabular spectra for the (n,nγ), (n,2n) and (n,3n) reactions were obtained. To clarify the competition of neutron, γ-emission and fission in case of (n,nx) and (n,2nx) reactions we have chosen the following presentation of spectra. Figure 5.1 shows the spectrum of 1st neutron of the reaction (n,nx) and its partial contributions for (n,nγ), (n,2n), (n,nf) (n,2nf) and (n,3n) reactions. Figure 5.2 shows the spectrum of 2nd neutron of the reaction (n,2nx) and its partial contributions for (n,2n), (n,3n) and (n,2nf) reactions. The spectra of 1st and 2nd neutrons are normalized to unity. The partial neutron spectra shown on figs. 5.1, 5.2 are normalized to the contributions of appropriate cross sections to the (n,nx) and (n,2nx) reaction cross sections, respectively.

Table 5.1 Average energies of secondary neutron spectra

E_n, MeV	1^{st} neutron average energy, MeV									
	(n, n')			(n, 2n)			(n, n'f)	(n, 3n)		(n, 2n'f)
	pres.	J - 3	B-6	pres.	B-6	J - 3	pres.	pres.	J - 3	pres.
2.0	0.55	0.58	0.40							
8.0	4.04	1.14.	1.22	1.17	0.70	1.14	0.82			
14.0	10.1	1.49	1.58	4.11	1.23	1.50	2.69	0.63	1.49	1.05
20.0	16.1	1.77	1.86	10.5	1.58	1.78	4.11	2.94	1.78	3.37

E_n, MeV	2^{nd}neutron average energy, MeV						3d neutron	
	(n, 2n)			(n, 3n)		(n, 2n'f)		
	pres.	B-6	J - 3	pres.	J - 3	pres.	pres.	J - 3
8.0	0.34	1.22	0.70					
14.0	0.82	1.47	1.04	0.52	1.08	0.73	0.18	0.70
20.0	0.77	1.86	1.41	1.17	1.41	1.17	0.66	0.90

The inclusion of pre-equilibrium emission changes significantly the average energies of emitted neutron spectra. That is shown in Table 5.1, where the average secondary neutron energies for current, JENDL-3 and ENDF/B-VI evaluations are compared. The most significant is the change of neutron

spectra of (n,nγ) reaction. Figures 5.3-5.7 demonstrate the discrepancies of secondary neutron spectra in current and JENDL-3 evaluations.

The 1st neutron spectra of (n,nf) reaction also becomes harder and that influences prompt fission neutron spectra. On the other hand, the spectra of 2nd and 3d neutrons become softer.

5.2 Prompt fission neutron spectra

Prompt fission neutron spectra were calculated within the framework of Madland-Nix model.[44]

5.2.1 Model calculations of prompt fission neutron spectra

The relevant model parameters, i.e. fragment masses, average total fission energies, total kinetic energies, average fission fragment separation energies and level density parameters, are defined just as described previously.[40]

5.2.1.1 Fragment masses. The fragment masses are defined as $A_L = 103$ and $A_H = 140$, in accordance with the data of Weber et al.[45] Fragment charges are defined using the ratios of

$$\langle A_{L,H} \rangle / (Z_{L,H} \mp 0.5) = A_F / Z_F.$$

The average fragments adopted are ^{103}Nb and ^{140}Xe

5.2.1.2 Energy parameters. Average total fission energies $\langle E_R \rangle$ and average fission-fragment separation energies are calculated as in Madland-Nix model using Mass Tables of Audi and Wapstra.[46] The values of $\langle TKE \rangle$ for fissioning nuclei ^{243}Am and ^{242}Am are defined fitting measured data on $\nu_p(E)$ below emissive fission threshold ^{242m}Am(n,f) and ^{241}Am(n,f), respectively. The value of $\langle TKE \rangle$ for ^{241}Am fissioning nucleus comes from systematics of Viola et al.[47]

5.2.2 Other parameters.

The level density parameter of the fermi-gas model is calculated as $a = A_{L,H}/10.2$, MeV^{-1}. Becchetti-Greenlees[48] spherical optical potential parameters are employed to calculate compound cross section.

5.2.3 Prompt fission neutron spectra evaluation

Below emissive fission threshold prompt fission neutron spectra are calculated with the parameters given in Table 5.2. Figure 5.8 shows the comparison of calculated thermal prompt fission neutron spectrum with maxwellian spectra of JENDL-3 ($T = 1.38$ MeV) and ENDF/B-VI ($T = 1.33$ MeV).

Average energy of fission spectrum equals 2.15 MeV, it is compatible with evaluated value of JENDL-3, however the spectra shapes are significantly different. Figures 5.9 and 5.10 demonstrate the discrepancies of our calculation with JENDL-3 and ENDF/B-VI evaluations. The discrepancies are due to incident neutron energy independent maxwellian fission spectrum representation in JENDL-3 and ENDF/B-VI as well as emissive fission contribution in present evaluation.

Above emissive fission threshold the fission neutron spectra $N(E)$ is the superposition of emissive fission spectra, i.e.

$$N(E) = (\frac{\sigma_{nf}}{\sigma_{nF}}\nu_1 N_1(E) + \frac{\sigma_{nn'f}}{\sigma_{nF}}\left[\Phi_{nn'f}(E) + \nu_2 N_2(E)\right]$$
$$+\frac{\sigma_{n2nf}}{\sigma_{nF}}\left[\Phi^1_{n2nf}(E) + \Phi^2_{n2nf}(E) + \nu_3 N_3(E)\right])/$$
$$\left[\frac{\sigma_{nf}}{\sigma_{nF}}\nu_1 + \frac{\sigma_{nn'f}}{\sigma_{nF}}(1+\nu_2) + \frac{\sigma_{n2nf}}{\sigma_{nF}}(2+\nu_3)\right],$$

where σ_{nF}, σ_{nf}, $\sigma_{nn'f}$, σ_{n2nf} are the total and i-th chance fission cross sections (i = 1,2,3); $\Phi_{nn'f}$, Φ^1_{n2nf}, and Φ^2_{n2nf} are emitted neutron spectra: for (n,nf) reaction, 1st and 2nd neutrons of (n,2nf) reaction, respectively; ν_i and N_i are multiplicity and prompt neutron spectra for the i-th fissioning nucleus. The pre-equilibrium emission of the first neutron is included, the secondary neutron spectra for emissive fission $\Phi^i_{n,xnf}$ are calculated with Weisscopf-Ewing evaporation model.[43]

The influence of pre-equilibrium pre-fission neutrons on prompt fission neutron multiplicity ν_i and prompt neutron spectra N_i predictions as well as $N(E)$ and $\nu(E)$, is illustrated in Table 5.3 and Fig. 5.11. In Table 5.3 $\langle E_i\rangle$ denotes average prompt fission neutron energy of i-th fissioning nucleus, $\langle E\rangle$ is the average fission neutron energy, $\langle E_{n'f}\rangle$, $\langle E_{2nf}\rangle^1$and $\langle E_{2nf}\rangle^2$are the average energies of neutrons, emitted in (n,nf) and 1st and 2nd neutrons emitted in (n,2nf) reactions, respectively. Figures 5.12-5.14 show the partial contributions of i-th chance fission to the total fission neutron spectrum at incident neutron energies of 8, 14 and 20 MeV.

Table 5.2

Parameters of the Madland-Nix model

Fissioning nucleus	A_L fragm.	A_H fragm.	$\langle E_R\rangle$, MeV	$\langle TKE\rangle$, MeV	B_n, MeV
^{243}Am	^{103}Nb	^{140}Xe	204.651	182.20-0.08E_n	6.367
^{242}Am	^{102}Nb	^{140}Xe	204.963	183.02-0.08E_n	5.538
^{241}Am	^{101}Nb	^{140}Xe	204.353	183.26-0.08E_n	6.641

6 Number of neutrons per fission

The number of prompt fission neutrons at thermal energies was measured in 1966 by Fultz et al.[49], in 1970 by Kroshkin and Zamyatnin[50] and Jaffey et al.[51] and in 1981 by Howe et al.[52] We renormalized these data to the recent reference values of ν_p for ^{233}U, ^{235}U, ^{239}Pu and ^{252}Cf. The resulted values are consistent within experimental errors. Therefore we adopted for thermal value of ν_p the mean weighted value of above measurements: ν_p^{th}= 3.26. The present evaluation of $\nu_p(E)$ is based on calculation within Madland-Nix model, fitted to the data of Howe et al.[52] in the energy range up to 5 MeV. The calculated $d\nu_p/dE$ = 0.145 MeV^{-1}in the first plateau region is consistently lower than $d\nu_p/dE$ = 0.128 MeV^{-1}, estimated by Howe et al.[52] in a linear least-squares data fit up to 30 MeV. That is essentially the same kind of discrepancy, that we have encountered in case of $\nu_p(E)$ data by Howe et al.[53] for ^{245}Cm(n,f) reaction, measured in the same environment. The calculated $d\nu_p/dE$ = 0.133 MeV^{-1} was considerably higher than $d\nu_p/dE$ = 0.08±0.015, MeV^{-1}, estimated by Howe et al.[53] However, calculated energy slope $\nu_p(E)$ was supported by recent data by Khokhlov et al.[54] To increase the $d\nu_p/dE$ within Madland-Nix model calculation even further, as systematics by Howerton[55] predicts (see ENDF/B-VI evaluation on Fig. 6.1), one should assume rather low value of $\langle TKE \rangle$ for ^{243}Am compound system. The comparison of $\nu_p(E)$ with measured data, JENDL-3 and ENDF/B-VI evaluations is shown in Fig. 6.1. The Madland-Nix model calculations predict non-linear decrease of $\nu_p(E)$ above emissive fission threshold. The influence of pre-equilibrium pre-fission neutrons manifests in additional appreciable decrease of $d\nu_p/dE$ above 12 MeV.

The delayed number of neutrons per fission ν_d and decay constants for six groups of delayed neutrons are taken from Brady and England.[56] Specifically, ν_d = 0.0078 for incident neutron energies up to 4 MeV and ν_d = 0.0043 for $E_n \geq 7$ MeV.

7 Angular distributions of secondary neutrons

The angular distributions of elastically scattered neutrons and those for neutrons, scattered on two levels of ground state band are calculated with the coupled channel method. The isotropic compound scattering contribution is taken into account by renormalizing l-th Legendre polynomial coefficients A_l^{cc}, calculated with coupled channels:

$$A_l = A_l^{cc}\sigma_{dir}/(\sigma_{dir}+\sigma_{comp}),$$

where σ_{dir} and σ_{comp} are the scattering cross section direct and compound contributions, respectively. For the other contributing reactions angular

distributions of secondary neutrons are assumed isotropic.

Table 5.3 Comparison of Madland-Nix and present approach

	E_n = 8 MeV		E_n = 14 MeV		E_n = 20 MeV	
Quantity	M-N model[53]	Present	M-N model[53]	Present	M-N model[50]	Present
$\langle E_1 \rangle$	2.350	2.350	2.478	2.478	2.598	2.598
ν_1	4.430	4.430	5.269	5.269	6.085	6.085
$\langle E_{n'f} \rangle$	1.176	0.821	1.543	2.688	1.834	4.106
$\langle E_2 \rangle$	2.180	2.189	2.316	2.289	2.442	2.393
ν_2	3.329	3.381	4.146	3.982	4.949	4.632
$\langle E_{2nf} \rangle^1$	-	-	1.543	1.048	1.834	3.365
$\langle E_{2nf} \rangle^2$	-	-	1.098	0.729	1.472	1.167
$\langle E_3 \rangle$	-	-	2.152	2.174	2.284	2.255
ν_3	-	-	3.105	3.232	3.880	3.704
$\langle E \rangle$	2.278	2.264	2.318	2.387	2.558	2.615
ν	4.411	4.421	5.211	5.155	5.992	5.807

8 Conclusions

The evaluated neutron data file for ^{242m}Am is compiled in ENDF/B-VI format and sent to the International Science and Technology Center (Moscow), Japan Nuclear Data Center at Japan Atomic Energy Research Institute and Nuclear Data Section of International Atomic Energy Agency (Austria).

Numerous discrepancies of experimental data coupled with possibility of some new data becoming available (for example, final ^{242m}Am(n,f) data by Fursov et al. (PPEI, Russia)) may urge some revision of data file. Present

version of ^{242m}Am data file may be revised before March of 1998, the expiration date of Project CIS-03-95.

9 Acknowledgement

The assistance of A.B. Klepatskij with numerical calculations of secondary neutron energy and angular distributions and number of neutrons per fission is appreciated.

10 References

1. Nakagawa T., Kikuchi Y., Proc. of the Int. Conf. on Nuclear Data and Technology, Gatlinburg, Tenn., USA, 9-13 May, 1994, Dickens J.K. (Editor), 709, ANS Inc., 1994.
2. C.L. Dunford, Nuclear Data for Science and Technology, Proc. Int. Conf. Julich, 1991,788. Springer-Verlag,1992, Berlin.
3. Nordborg C., Salvatores M. Nuclear Data for Science and Technology, Proc. of the Int. Conf., Gatlinburg, Tennessee, USA, May 9-13, 1994, v.2, p. 680.
4. Japanese Evaluated Data Library, Version 3, JAERI 1319, 1990.
5. Bowman C.D., Auchampaugh G.F., Fultz S.C., Hoff R.W., Phys. Rev. 166, 1219 (1968).
6. Seeger P.A., Hemmendinger A., Diven B.C. Nucl. Phys. A96, 605 (1967).
7. Browne J.C., White R.M., Howe R.E. et al. Phys. Rev. 29, 2188 (1984).
8. Dabbs J.W. , Bemis C.E., Raman S., et al., Nucl. Sci. Engng. 84, 1 (1983).
9. Hulet E.K., Hoff R.W., Bowman H.R., Michel M.C. Phys. Rev., 107, 1294 (1957).
10. Wolfsberg K., Ford G.P., Smith H.L. Nucl. Sci. Engng. 20, 588 (1966).
11. Ihle H., Michael H., Neubert A. et al., J. Inorg. Nucl. Chem., 34, 2427 (1972).
12. Wolfsberg K., Ford G.P. Phys. Rev., C3, 1333, (1971).
13. Zhuravlev K.D., Kroshkin N.I., Chetverikov A.P., Atomnaya Energiya, 39, 285 (1975).
14. Street K., Jr., Ghiorso A., Thompson S.G., Phys. Rev., 85, 135 (1952).
15. Dunford C.L.: "ENDF Utility Codes Release 6.9", IAEA-NDS-29 (1993).
16. Porodzinskij Yu.V., Sukhovitskij E.Sh., Nuclear Constants, 4, p.27, 1987 (in Russian).
17. Jaynes F.J., Trans. Systems Sci. and Cybern., 4, 227 (1968).
18. Ignatjuk A.V., Istekov K.K., Smirenkin G.N. Sov. J. Nucl. Phys. 29, 450 (1979).
19. Maslov V.M., Porodzinskij Yu.V., Sukhovitskij E.Sh., Klepatskij A.B., Morogovskij G.B., INDC(BLR)-5, 1996.
20. Haouat, Lachkar J., Lagrange Ch., et al., Nucl.Sci. Engng. 81, 491 (1982).
21. Phillips T.W., Howe R.E. Nucl. Sci. Engng., 69, 375 (1979).
22. Klepatskij A.B., Sukhovitskij E.Sh., private communication.
23. Fomushkin E.F., Novoselov G.F., Vinogradov Yu.I., et al. Yad. Fyz.., 33, 620 (1981).
24. Fursov B.I., Samylin B.F., Smirenkin G.N., Polynov V.N., Nuclear Data for Science and Technology, Proc. of the Int. Conf., Gatlinburg, Tennessee,

USA, May 9-13, 1994, v.I, p. 269.
25. Ignatjuk A.V., Maslov V.M., Proc. Int. Symp. Nuclear Data Evaluation Methodology, Brookhaven,USA, October 12-16, 1992, p.440, World Scientific, 1993.
26. Maslov V.M. and Y. Kikuchi JAERI-Research, 1996.
27. Maslov V.M. Sov. J. At. Energy 64, 478 (1988).
28. Maslov V.M., Proc. Int. Seminar on Interactions of Neutrons with Nuclei, Dubna, Russia, April, 27-30, 1996.
29. Bolsterli M., Fiset E.O., Nix J.R., Norton J.L. Phys.Rev., C 5, 1050 (1972).
30. Howard W.M., Moller P. Atomic Data and Nuclear Data Tables,25, 219 (1980).
31. Maslov V.M., Porodzinskij Yu.V., Sukhovitskij E.Sh., Klepatskij A.B., Morogovskij G.B., INDC(BLR)-4, 1996.
32. Fu C. Nucl. Sci. Engng. 86, 344 (1984).
33. Maslov V.M. Zeit. Phys. A, Hadrons & Nuclei, 347, 211 (1994).
34. Tepel J.W., Hoffman H.M., Weidenmuller H.A. Phys. Lett. 49, 1 (1974).
35. Klepatskij A.B., Maslov V.M., Sukhovitskij E.Sh., private communication.
36. Ignatjuk A.V., Maslov V.M., Pashchenko A.B. Sov. J. Nucl. Phys. 47, 224 (1988).
37. Uhl M. and Strohmaier B., Report IRK - 76/10 (Vienna,1976).
38. Maslov V.M., Porodzinskij Yu.V., Sukhovitskij E.Sh., Klepatskij A.B., Morogovskij G.B., INDC(BLR)-4, 1996.
39. White R.M., Browne J.C., in: Nuclear Data for Science and Technology (North-Holland, 1983), p.281.
40. Maslov V.M., Porodzinskij Yu.V., Sukhovitskij E.Sh., Klepatskij A.B., Morogovskij G.B., INDC(BLR)-6, 1996.
41. ENSDF, 1995.
42. Sood P.C., Singh R.N. Nucl. Phys. A373, 519 (1982).
43. Maslov V.M., Porodzinskij Yu.V.,Sukhovitskij E.Sh., Proc. Int. Conf. on Neutron Physics, 14-18 Sept., Kiev, USSR, V.1, p.413, 1988.
44. Madland D.G., Nix J.R., Nucl. Sci. Engng. 81, 213 (1982).
45. Weber et al., Phys. Rev. C, 13, 189 (1976).
46. Audi G., Wapstra A.H., Nuclear Physics A, 565, 1 (1980).
47. Viola V.E., Kwiatkowski K., Walker M., Phys. Rev., 31, 1550 (1985).
48. Becchetti F.D., Greenlees G.W., Phys. Rev. 182, 1190 (1969).
49. Fultz S.C., Caldwell J.T., Berman B.L., et al. Phys. Rev., 152, 1046 (1966).
50. Kroshkin N.I., Zamyatnin Yu. S. Sov. Atomic Energy, 29, 790 (1970).
51. Jaffey A.H., Lerner J.L., Nucl. Phys. A, 145, 1 (1970).
52. Howe R.E., Browne J.C., Dougan R.J., Dupzyk R.J., Landrum J.H.

Nucl. Sci. Eng. 77,454 (1981).
53. Howe R.E., White R.M., Browne J.C., Landrum J.H., Dougan R.J., Lougheed R.W., Dupzyk R.J., Nucl. Phys., A407, 193 (1983).
54. Khokhlov Yu.A. et al., Nuclear Data for Science and Technology, Proc. of the Int. Conf., Gatlinburg, Tennessee, USA, May 9-13, 1994, v.I, p. 272.
55. Howerton R.J. Nucl. Sci. Engng., 62, 438 (1977).
56. Brady M.C. and England T.R., Nucl.Sci. Engng. 103, 129 (1989).

11 Figure captions

Fig. 2.1 Fission cross section of ^{242m}Am below 0.1 eV.
Fig. 2.2 Fission cross section of ^{242m}Am in the energy region below 1 eV.
Fig. 2.3 Fission cross section of ^{242m}Am in the energy region below 5 eV.
Fig. 2.4 Fission cross section of ^{242m}Am in the energy region below 10 eV.
Fig. 2.5 Fission cross section of ^{242m}Am below 15 eV.
Fig. 2.6 Fission cross section of ^{242m}Am in the energy region below 20 eV.
Fig. 2.7 Fission cross section of ^{242m}Am in the energy region below 26 eV.
Fig. 2.8 Fission cross section of ^{242m}Am in the energy region below 33 eV.
Fig. 2.9 Fission cross section of ^{242m}Am in the energy region below 38.5 eV.
Fig. 2.10 Fission cross section of ^{242m}Am in the energy region below 43.5 eV.
Fig. 2.11 Distribution of fission widths for ^{242m}Am.
Fig. 3.1 Cumulative sum of neutron resonance levels of ^{242m}Am.
Fig. 3.2 Cumulative sum of reduced neutron widths of ^{242m}Am.
Fig. 3.3 Distribution of reduced neutron widths for ^{242m}Am.
Fig. 3.4 Neutron resonance spacing distribution for ^{242m}Am.
Fig. 3.5 Fission cross section of ^{242m}Am in unresolved resonance region.
Fig. 3.6 Fission cross section of ^{242m}Am in unresolved resonance region.
Fig. 3.7 Capture cross section of ^{242m}Am in unresolved resonance region.
Fig. 4.1 Compound reaction cross section of ^{242m}Am.
Fig. 4.2 Total cross section of ^{242m}Am.
Fig. 4.3 Elastic scattering cross section of ^{242m}Am.
Fig. 4.4 Fission cross section of ^{242m}Am.
Fig. 4.5 Fission cross section of ^{242m}Am.
Fig. 4.6 Fission cross section of ^{242m}Am.
Fig. 4.7 Fission cross section of ^{241}Am.
Fig. 4.8 Fission cross section of ^{243}Am.
Fig. 4.9 Fission cross section of ^{242m}Am.
Fig. 4.10 Cumulative number of levels of ^{242}Am.
Fig. 4.11 Inelastic scattering cross section of ^{242m}Am.
Fig. 4.12 Continuum inelastic scattering cross section of ^{242m}Am.
Fig. 4.13 Cross section of ^{242m}Am: 0.064 MeV, 6^- level excitation.
Fig. 4.14Cross section of ^{242m}Am: 0.141 MeV, 7^- level excitation.
Fig. 4.15 Cumulative number of levels of ^{243}Am.
Fig. 4.16 Radiative capture cross section of ^{242m}Am.
Fig. 4.17 ^{242m}Am(n,2n) reaction cross section.
Fig. 4.18 ^{242m}Am(n,3n) reaction cross section.
Fig. 5.1 Components of first neutron spectrum of ^{242m}Am for incident neu-

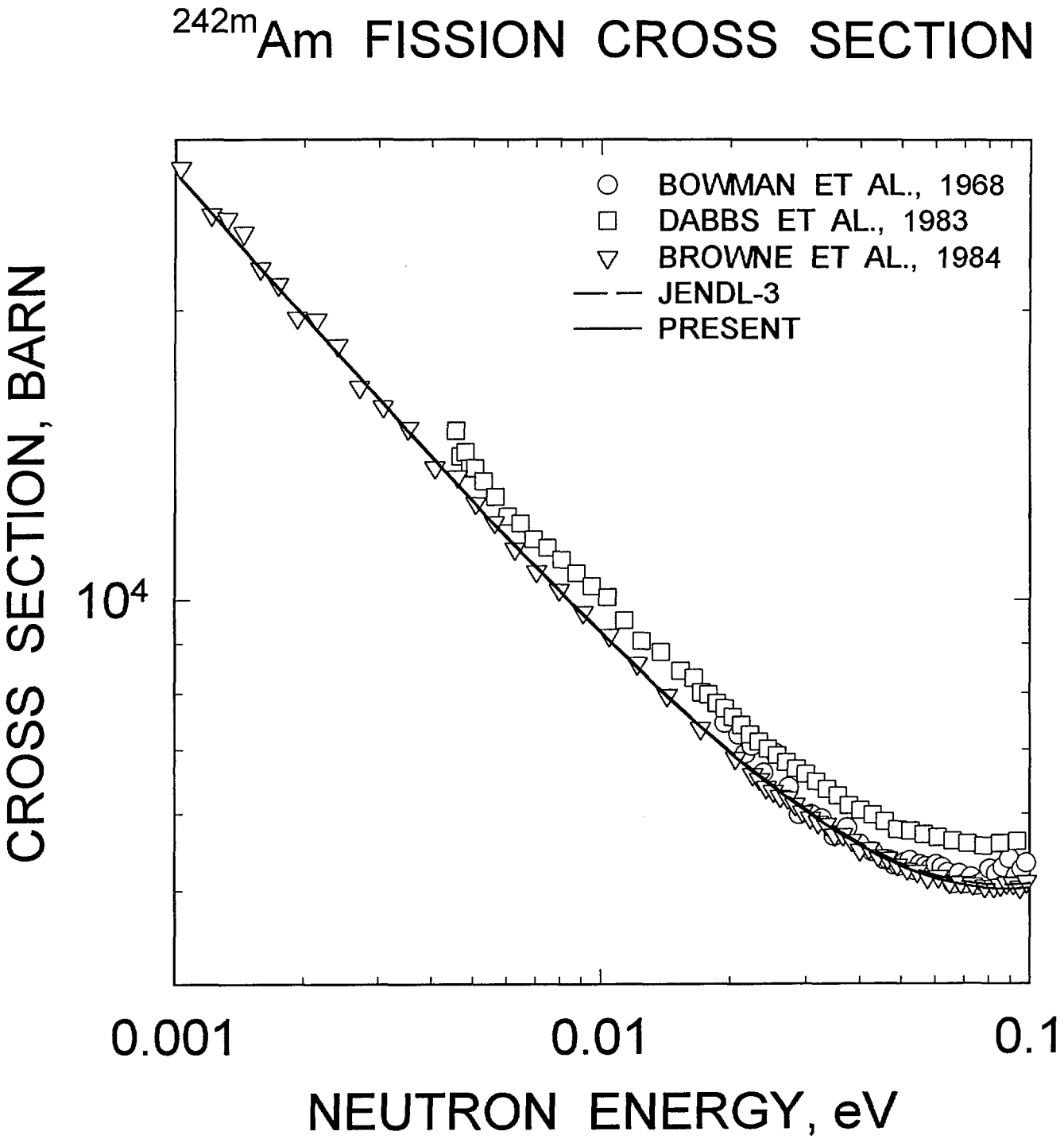
242mAm FISSION CROSS SECTION
BOWMAN ET AL., 1968
DABBS ET AL., 1983
BROWNE ET AL., 1984
JENDL-3
PRESENT
CROSS SECTION, BARN
10^4
0.001
0.01
0.1
NEUTRON ENERGY, eV

FIG.2.1

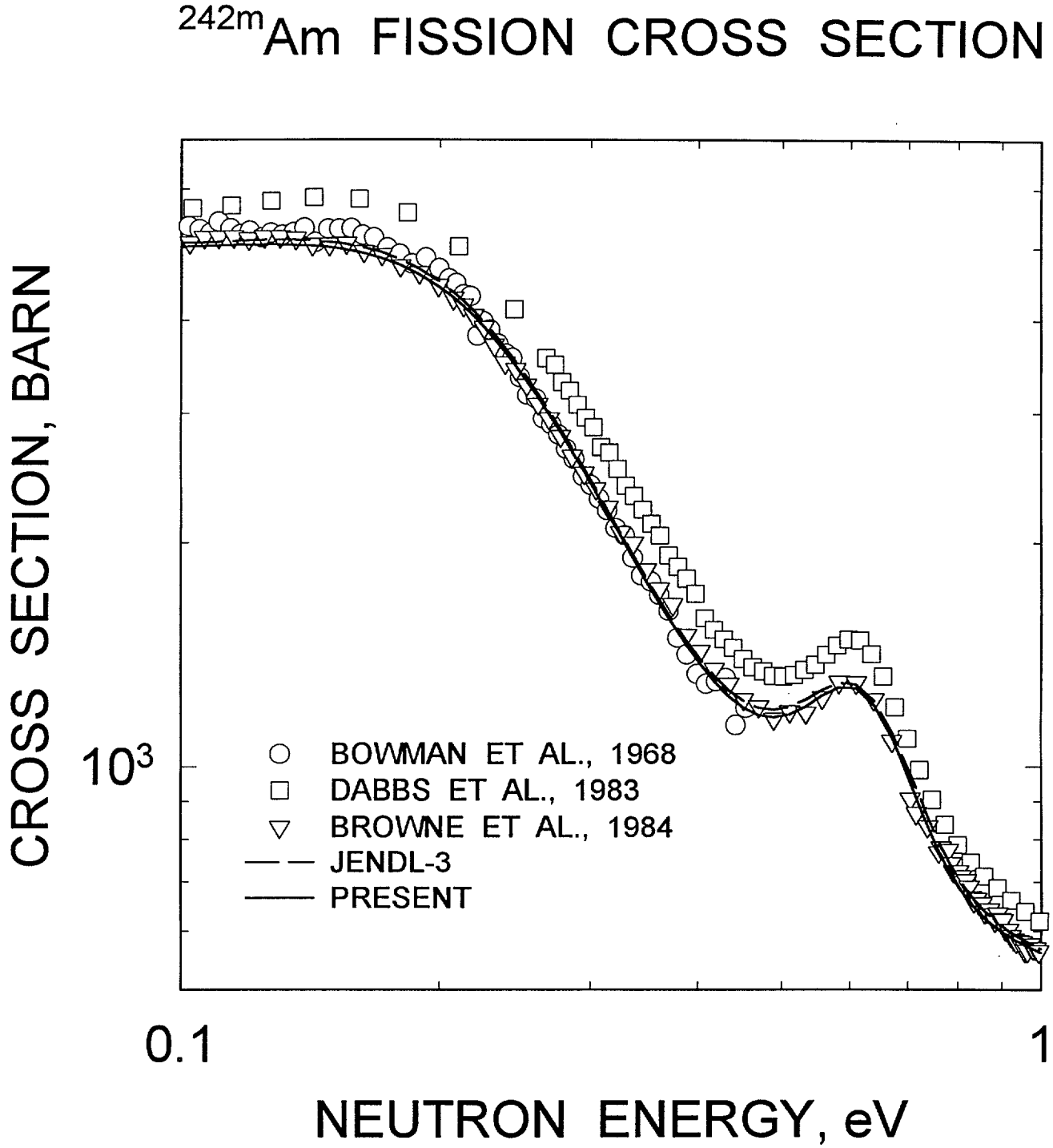
^{242m}Am FISSION CROSS SECTION
CROSS SECTION, BARN
10^3
BOWMAN ET AL., 1968
DABBS ET AL., 1983
BROWNE ET AL., 1984
JENDL-3
PRESENT
0.1
1
NEUTRON ENERGY, eV

FIG.2.2

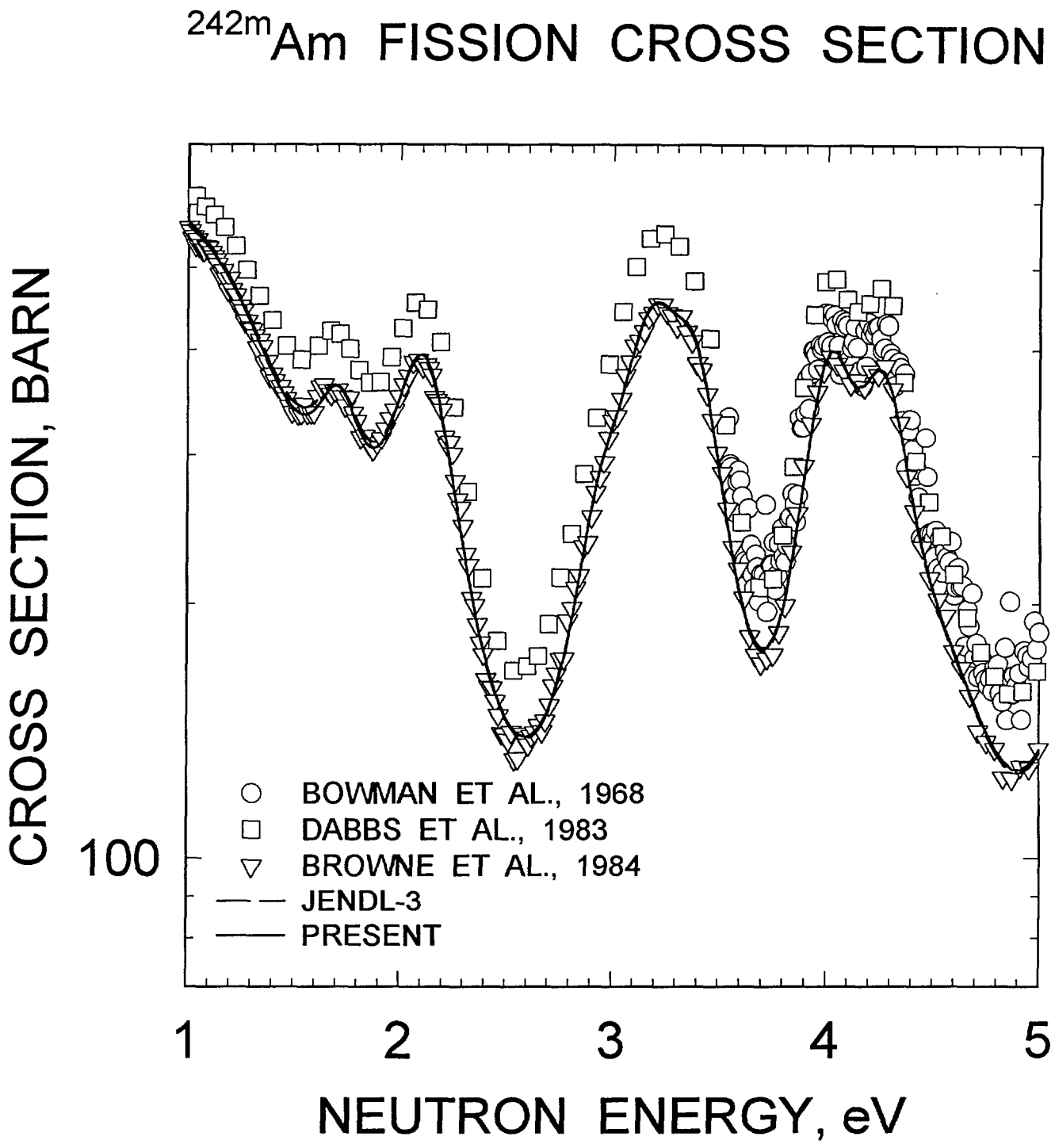
242mAm FISSION CROSS SECTION
CROSS SECTION, BARN
100
BOWMAN ET AL., 1968
DABBS ET AL., 1983
BROWNE ET AL., 1984
JENDL-3
PRESENT
1
2
3
4
5
NEUTRON ENERGY, eV

FIG.2.3

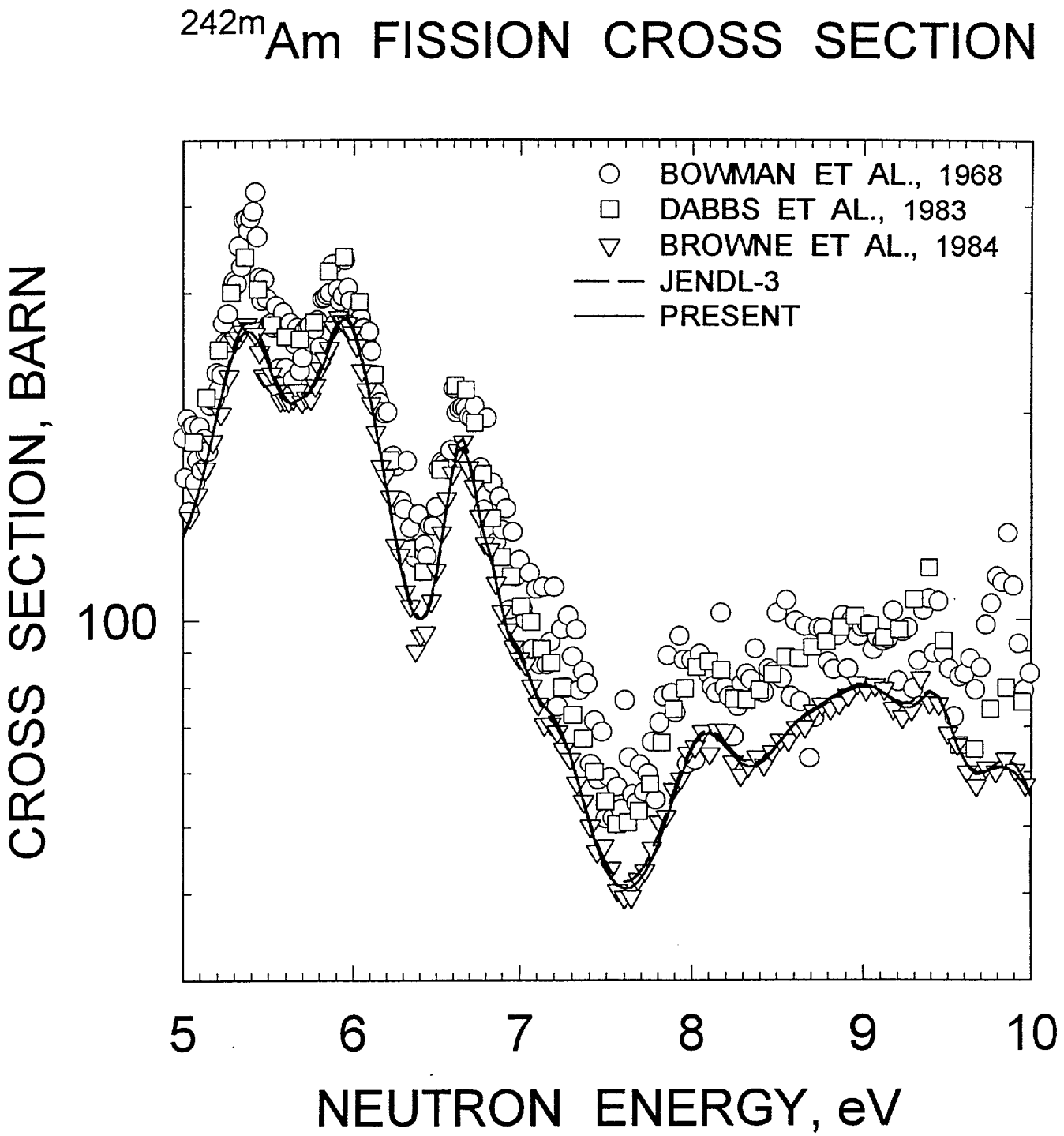
^{242m}Am FISSION CROSS SECTION
BOWMAN ET AL., 1968
DABBS ET AL., 1983
BROWNE ET AL., 1984
JENDL-3
PRESENT
CROSS SECTION, BARN
100
5
6
7
8
9
10
NEUTRON ENERGY, eV

FIG.2.4

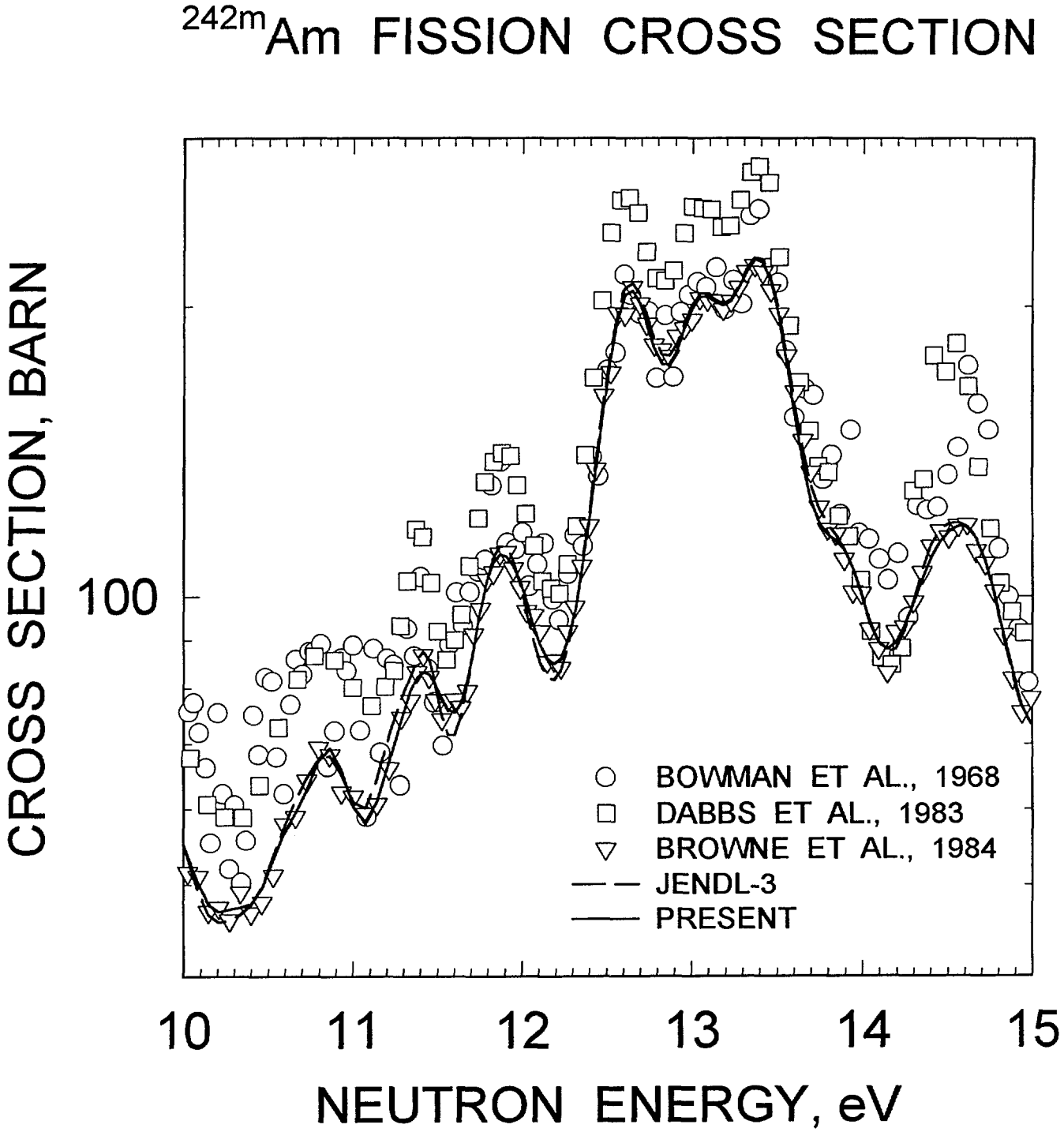
242mAm FISSION CROSS SECTION
CROSS SECTION, BARN
100
10
11
12
13
14
15
NEUTRON ENERGY, eV
BOWMAN ET AL., 1968
DABBS ET AL., 1983
BROWNE ET AL., 1984
JENDL-3
PRESENT

FIG.2.5

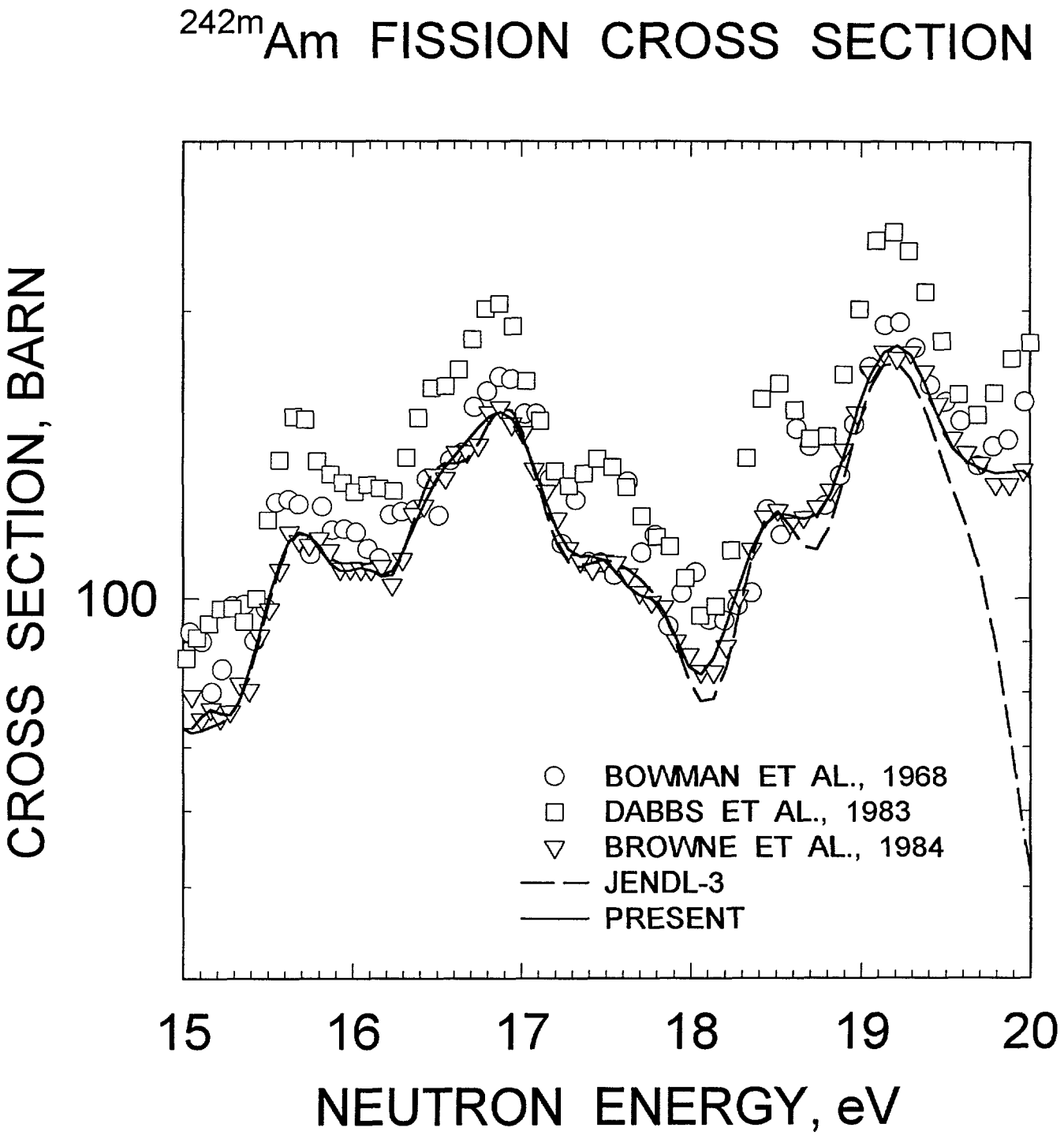
242mAm FISSION CROSS SECTION
CROSS SECTION, BARN
100
BOWMAN ET AL., 1968
DABBS ET AL., 1983
BROWNE ET AL., 1984
JENDL-3
PRESENT
15
16
17
18
19
20
NEUTRON ENERGY, eV

FIG.2.6

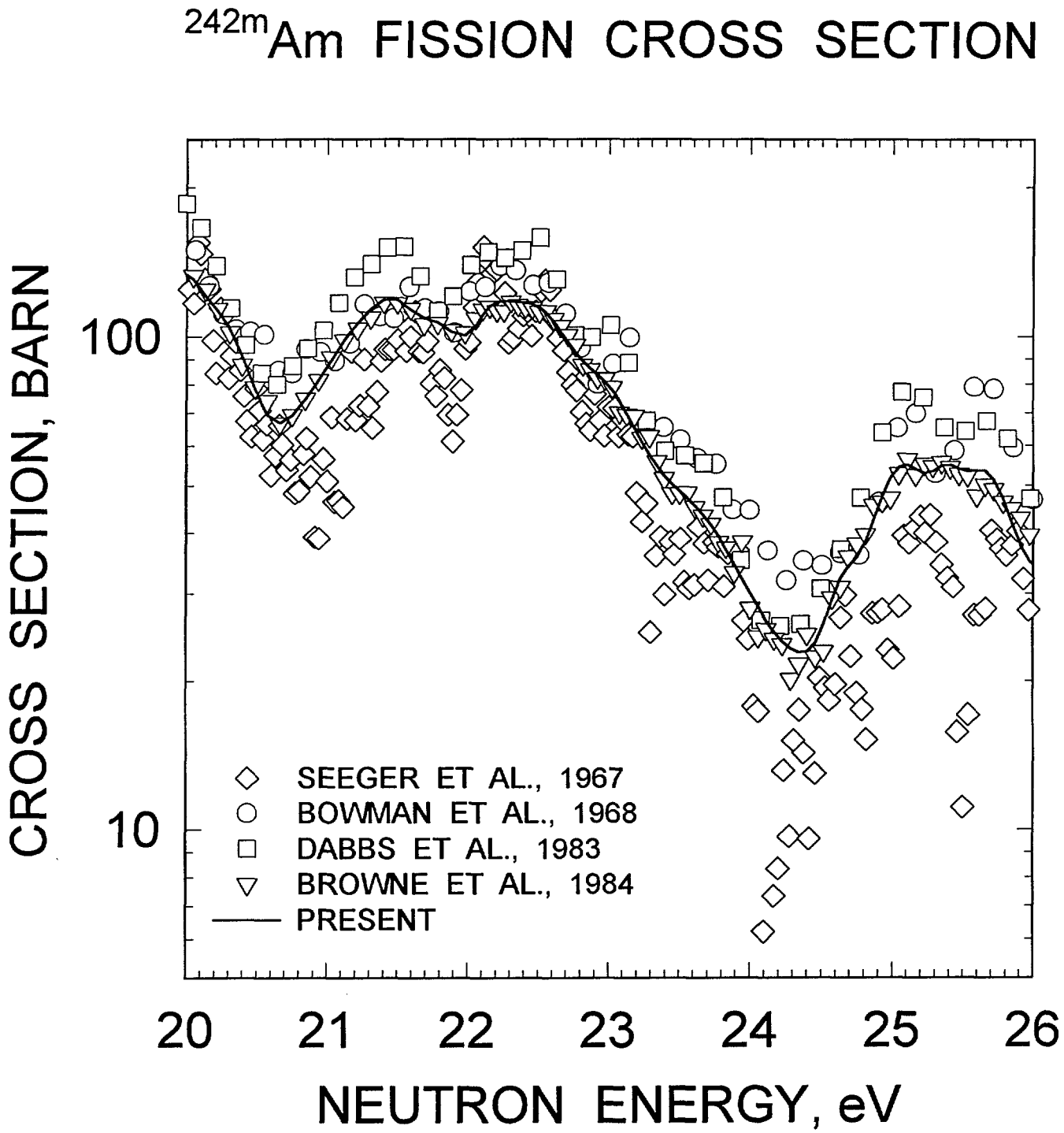
^{242m}Am FISSION CROSS SECTION
CROSS SECTION, BARN
100
10
SEEGER ET AL., 1967
BOWMAN ET AL., 1968
DABBS ET AL., 1983
BROWNE ET AL., 1984
PRESENT
20
21
22
23
24
25
26
NEUTRON ENERGY, eV

FIG.2.7

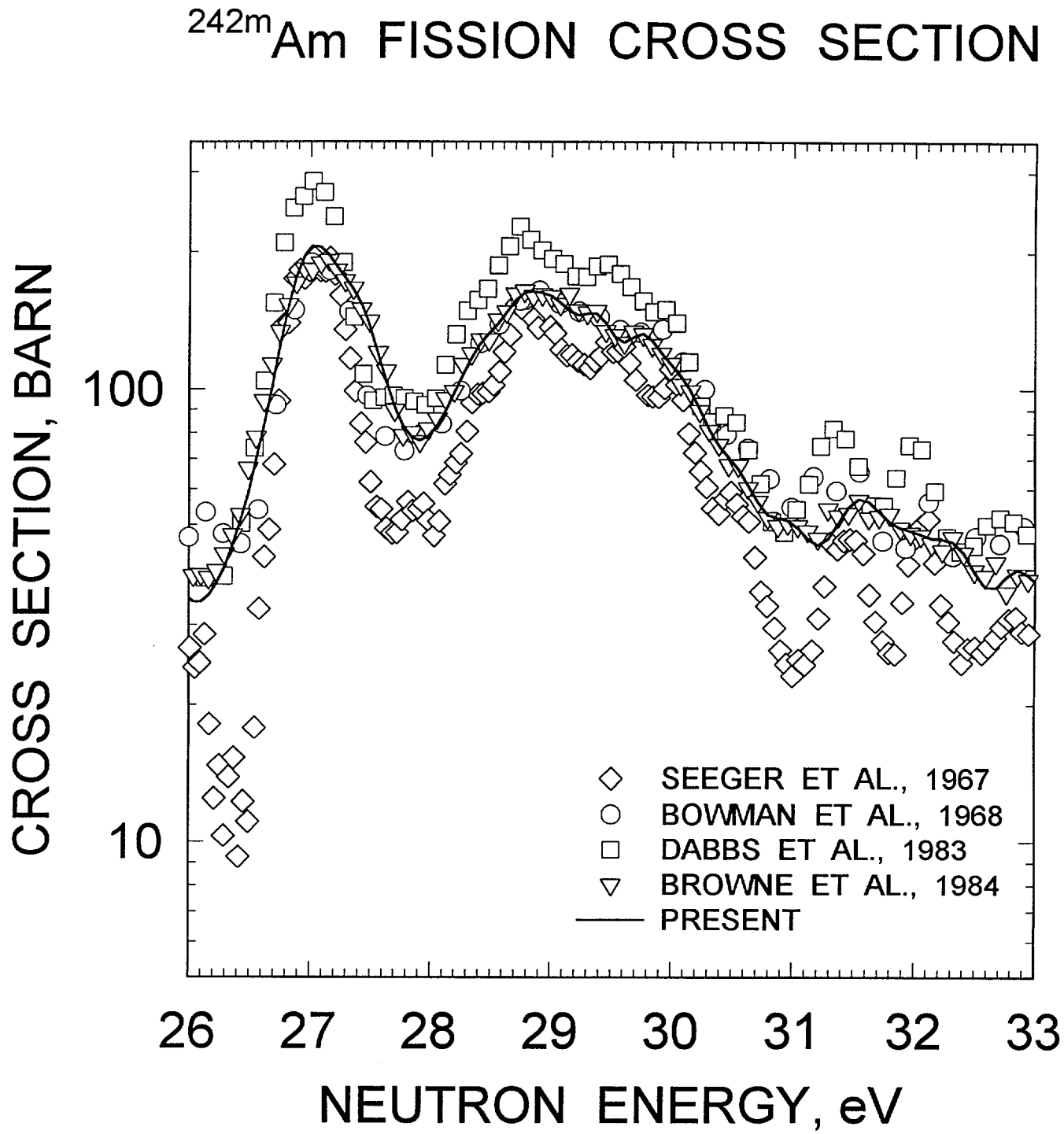
242mAm FISSION CROSS SECTION
CROSS SECTION, BARN
100
10
SEEGER ET AL., 1967
BOWMAN ET AL., 1968
DABBS ET AL., 1983
BROWNE ET AL., 1984
PRESENT
26
27
28
29
30
31
32
33
NEUTRON ENERGY, eV

FIG.2.8

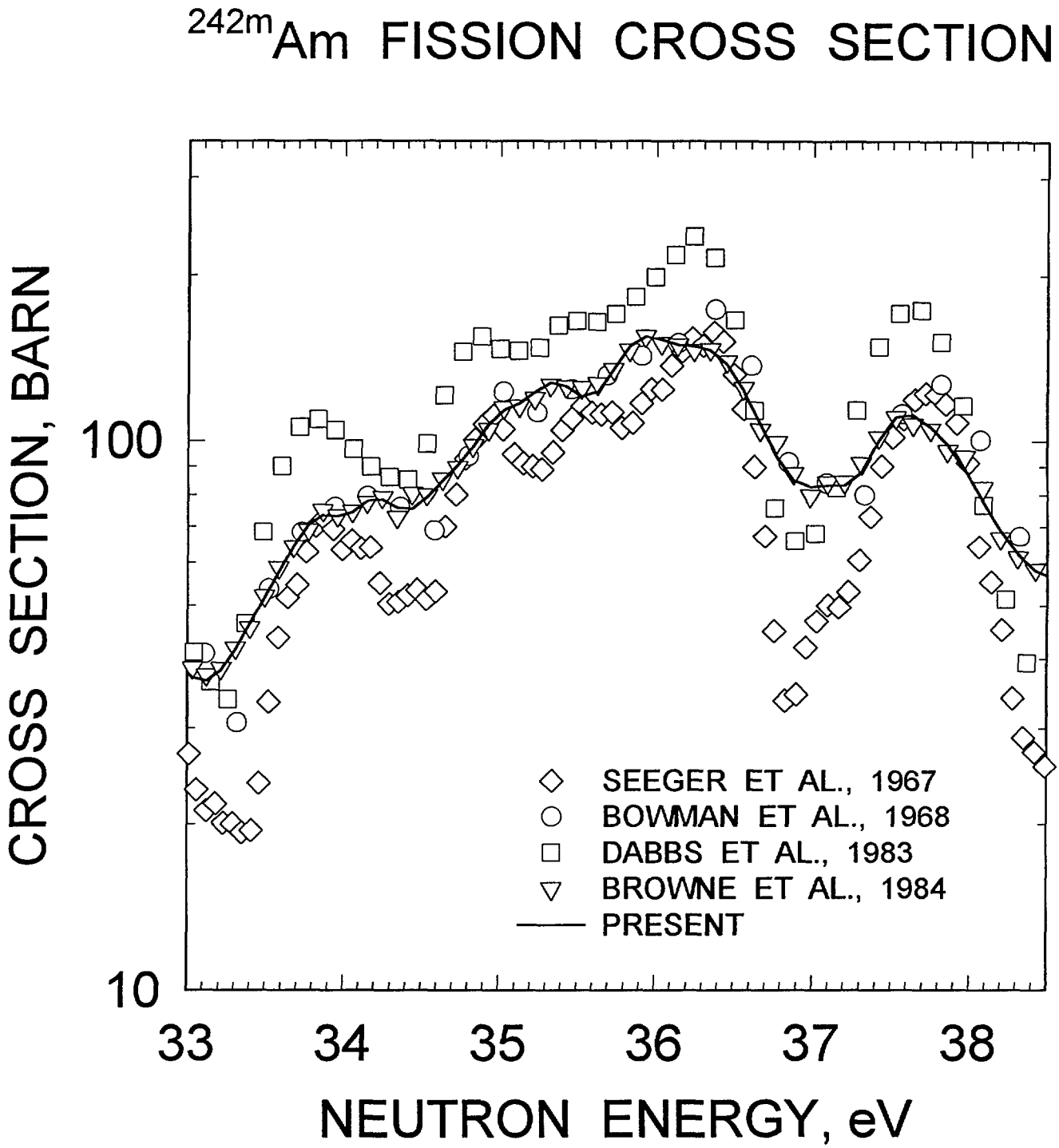
242mAm FISSION CROSS SECTION
CROSS SECTION, BARN
100
10
33
34
35
36
37
38
NEUTRON ENERGY, eV
SEEGER ET AL., 1967
BOWMAN ET AL., 1968
DABBS ET AL., 1983
BROWNE ET AL., 1984
PRESENT

FIG.2.9

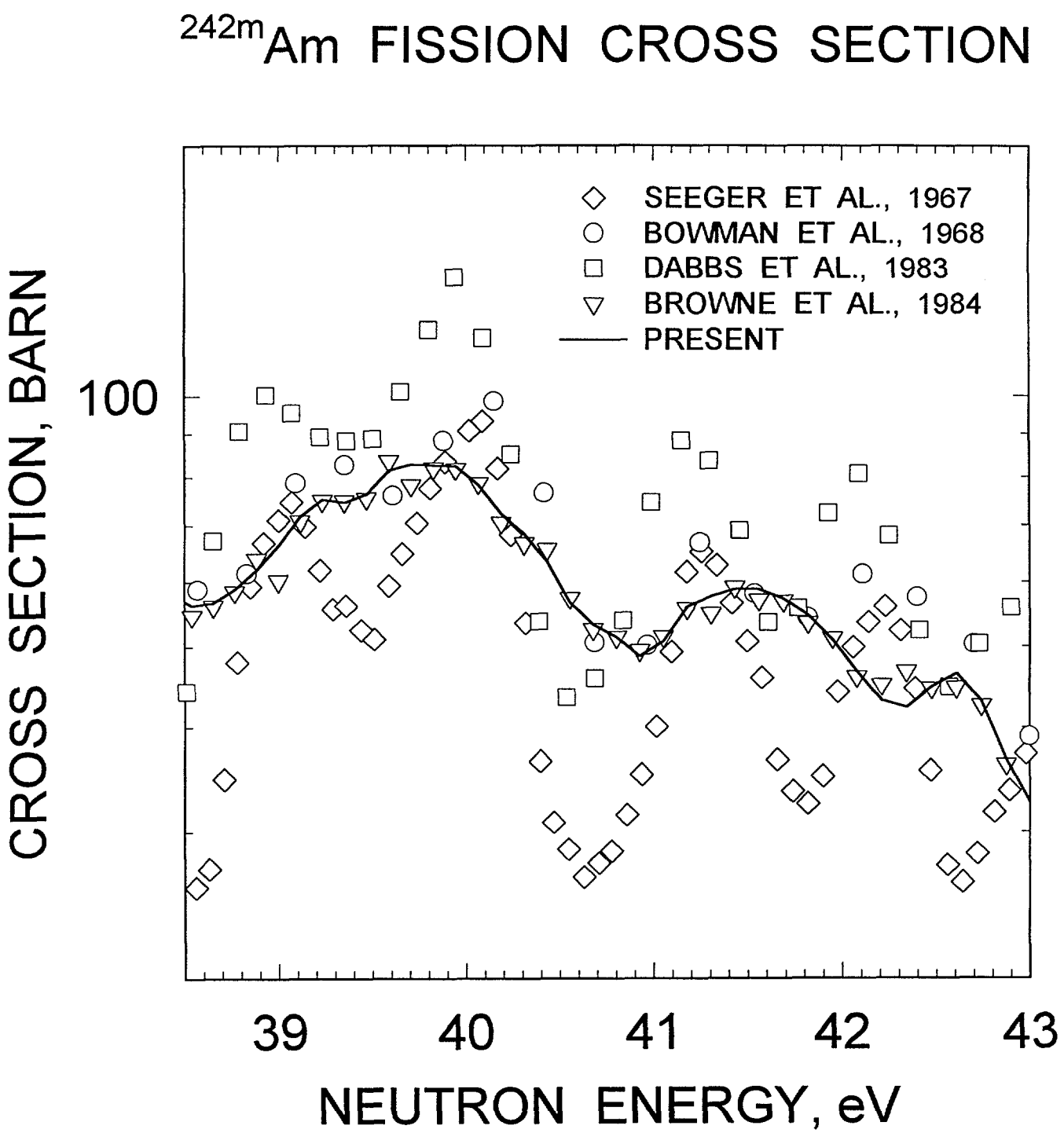
242mAm FISSION CROSS SECTION
SEEGER ET AL., 1967
BOWMAN ET AL., 1968
DABBS ET AL., 1983
BROWNE ET AL., 1984
PRESENT
CROSS SECTION, BARN
100
39
40
41
42
43
NEUTRON ENERGY, eV

FIG.2.10

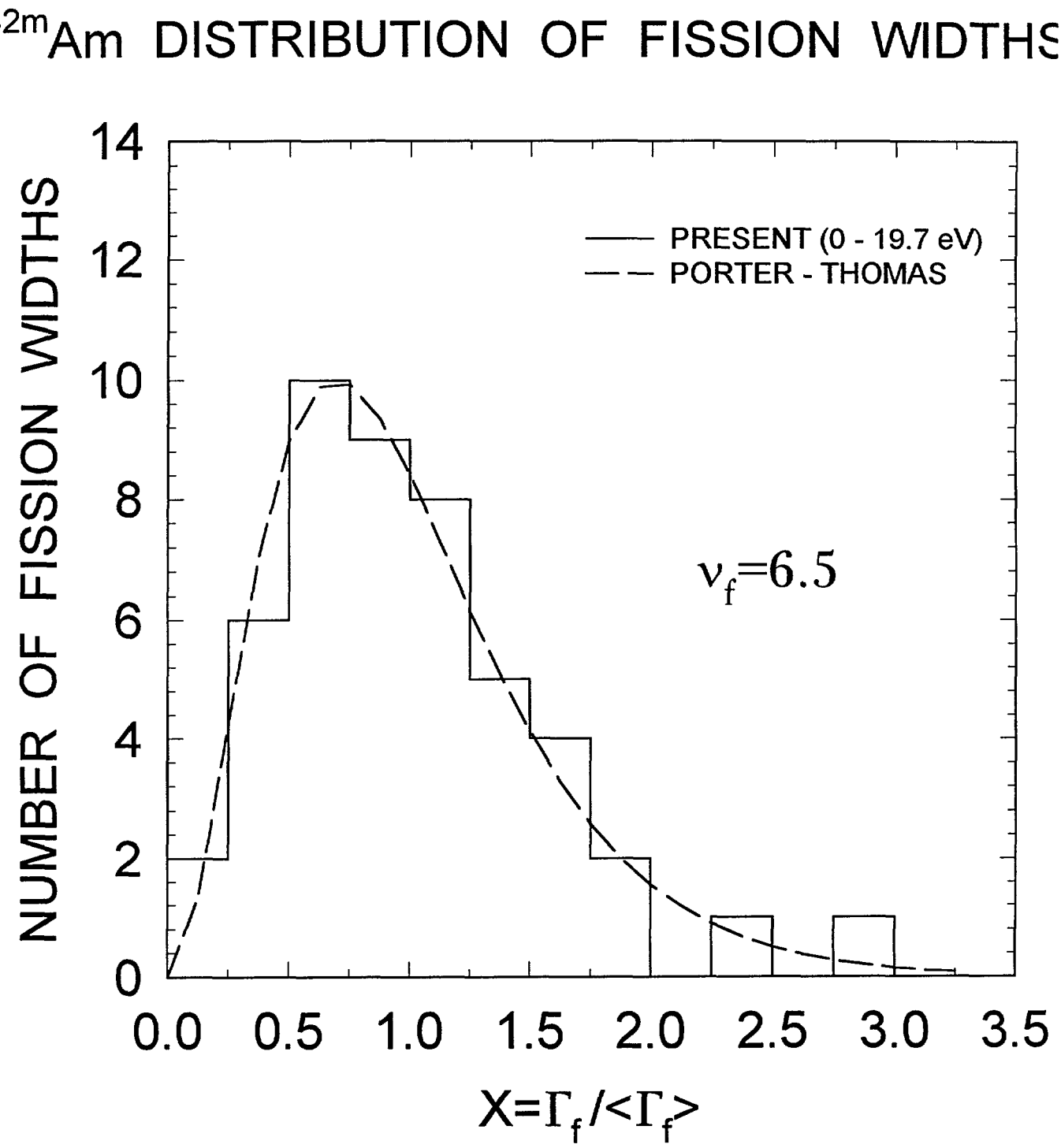
242mAm DISTRIBUTION OF FISSION WIDTHS
NUMBER OF FISSION WIDTHS
14
12
10
8
6
4
2
0
0.0
0.5
1.0
1.5
2.0
2.5
3.0
3.5
X=Γf/<Γf>
PRESENT (0 - 19.7 eV)
PORTER - THOMAS
νf=6.5

FIG.2.11

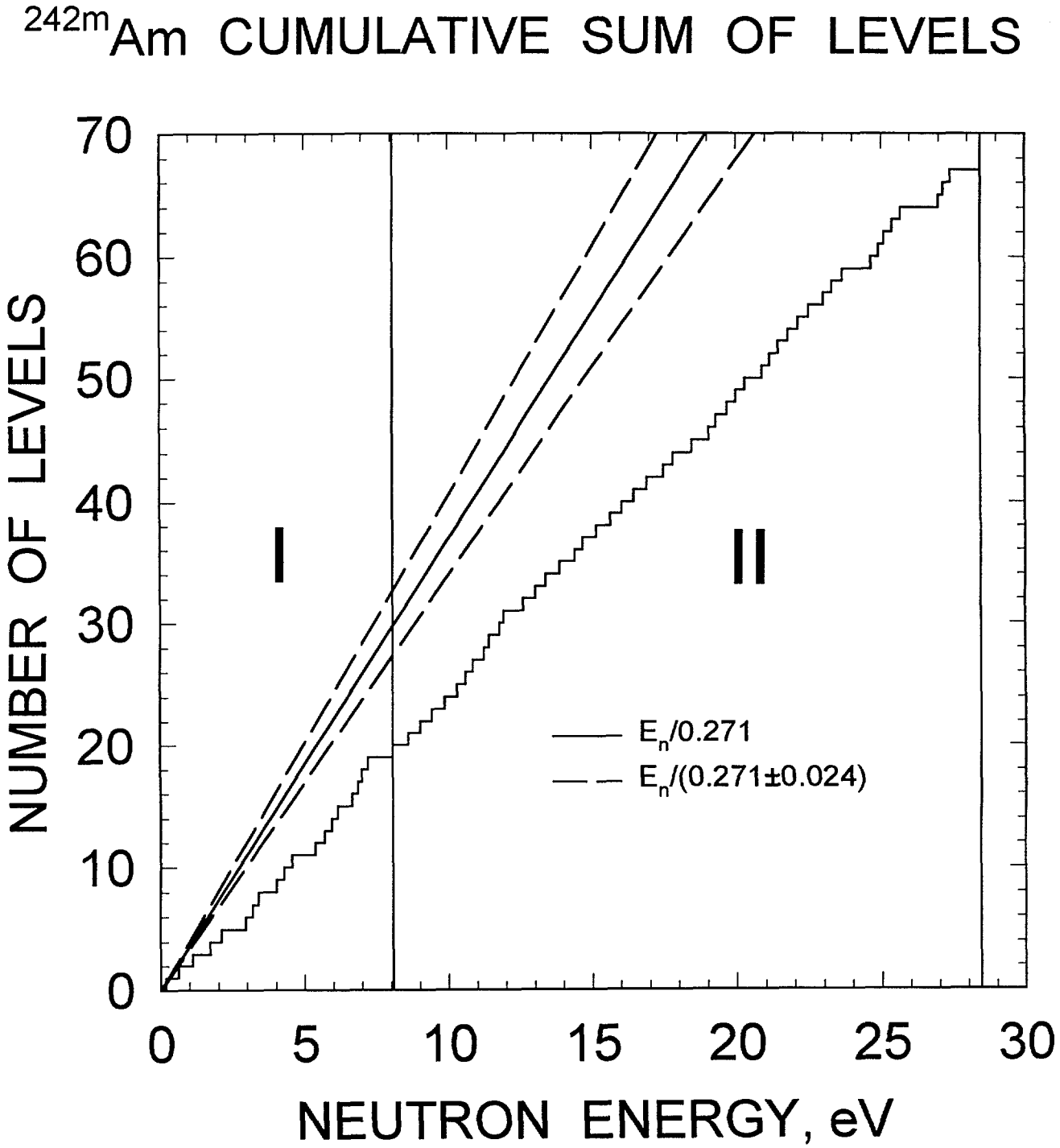
^{242m}Am CUMULATIVE SUM OF LEVELS
NUMBER OF LEVELS
70
60
50
40
30
20
10
0
I
II
E_n/0.271
E_n/(0.271±0.024)
0
5
10
15
20
25
30
NEUTRON ENERGY, eV

FIG.3.1

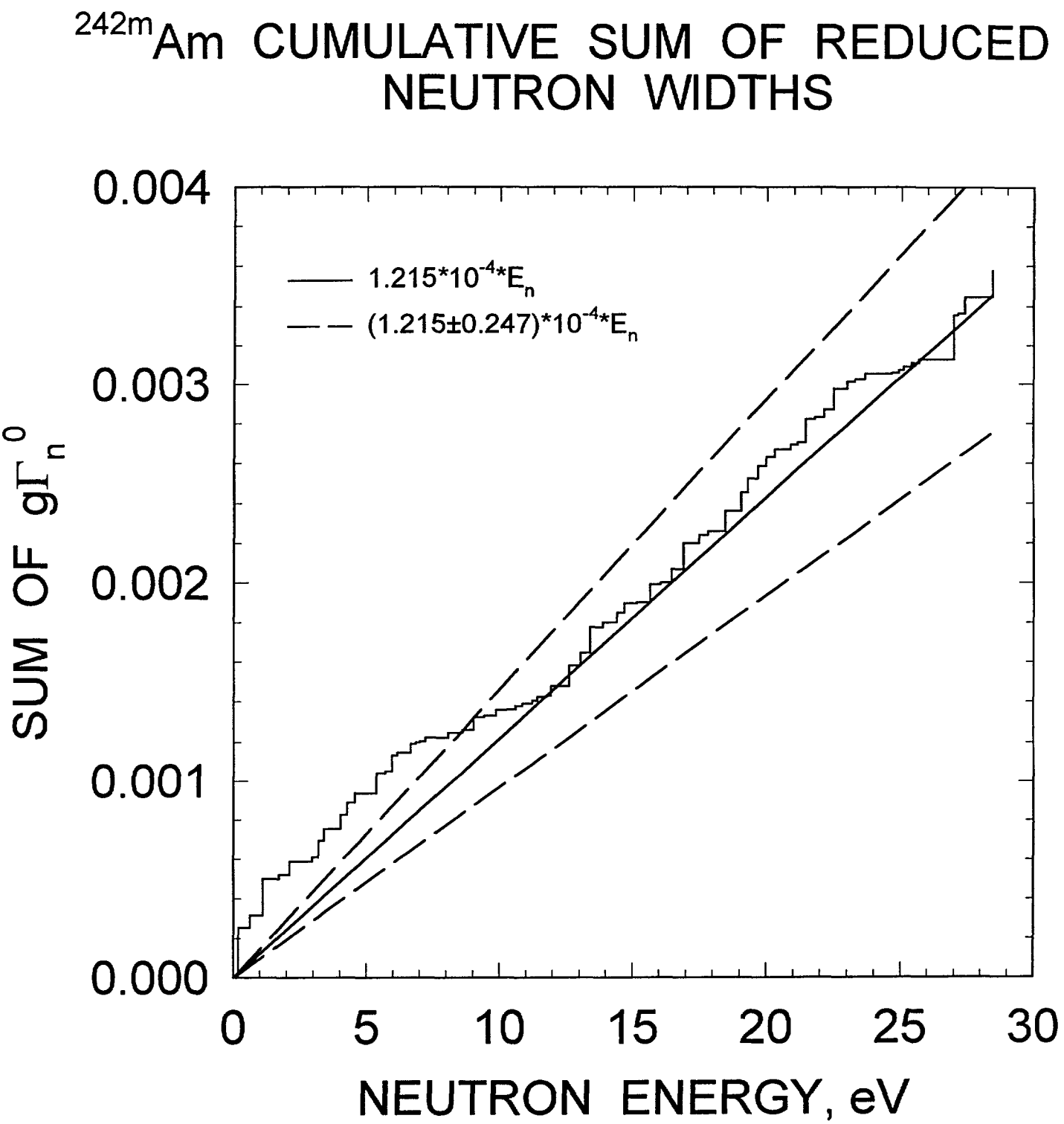
^{242m}Am CUMULATIVE SUM OF REDUCED NEUTRON WIDTHS
0.004
0.003
0.002
0.001
0.000
SUM OF $g\Gamma_n^0$
$1.215*10^{-4}*E_n$
$(1.215\pm0.247)*10^{-4}*E_n$
0
5
10
15
20
25
30
NEUTRON ENERGY, eV

FIG.3.2

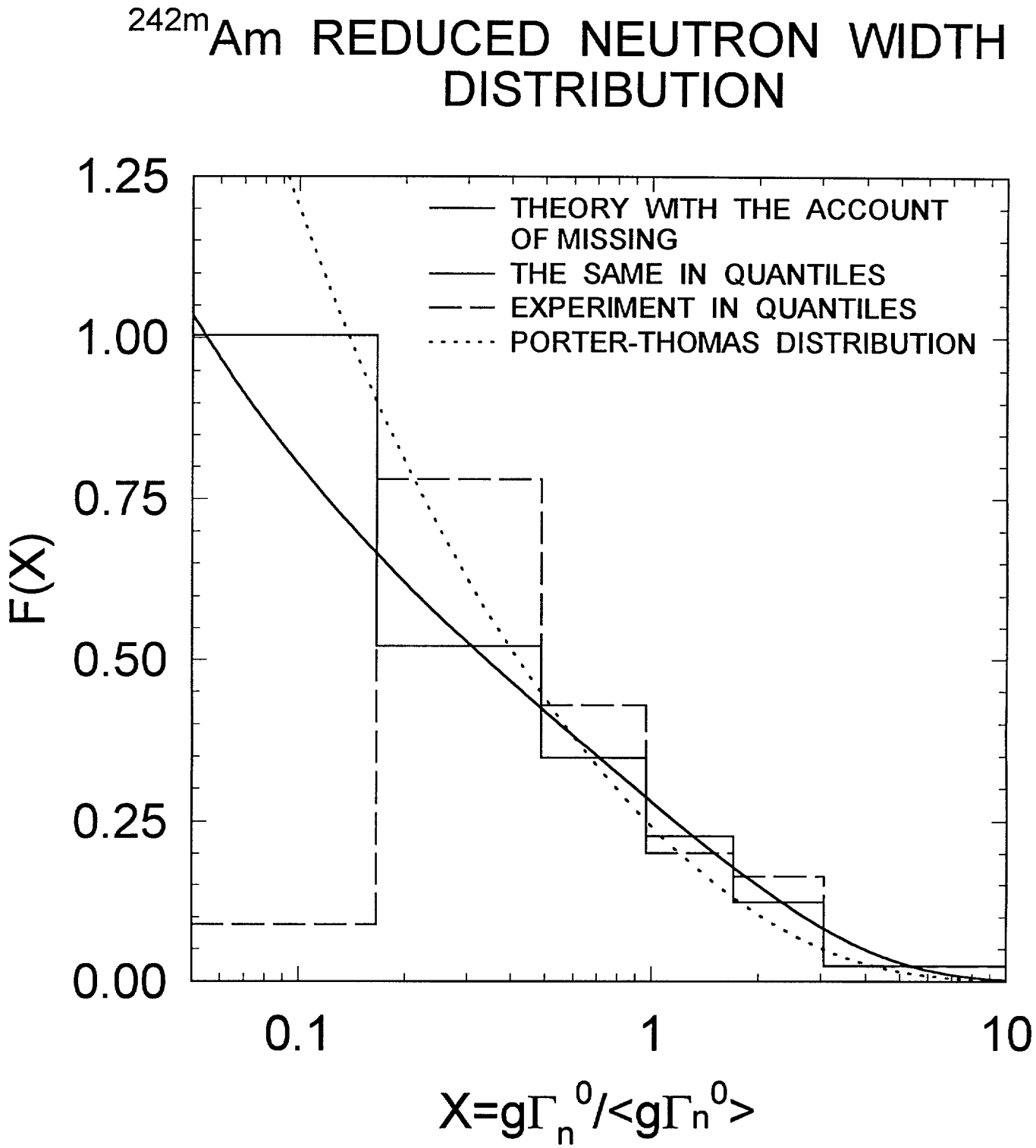
^{242m}Am REDUCED NEUTRON WIDTH DISTRIBUTION
THEORY WITH THE ACCOUNT OF MISSING
THE SAME IN QUANTILES
EXPERIMENT IN QUANTILES
PORTER-THOMAS DISTRIBUTION
F(X)
1.25
1.00
0.75
0.50
0.25
0.00
0.1
1
10
X=gΓn0/<gΓn0>

FIG.3.3

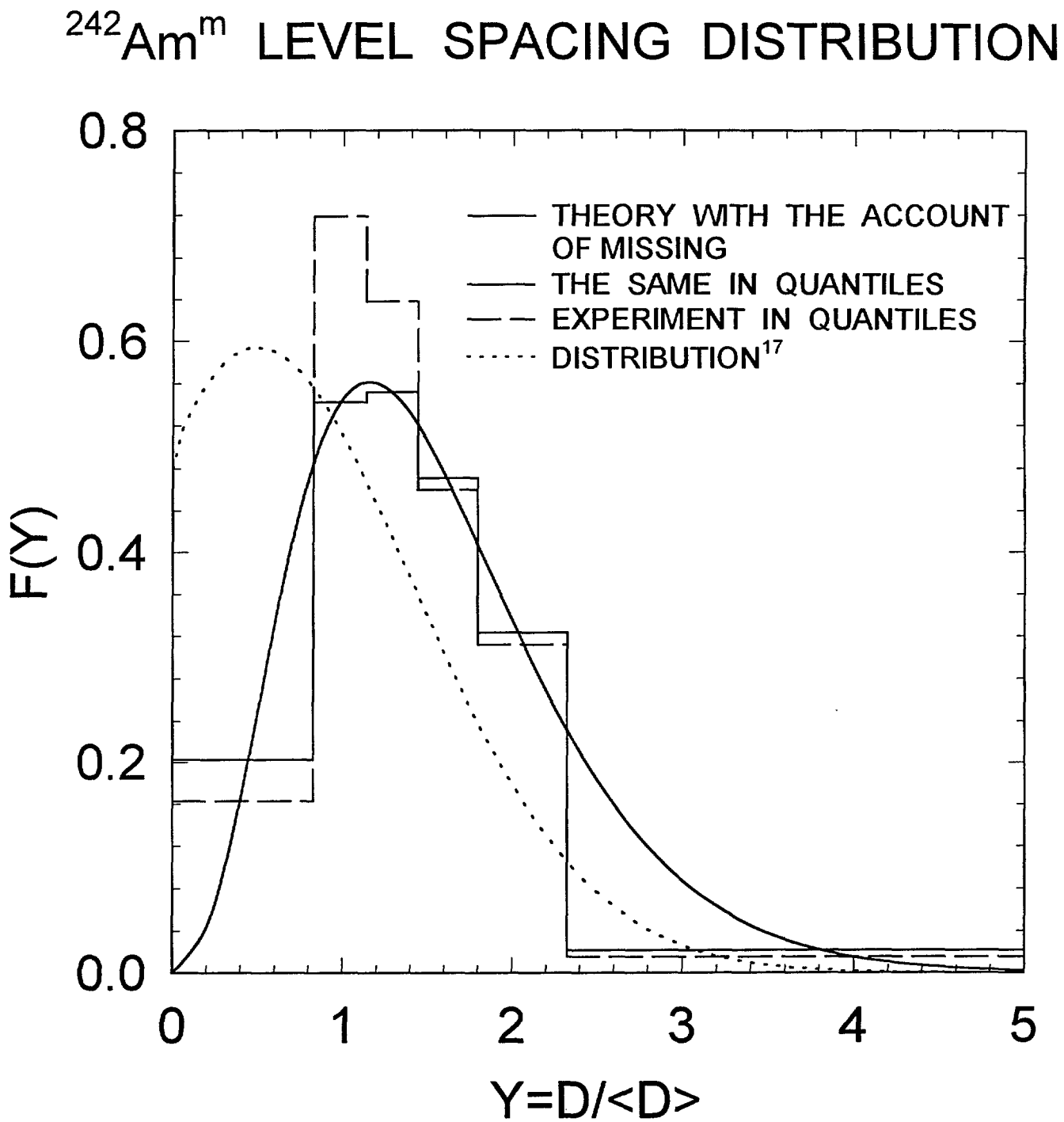
$^{242}Am^{m}$ LEVEL SPACING DISTRIBUTION
0.8
0.6
0.4
0.2
0.0
F(Y)
0
1
2
3
4
5
Y=D/<D>
THEORY WITH THE ACCOUNT OF MISSING
THE SAME IN QUANTILES
EXPERIMENT IN QUANTILES
DISTRIBUTION[17]

FIG.3.4

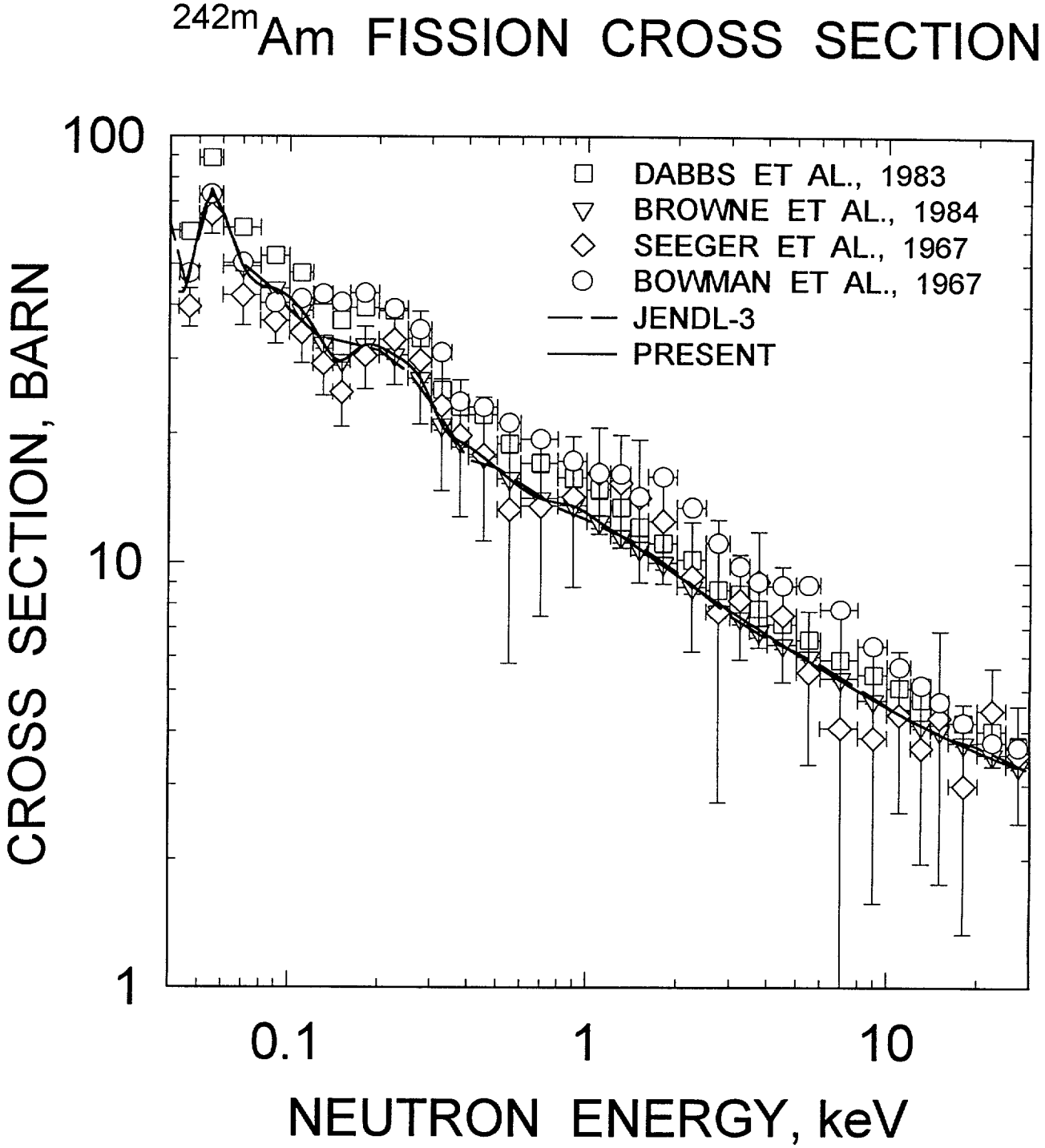
242mAm FISSION CROSS SECTION
100
10
1
CROSS SECTION, BARN
0.1
1
10
NEUTRON ENERGY, keV
DABBS ET AL., 1983
BROWNE ET AL., 1984
SEEGER ET AL., 1967
BOWMAN ET AL., 1967
JENDL-3
PRESENT

FIG.3.5

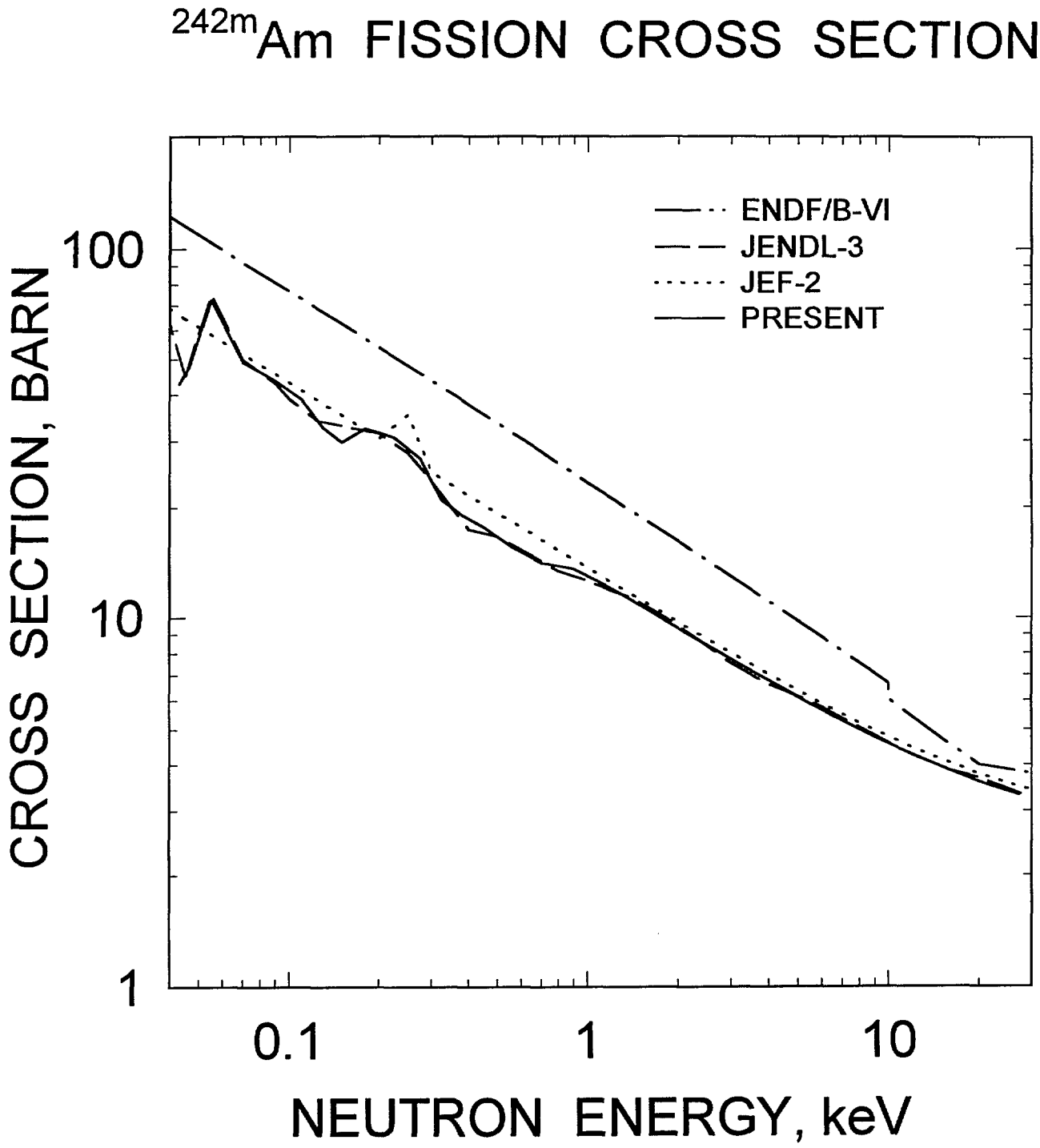
242mAm FISSION CROSS SECTION
ENDF/B-VI
JENDL-3
JEF-2
PRESENT
CROSS SECTION, BARN
100
10
1
0.1
1
10
NEUTRON ENERGY, keV

FIG.3.6

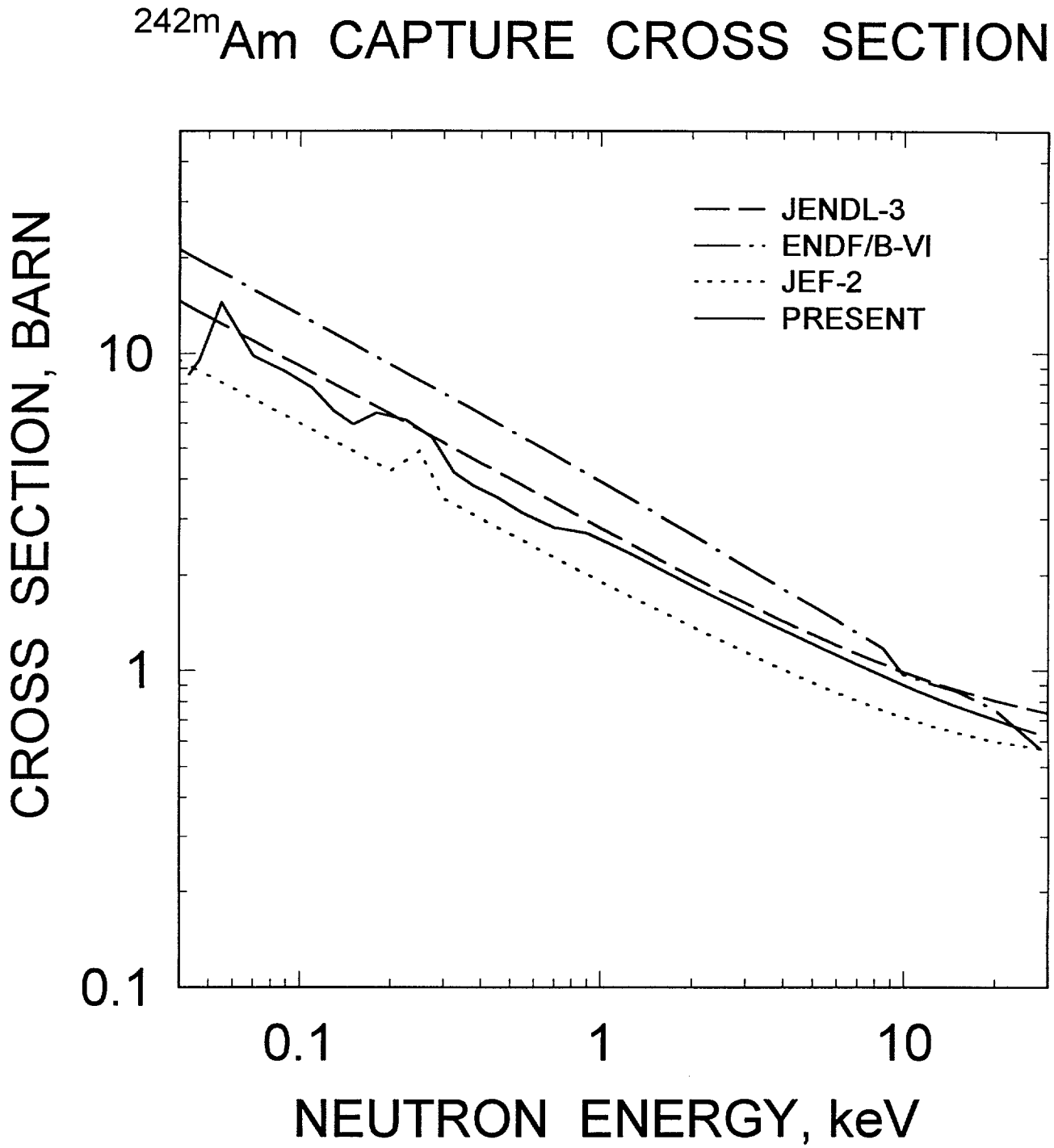
242mAm CAPTURE CROSS SECTION
JENDL-3
ENDF/B-VI
JEF-2
PRESENT
CROSS SECTION, BARN
10
1
0.1
0.1
1
10
NEUTRON ENERGY, keV

FIG.3.7

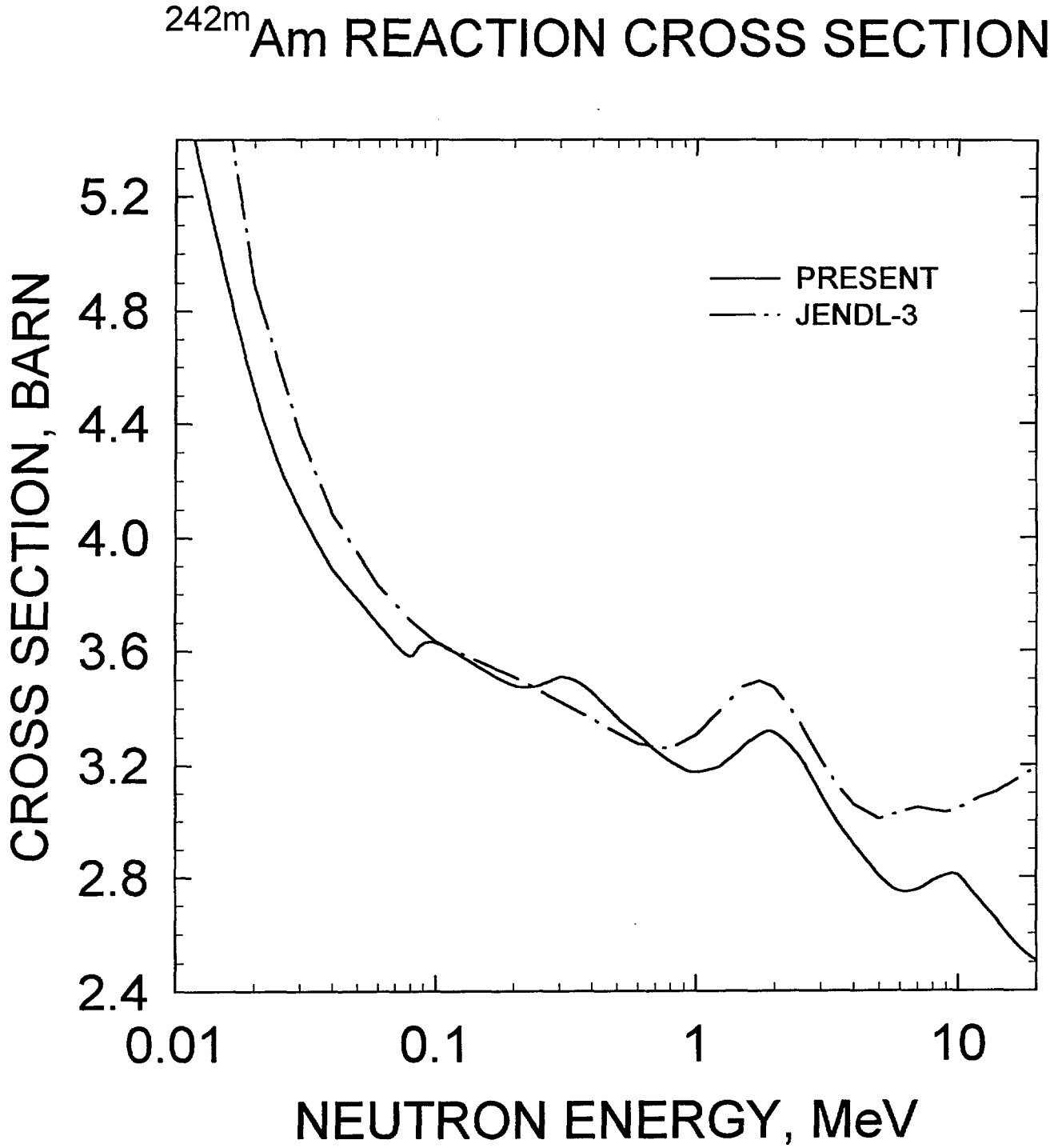
242mAm REACTION CROSS SECTION
CROSS SECTION, BARN
5.2
4.8
4.4
4.0
3.6
3.2
2.8
2.4
0.01
0.1
1
10
NEUTRON ENERGY, MeV
PRESENT
JENDL-3

FIG.4.1

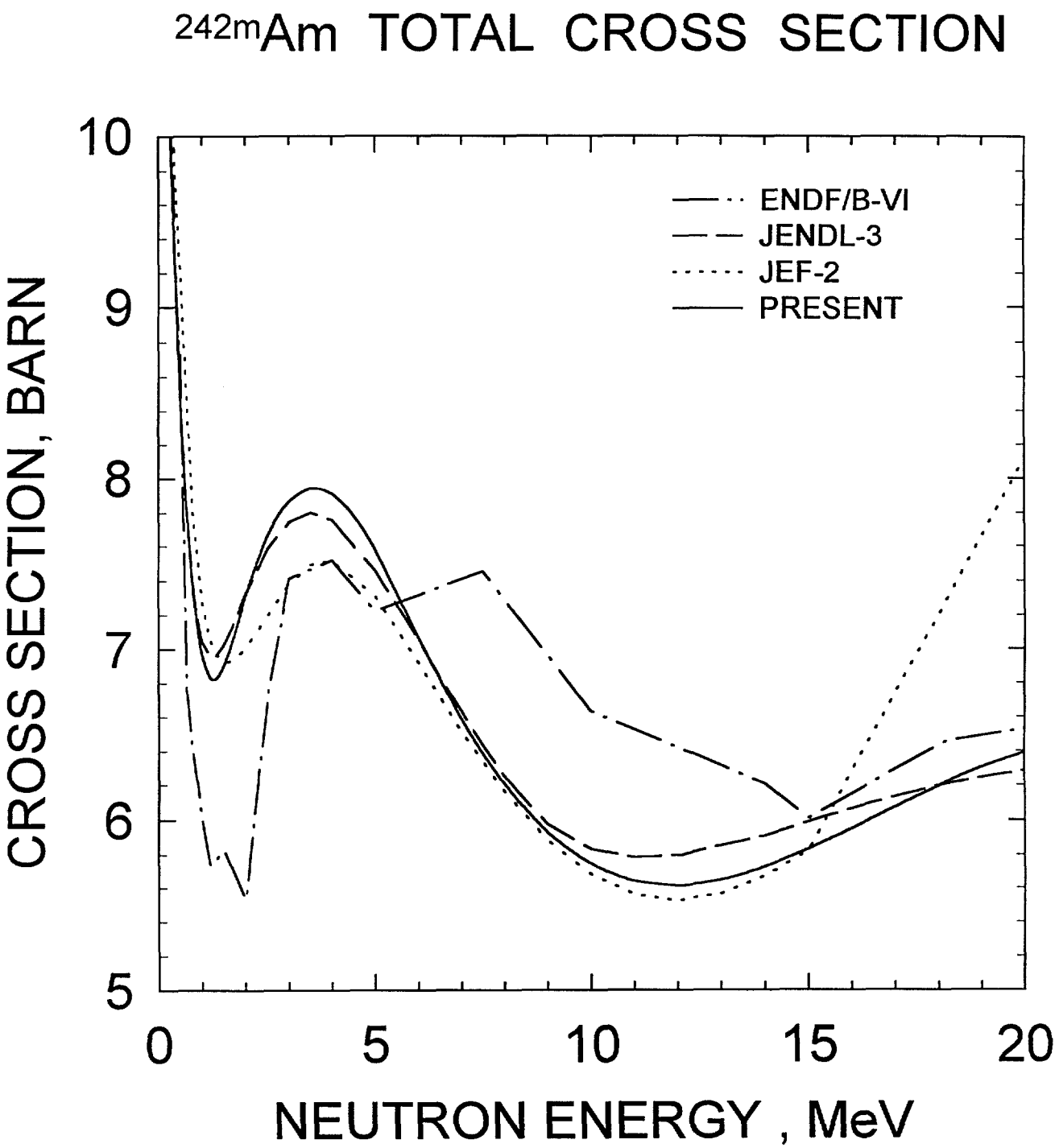
242mAm TOTAL CROSS SECTION
CROSS SECTION, BARN
NEUTRON ENERGY , MeV
ENDF/B-VI
JENDL-3
JEF-2
PRESENT
10
9
8
7
6
5
0
5
10
15
20

FIG.4.2

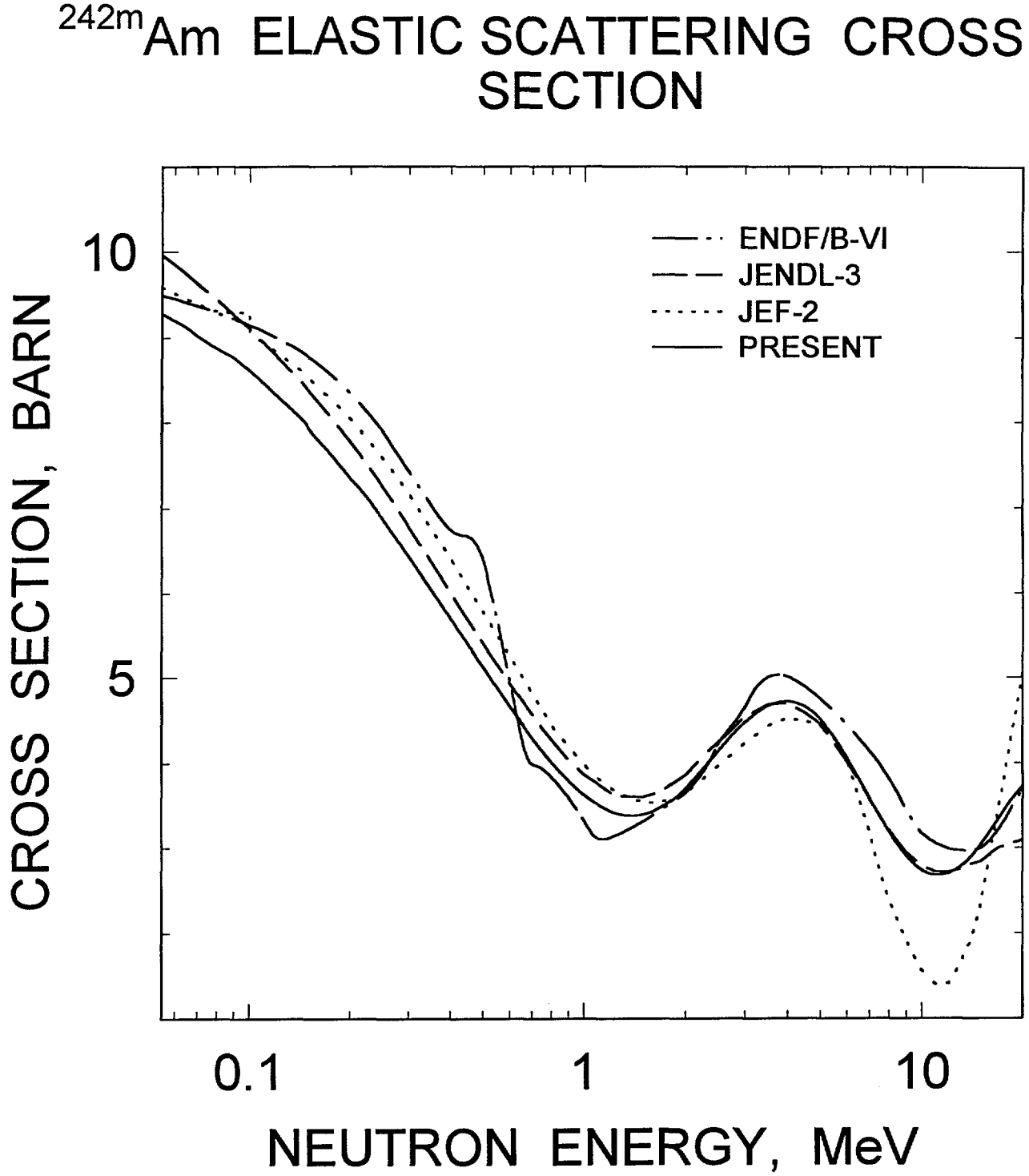
^{242m}Am ELASTIC SCATTERING CROSS SECTION
ENDF/B-VI
JENDL-3
JEF-2
PRESENT
CROSS SECTION, BARN
10
5
0.1
1
10
NEUTRON ENERGY, MeV

FIG.4.3

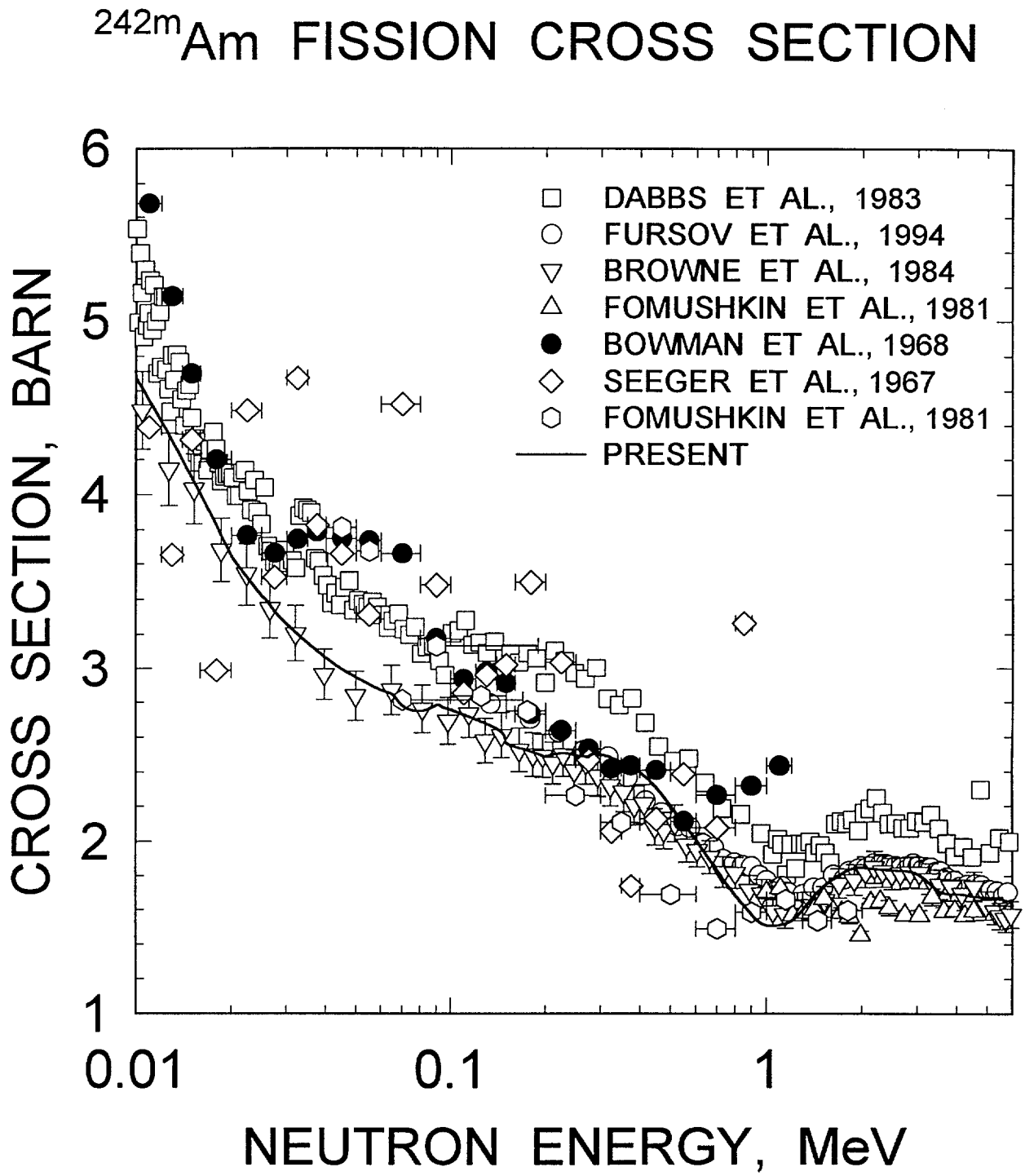
242mAm FISSION CROSS SECTION
CROSS SECTION, BARN
NEUTRON ENERGY, MeV
6
5
4
3
2
1
0.01
0.1
1
DABBS ET AL., 1983
FURSOV ET AL., 1994
BROWNE ET AL., 1984
FOMUSHKIN ET AL., 1981
BOWMAN ET AL., 1968
SEEGER ET AL., 1967
FOMUSHKIN ET AL., 1981
PRESENT

FIG. 4.4

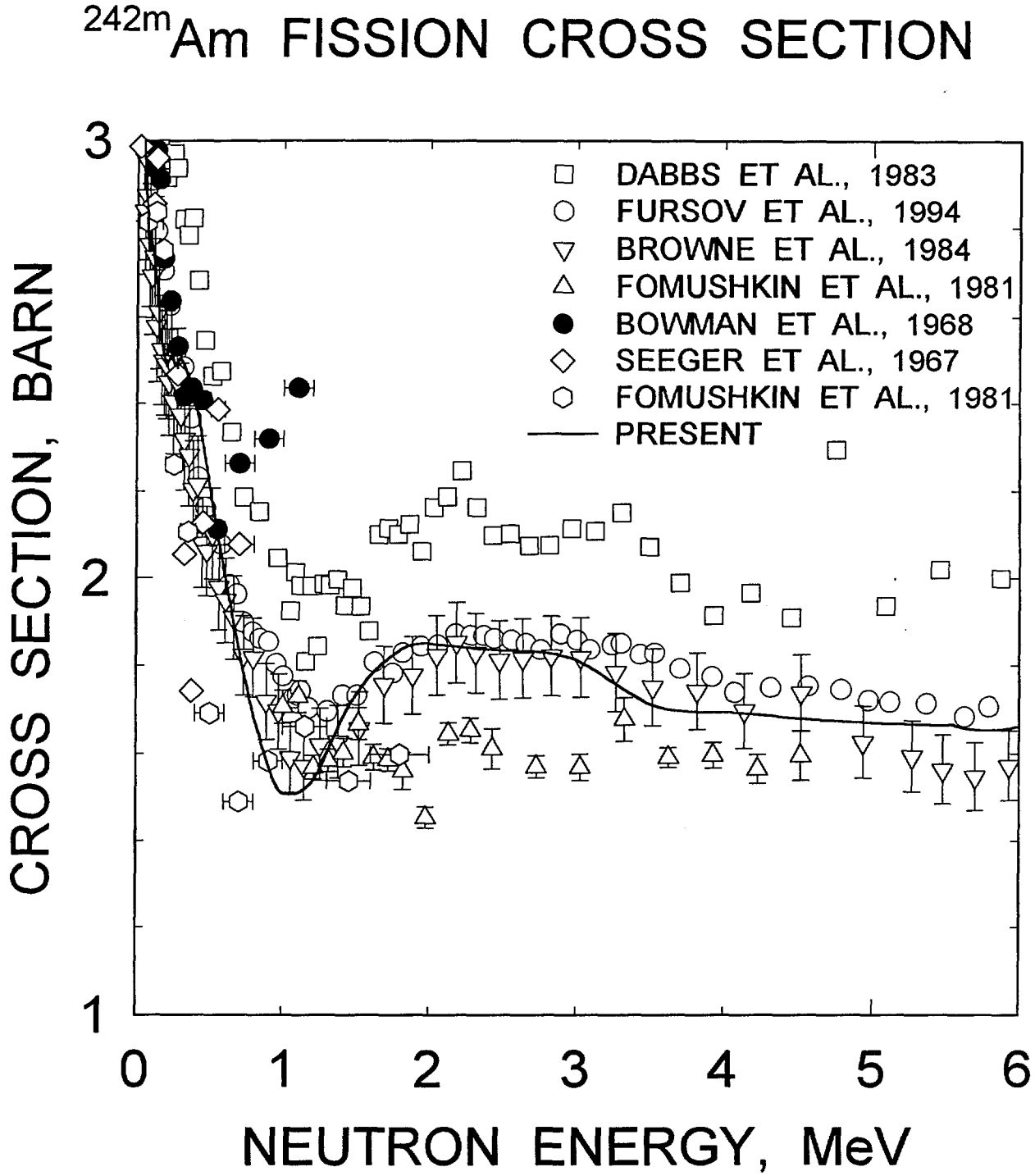
242mAm FISSION CROSS SECTION
CROSS SECTION, BARN
NEUTRON ENERGY, MeV
DABBS ET AL., 1983
FURSOV ET AL., 1994
BROWNE ET AL., 1984
FOMUSHKIN ET AL., 1981
BOWMAN ET AL., 1968
SEEGER ET AL., 1967
FOMUSHKIN ET AL., 1981
PRESENT
1
2
3
0
1
2
3
4
5
6

FIG. 4.5

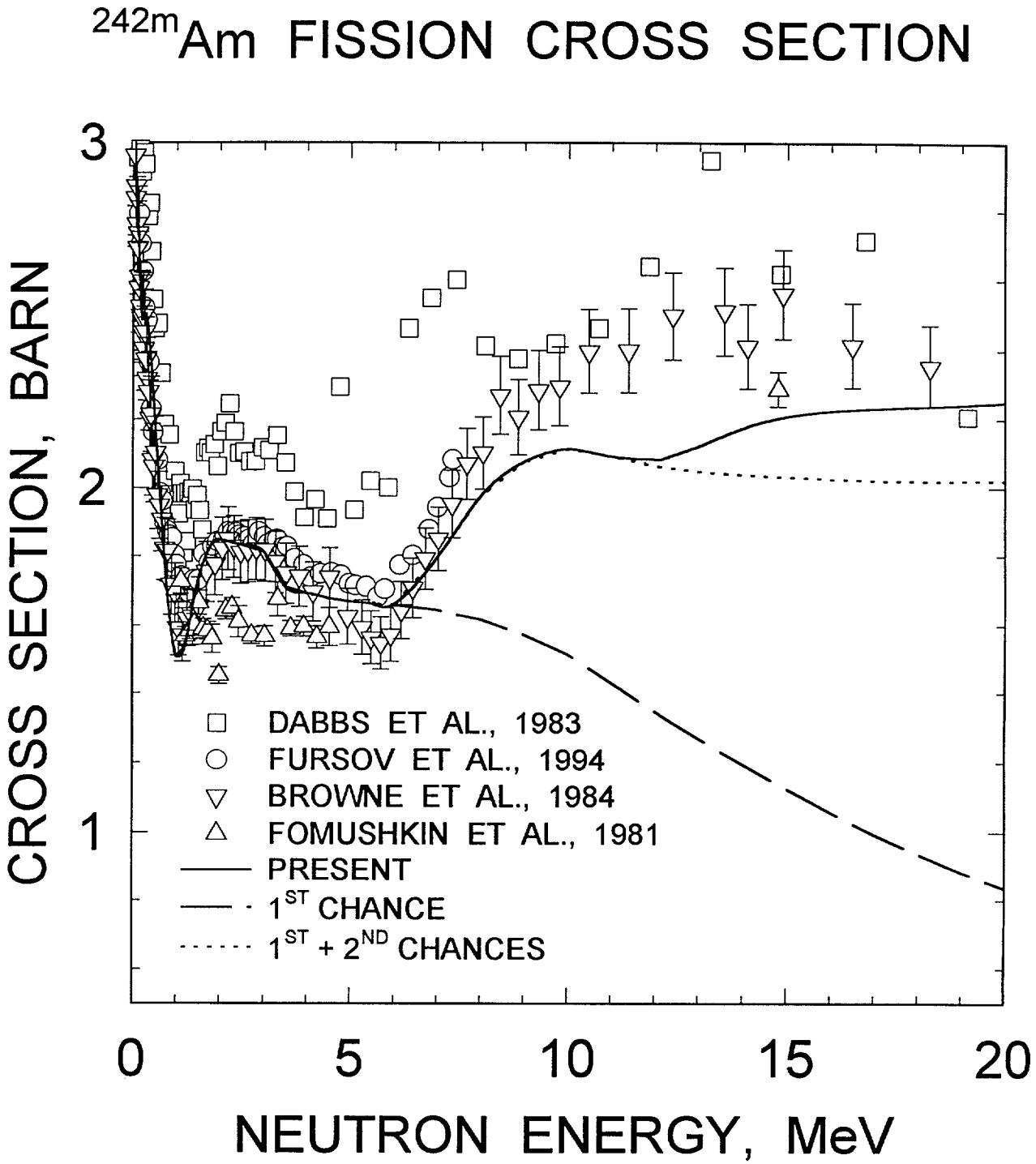
242mAm FISSION CROSS SECTION
CROSS SECTION, BARN
3
2
1
0
5
10
15
20
NEUTRON ENERGY, MeV
DABBS ET AL., 1983
FURSOV ET AL., 1994
BROWNE ET AL., 1984
FOMUSHKIN ET AL., 1981
PRESENT
1ST CHANCE
1ST + 2ND CHANCES

FIG. 4.6

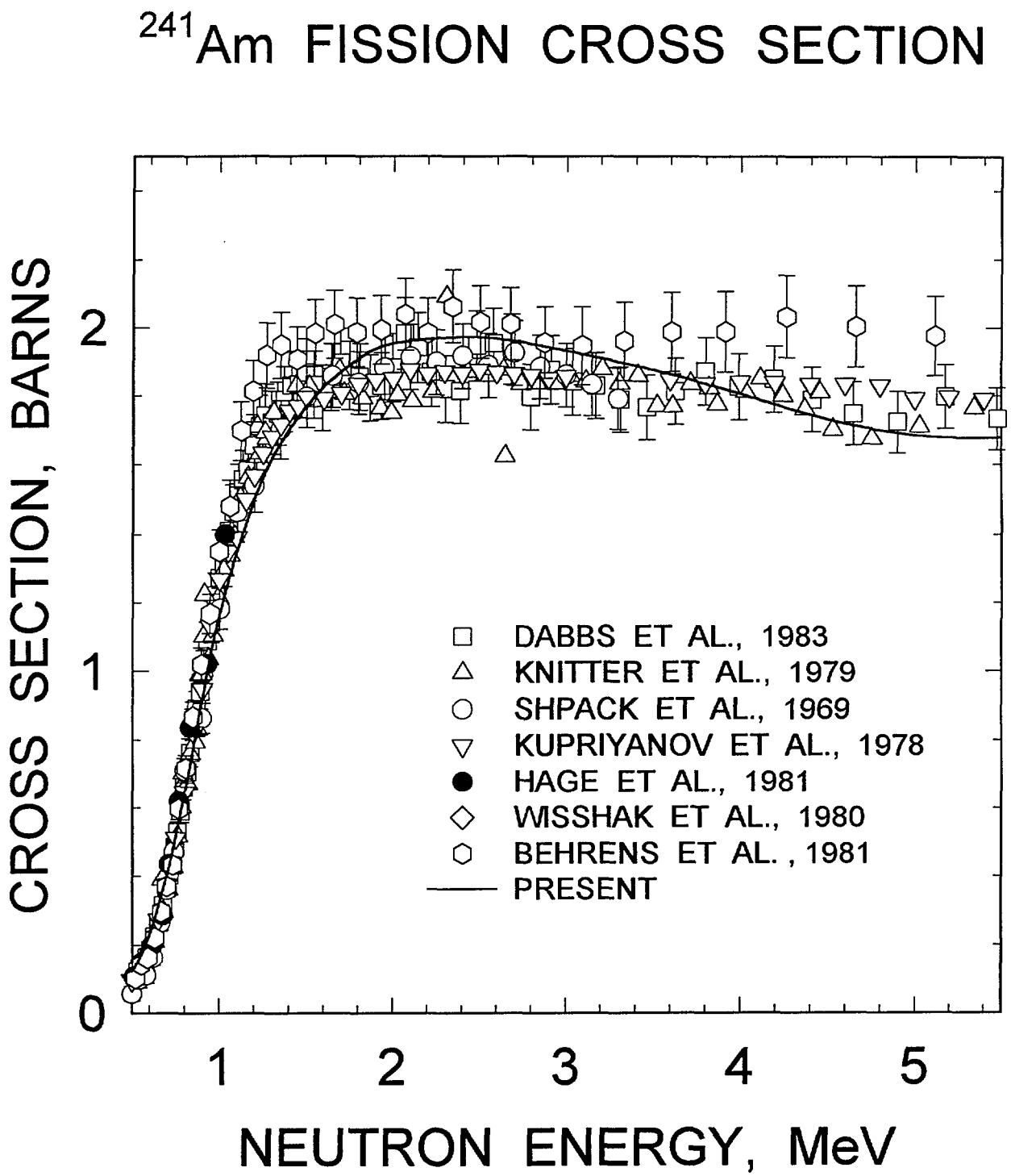
^{241}Am FISSION CROSS SECTION
CROSS SECTION, BARNS
0
1
2
1
2
3
4
5
NEUTRON ENERGY, MeV
DABBS ET AL., 1983
KNITTER ET AL., 1979
SHPACK ET AL., 1969
KUPRIYANOV ET AL., 1978
HAGE ET AL., 1981
WISSHAK ET AL., 1980
BEHRENS ET AL., 1981
PRESENT

FIG. 4.7

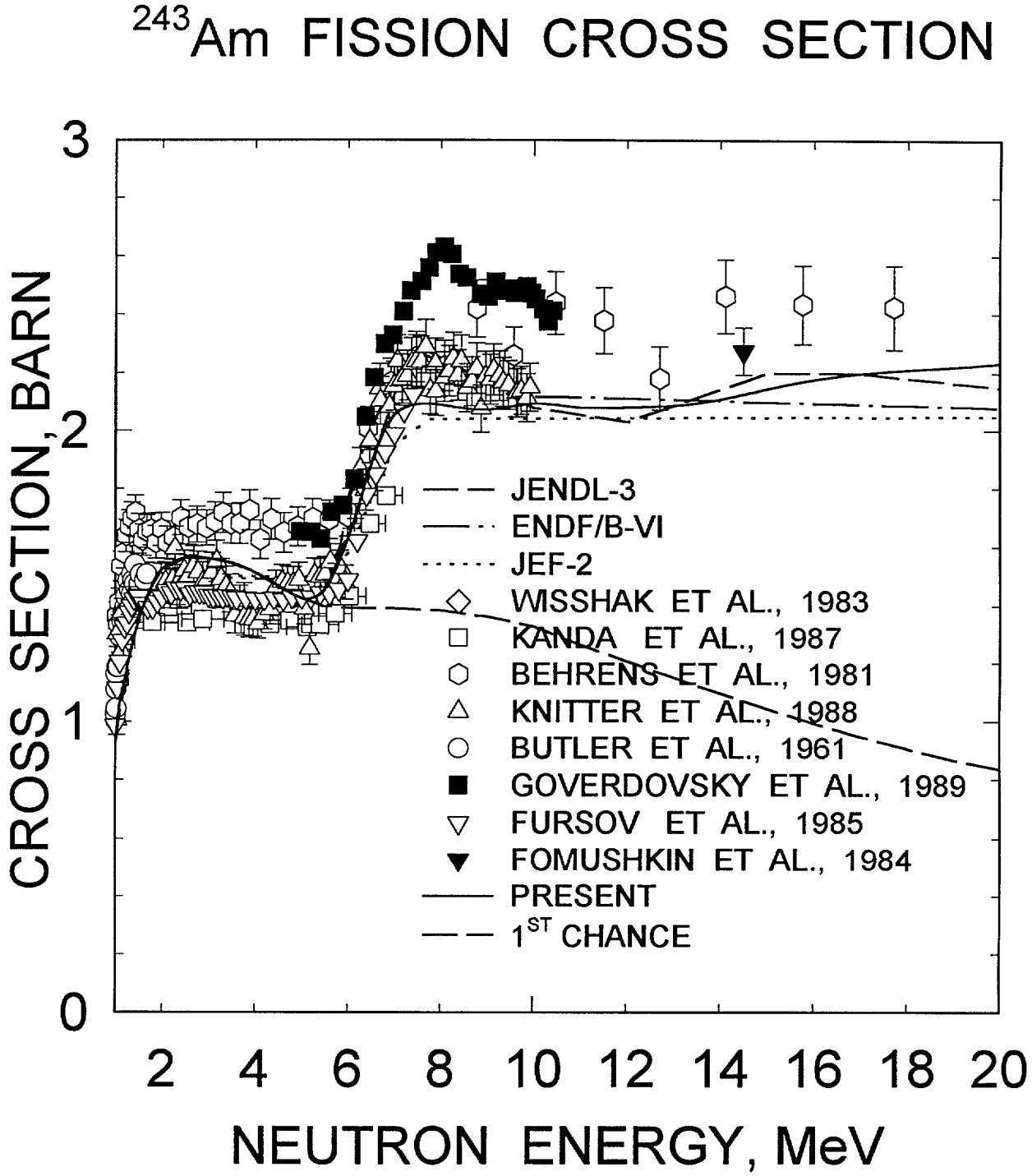
^{243}Am FISSION CROSS SECTION
CROSS SECTION, BARN
NEUTRON ENERGY, MeV
0
1
2
3
2
4
6
8
10
12
14
16
18
20
JENDL-3
ENDF/B-VI
JEF-2
WISSHAK ET AL., 1983
KANDA ET AL., 1987
BEHRENS ET AL., 1981
KNITTER ET AL., 1988
BUTLER ET AL., 1961
GOVERDOVSKY ET AL., 1989
FURSOV ET AL., 1985
FOMUSHKIN ET AL., 1984
PRESENT
1ST CHANCE

FIG.4.8

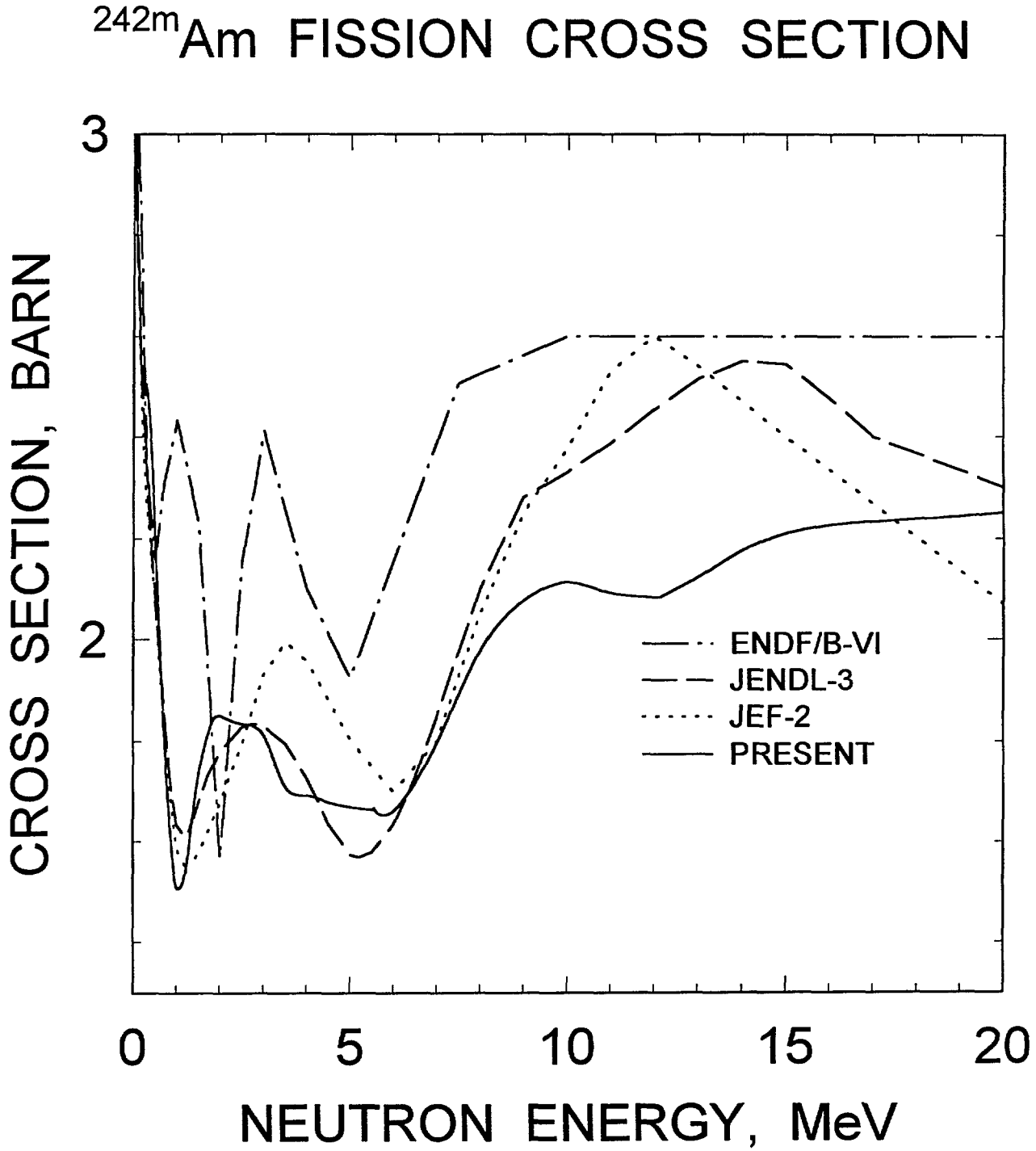
242mAm FISSION CROSS SECTION
CROSS SECTION, BARN
3
2
0
5
10
15
20
NEUTRON ENERGY, MeV
ENDF/B-VI
JENDL-3
JEF-2
PRESENT

FIG. 4.9

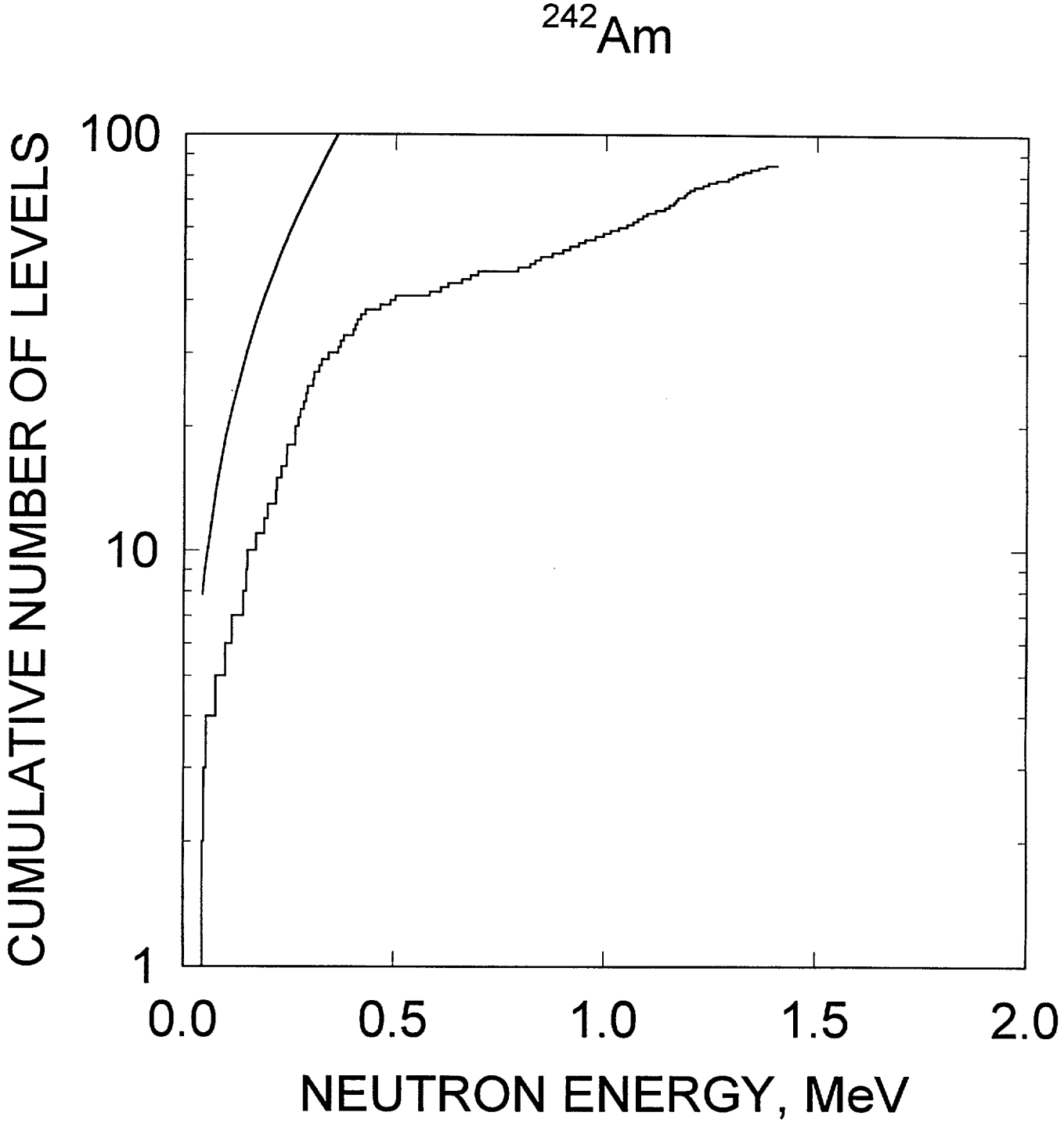
^{242}Am
CUMULATIVE NUMBER OF LEVELS
100
10
1
0.0
0.5
1.0
1.5
2.0
NEUTRON ENERGY, MeV

FIG. 4.10

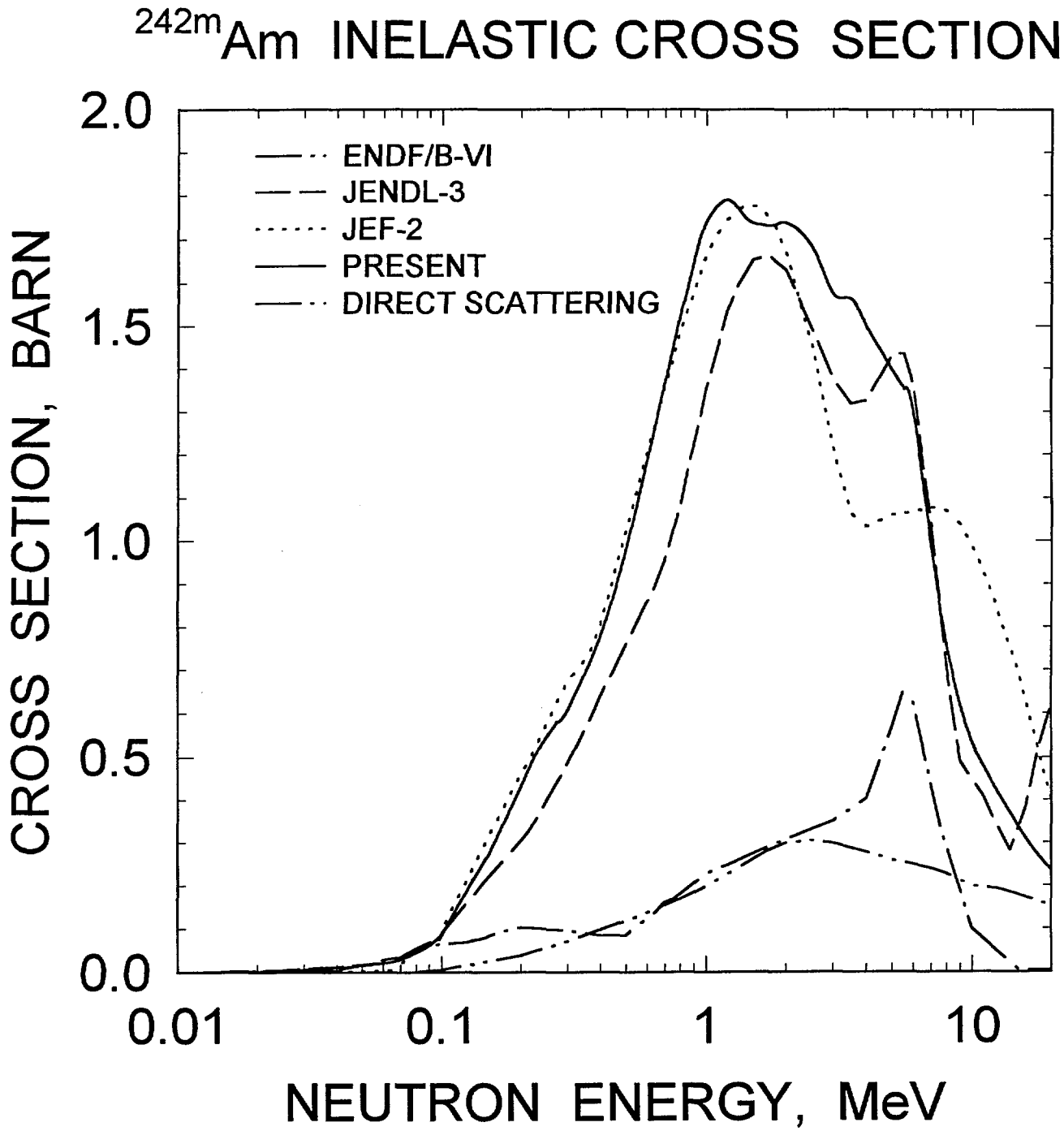
^{242m}Am INELASTIC CROSS SECTION
ENDF/B-VI
JENDL-3
JEF-2
PRESENT
DIRECT SCATTERING
CROSS SECTION, BARN
2.0
1.5
1.0
0.5
0.0
0.01
0.1
1
10
NEUTRON ENERGY, MeV

FIG.4.11

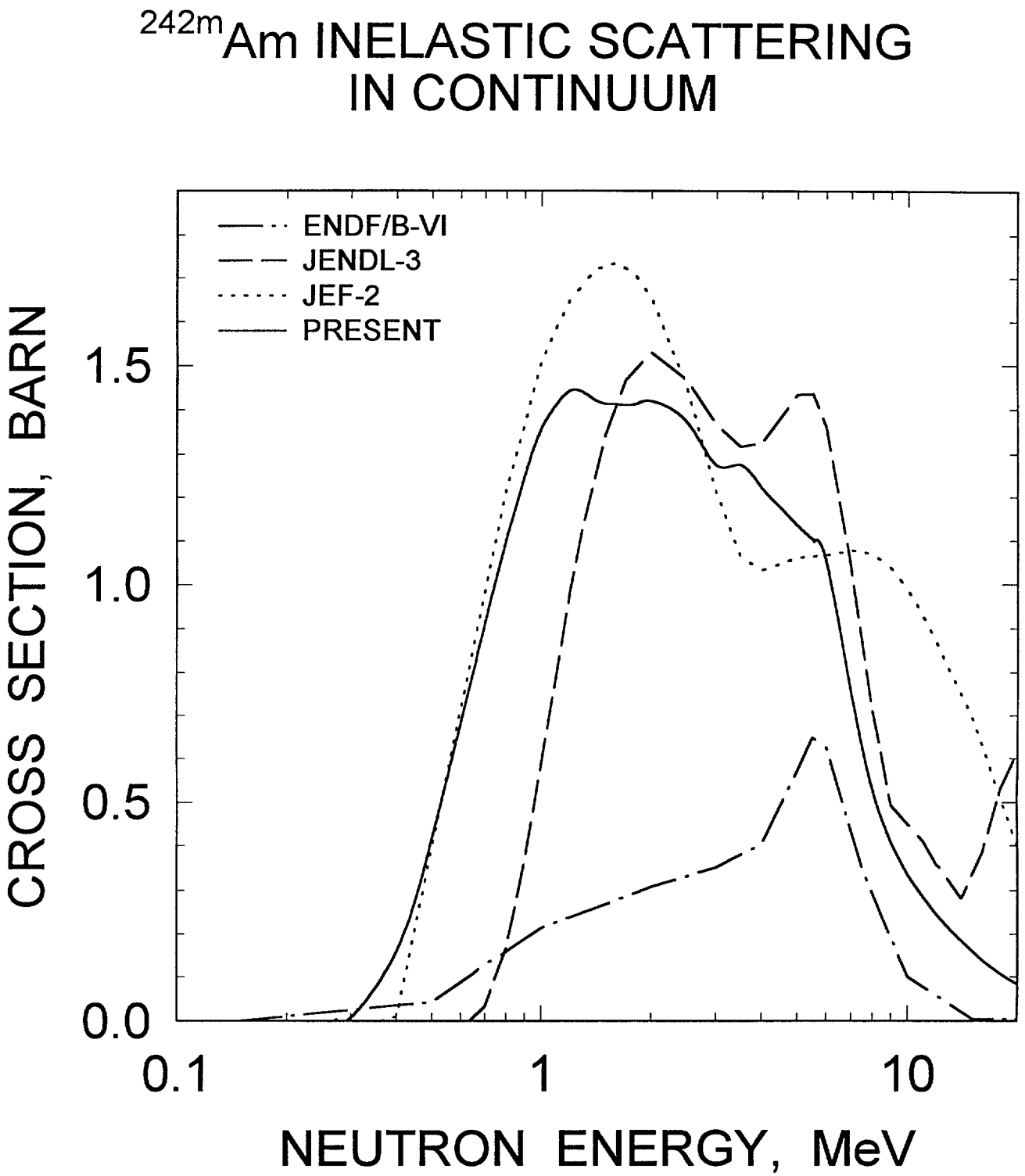
242mAm INELASTIC SCATTERING
IN CONTINUUM
ENDF/B-VI
JENDL-3
JEF-2
PRESENT
CROSS SECTION, BARN
0.0
0.5
1.0
1.5
0.1
1
10
NEUTRON ENERGY, MeV

FIG.4.12

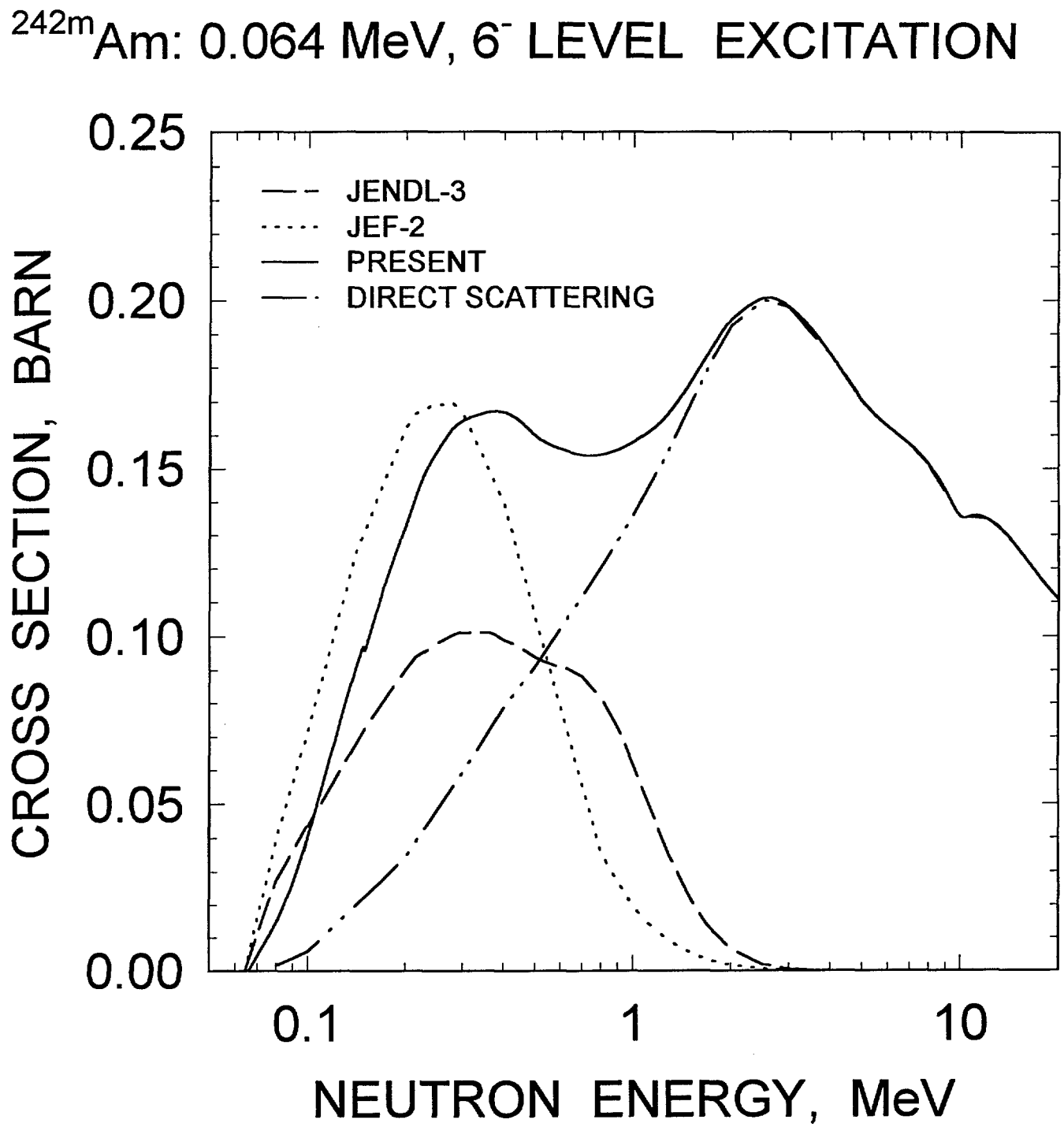
^{242m}Am: 0.064 MeV, 6$^-$ LEVEL EXCITATION
JENDL-3
JEF-2
PRESENT
DIRECT SCATTERING
CROSS SECTION, BARN
0.25
0.20
0.15
0.10
0.05
0.00
0.1
1
10
NEUTRON ENERGY, MeV

FIG.4.13

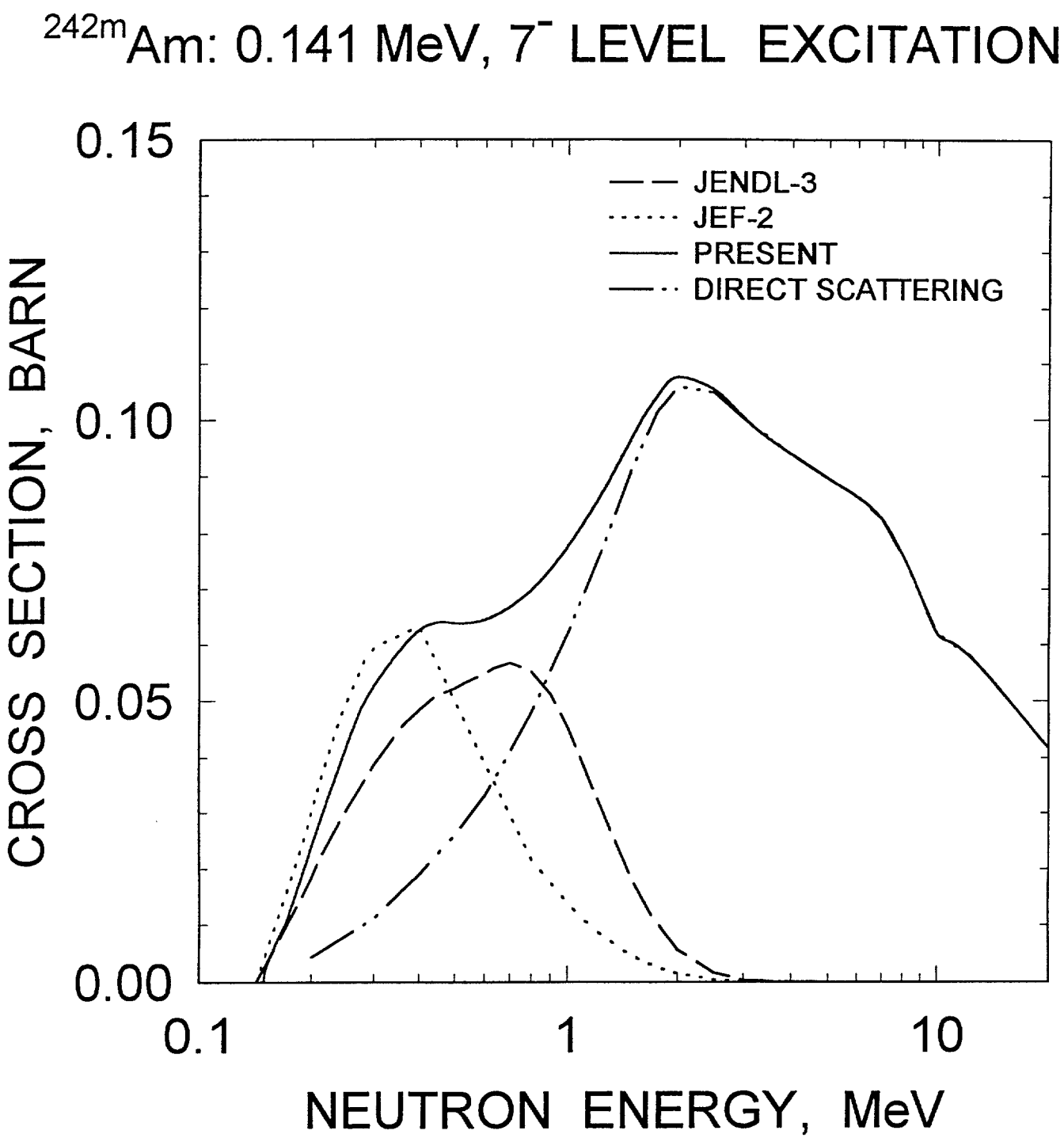
^{242m}Am: 0.141 MeV, 7$^-$ LEVEL EXCITATION
JENDL-3
JEF-2
PRESENT
DIRECT SCATTERING
CROSS SECTION, BARN
0.15
0.10
0.05
0.00
0.1
1
10
NEUTRON ENERGY, MeV

FIG.4.14

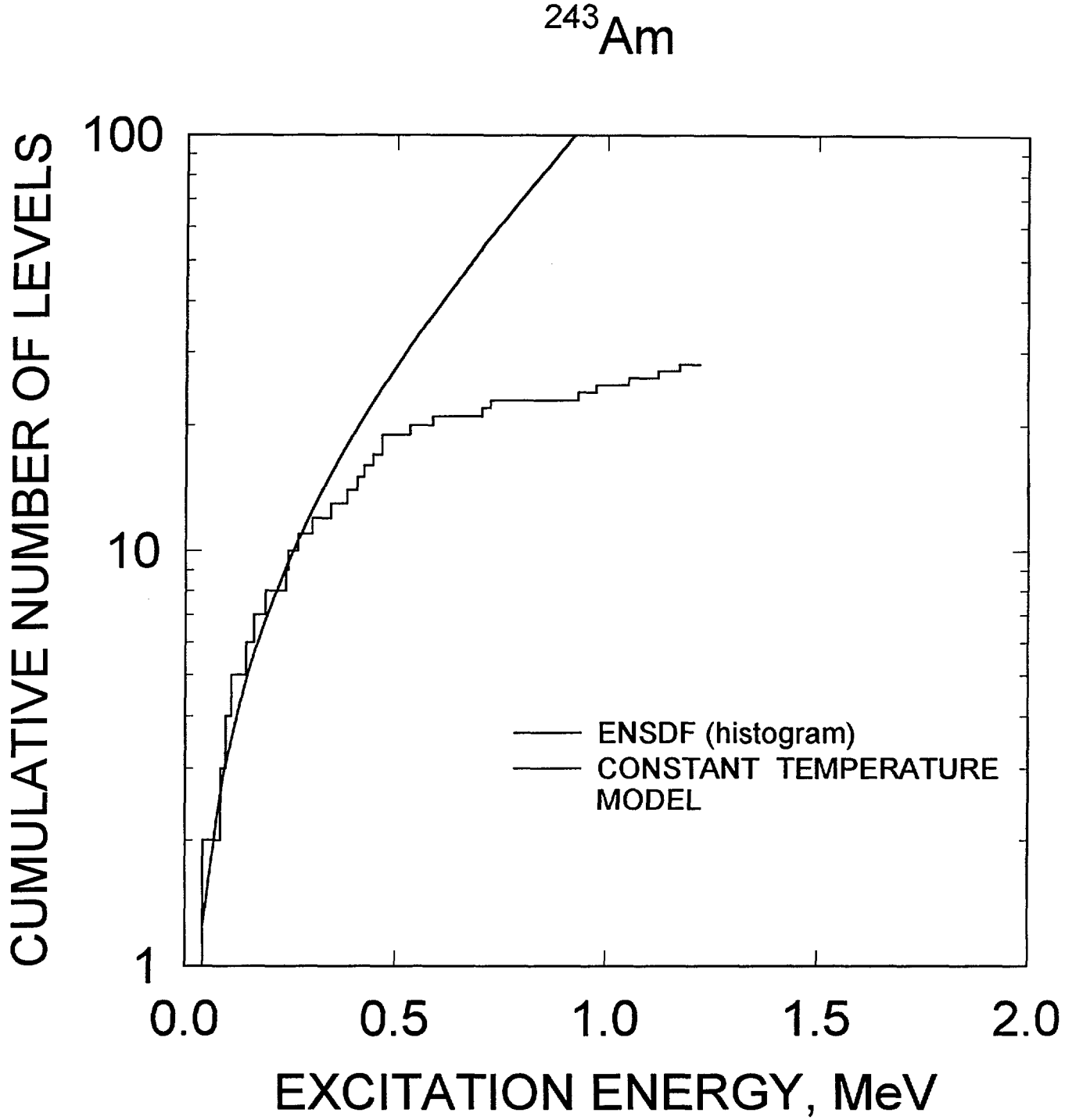
^{243}Am
CUMULATIVE NUMBER OF LEVELS
100
10
1
0.0
0.5
1.0
1.5
2.0
EXCITATION ENERGY, MeV
ENSDF (histogram)
CONSTANT TEMPERATURE MODEL

FIG. 4.15

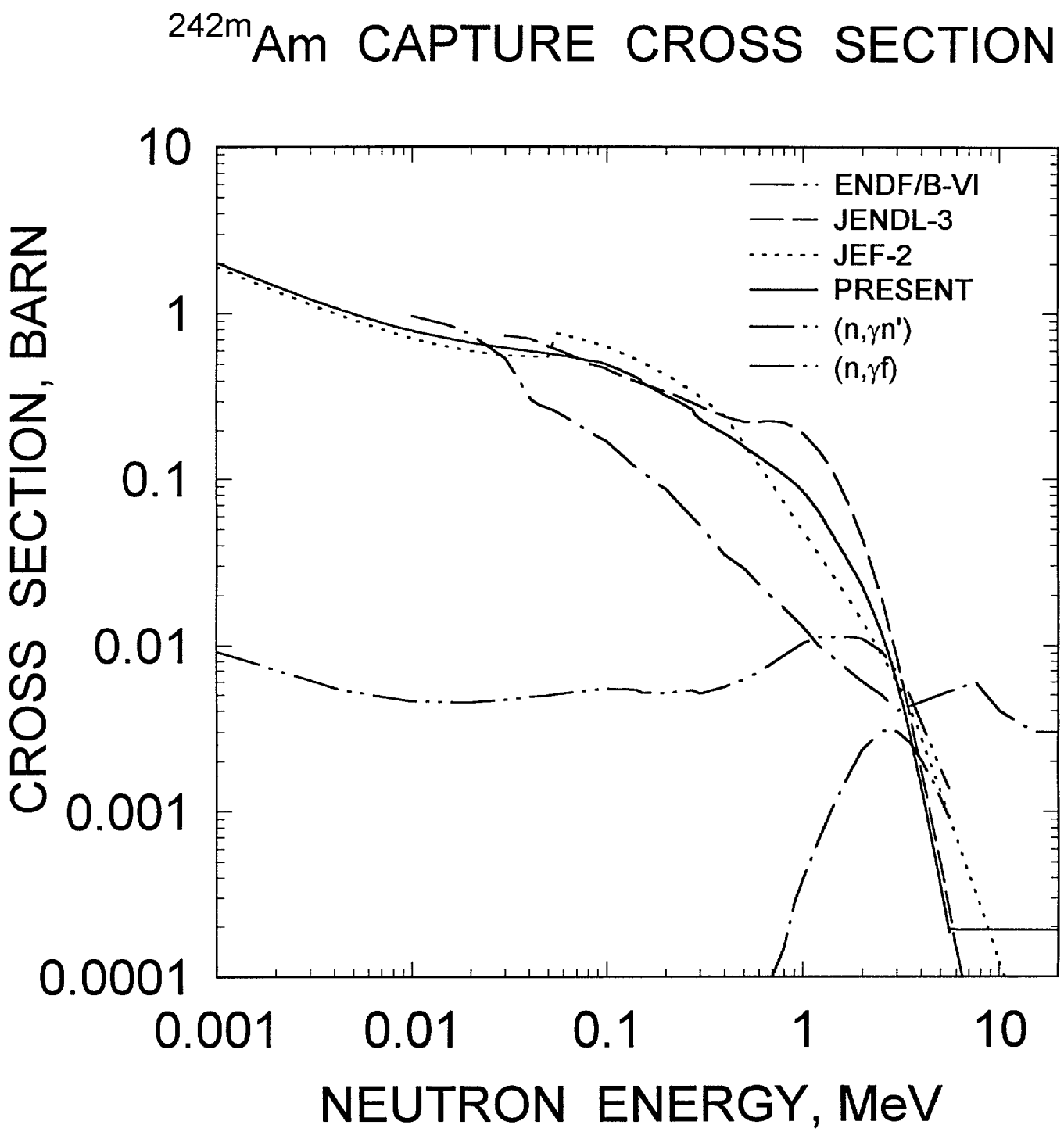
^{242m}Am CAPTURE CROSS SECTION
CROSS SECTION, BARN
10
1
0.1
0.01
0.001
0.0001
0.001
0.01
0.1
1
10
NEUTRON ENERGY, MeV
ENDF/B-VI
JENDL-3
JEF-2
PRESENT
(n,γn')
(n,γf)

FIG.4.16

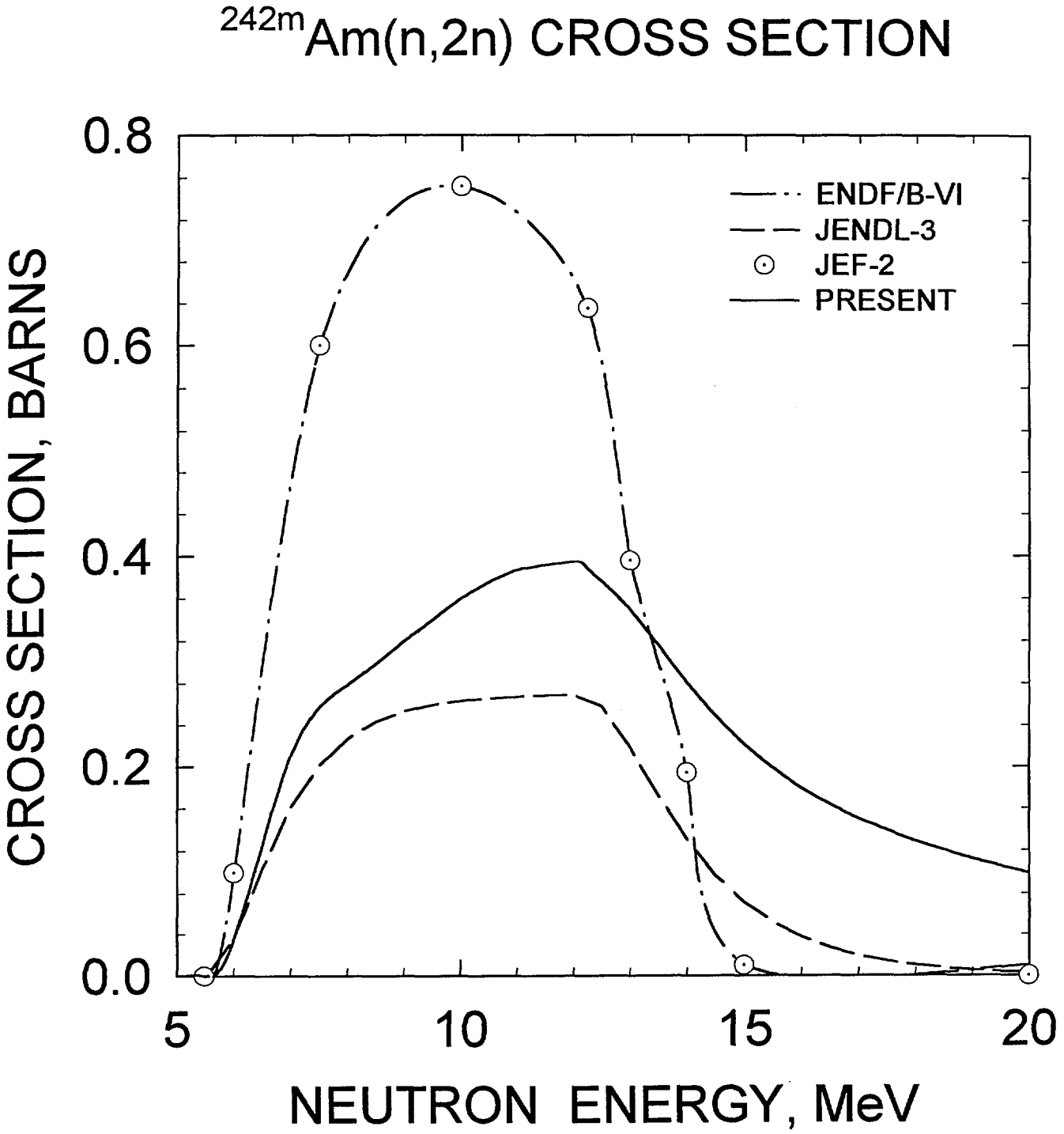
^{242m}Am(n,2n) CROSS SECTION
CROSS SECTION, BARNS
0.0
0.2
0.4
0.6
0.8
5
10
15
20
NEUTRON ENERGY, MeV
ENDF/B-VI
JENDL-3
JEF-2
PRESENT

FIG. 4.17

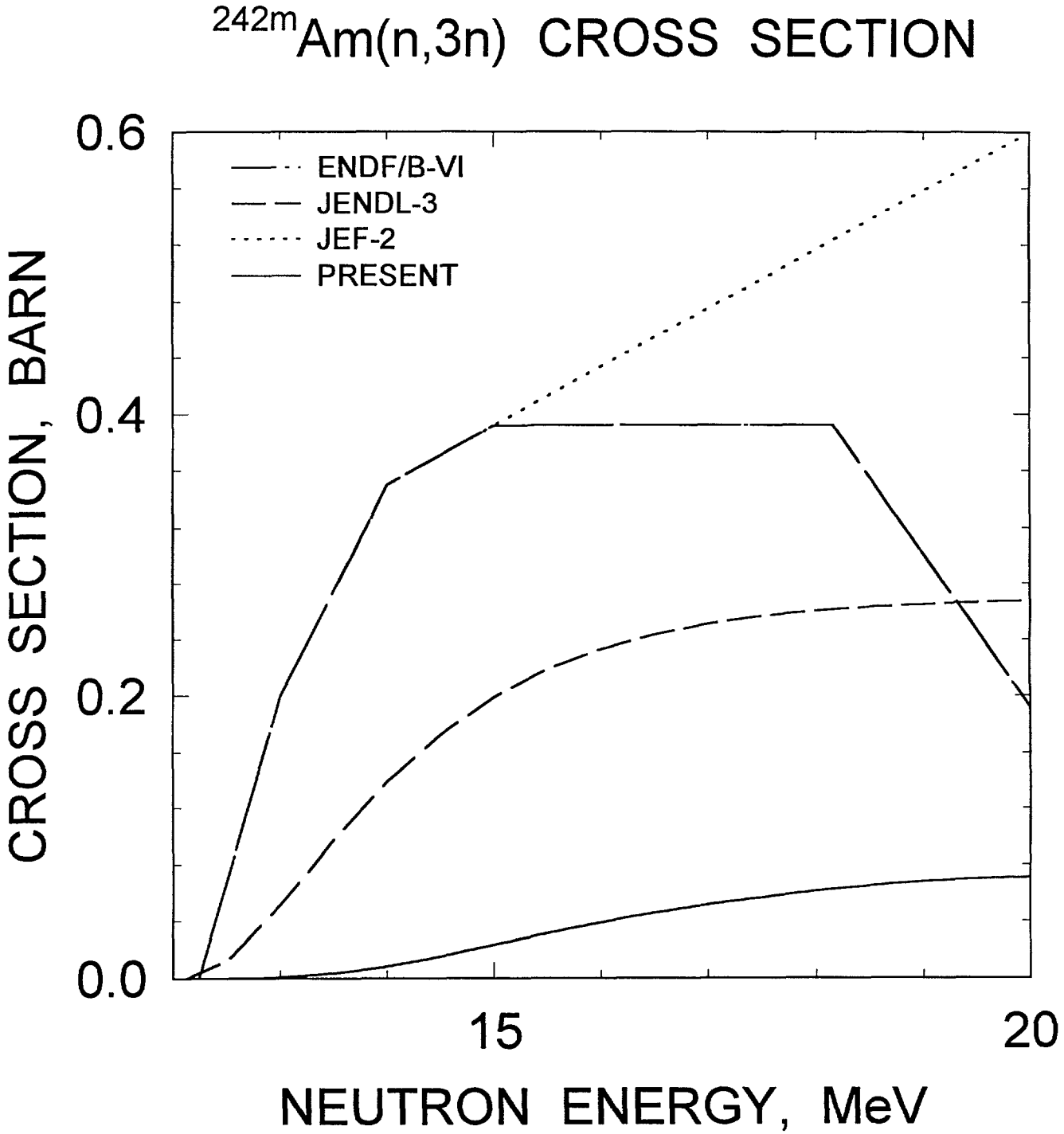
^{242m}Am(n,3n) CROSS SECTION
ENDF/B-VI
JENDL-3
JEF-2
PRESENT
CROSS SECTION, BARN
0.6
0.4
0.2
0.0
15
20
NEUTRON ENERGY, MeV

FIG.4.18

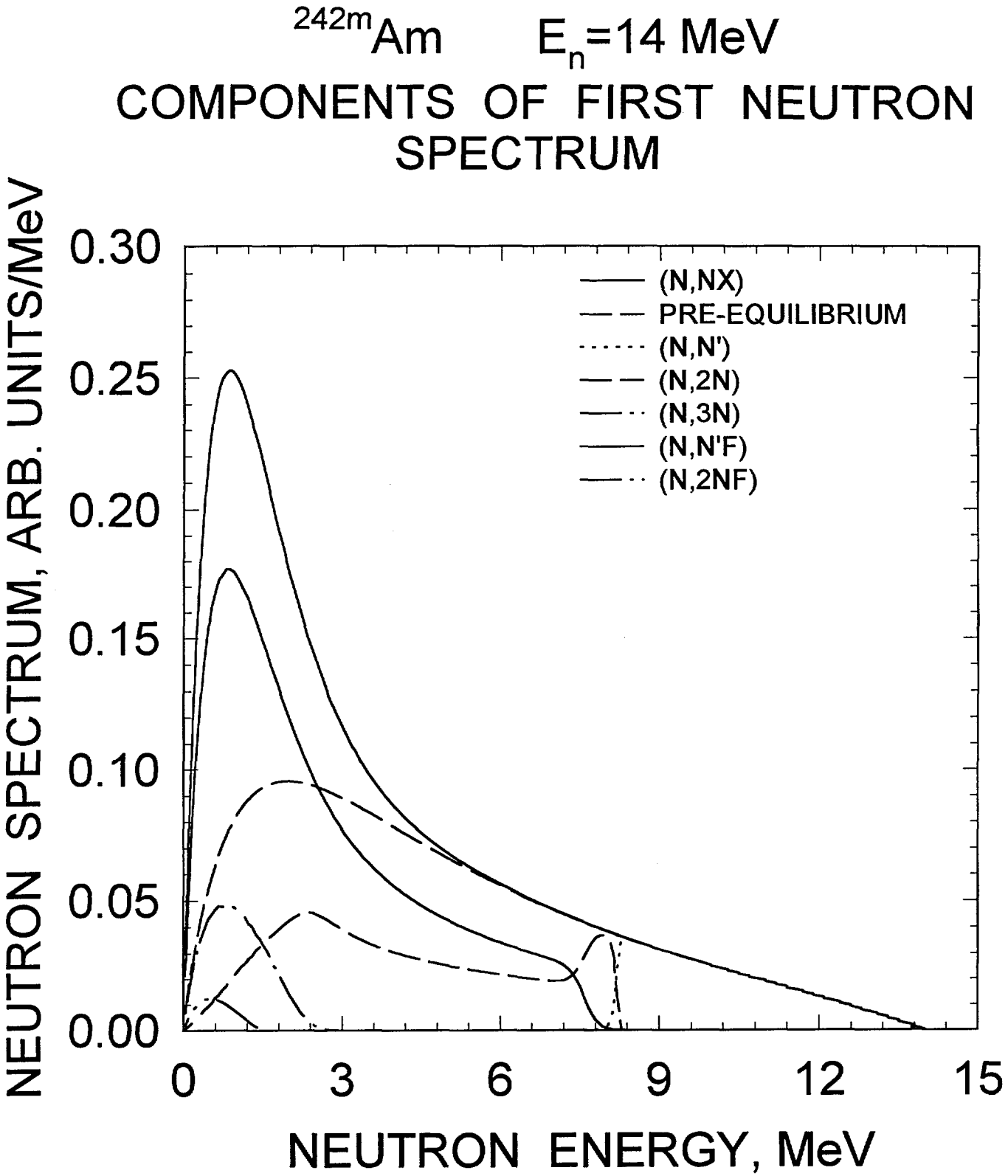
^{242m}Am E_n=14 MeV
COMPONENTS OF FIRST NEUTRON SPECTRUM
NEUTRON SPECTRUM, ARB. UNITS/MeV
0.30
0.25
0.20
0.15
0.10
0.05
0.00
0
3
6
9
12
15
NEUTRON ENERGY, MeV
(N,NX)
PRE-EQUILIBRIUM
(N,N')
(N,2N)
(N,3N)
(N,N'F)
(N,2NF)

FIG.5.1

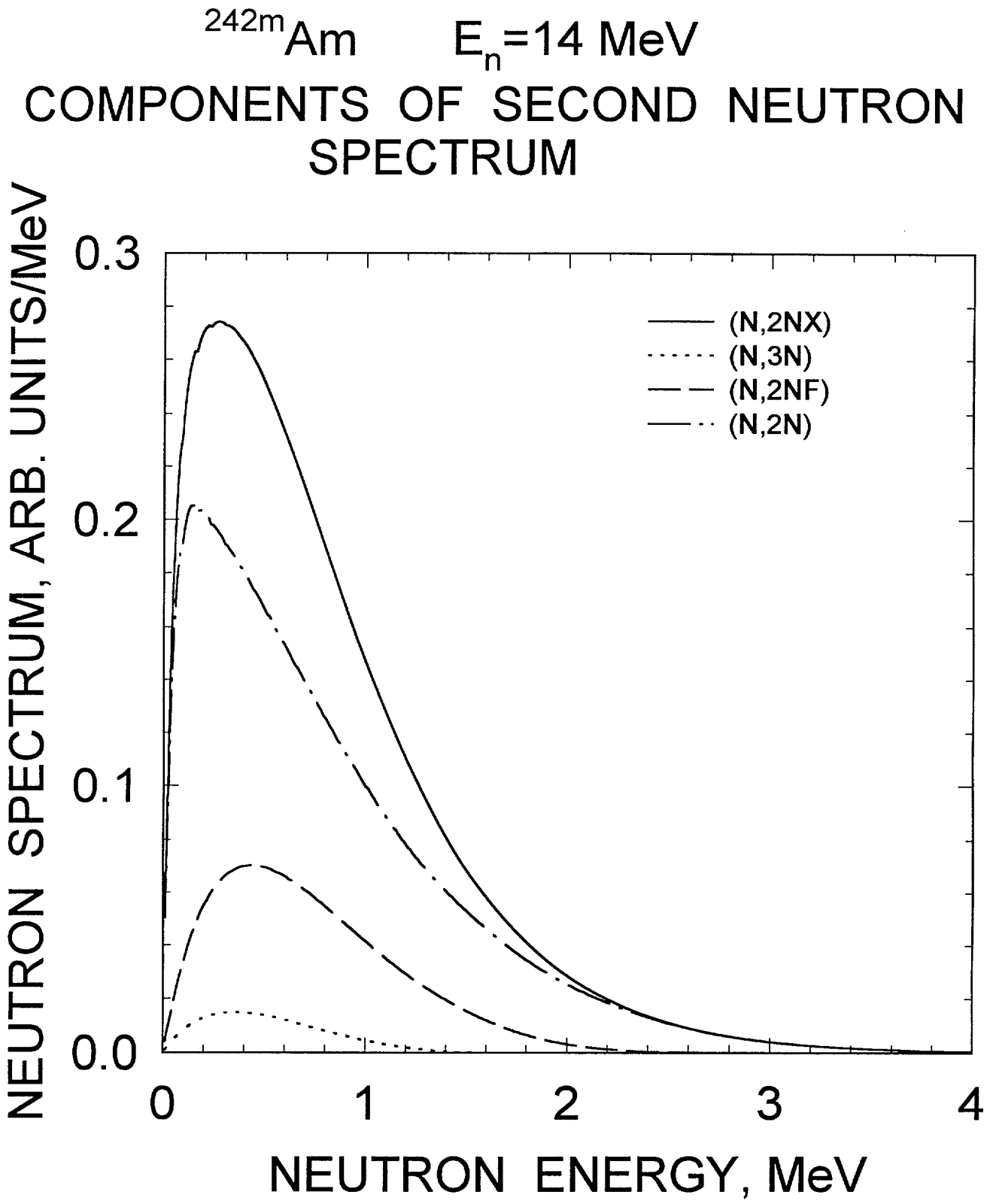
^{242m}Am E_n=14 MeV
COMPONENTS OF SECOND NEUTRON SPECTRUM
NEUTRON SPECTRUM, ARB. UNITS/MeV
0.3
0.2
0.1
0.0
0
1
2
3
4
NEUTRON ENERGY, MeV
(N,2NX)
(N,3N)
(N,2NF)
(N,2N)

FIG.5.2

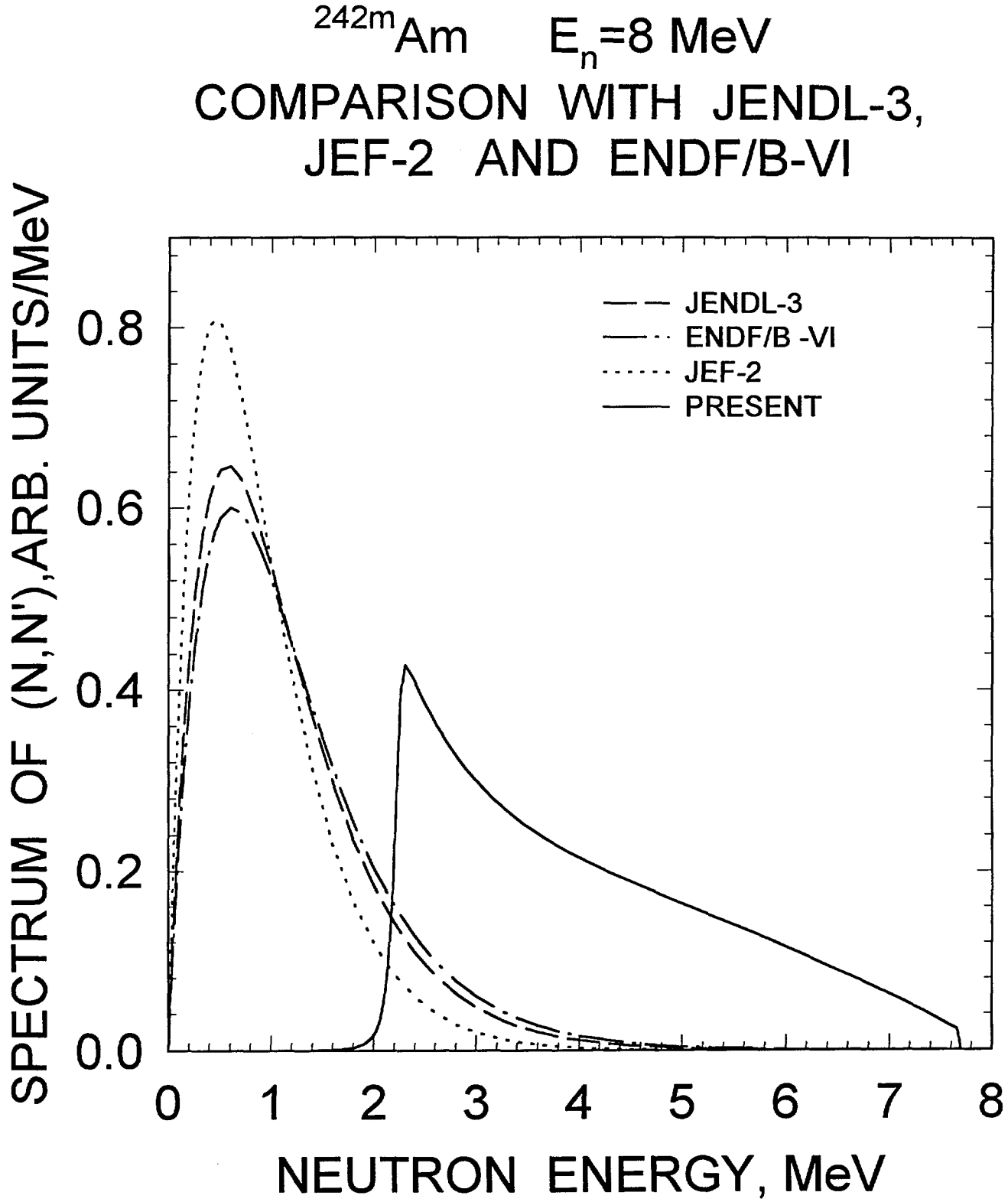
^{242m}Am E_n=8 MeV
COMPARISON WITH JENDL-3, JEF-2 AND ENDF/B-VI
SPECTRUM OF (N,N'),ARB. UNITS/MeV
0.0
0.2
0.4
0.6
0.8
0
1
2
3
4
5
6
7
8
NEUTRON ENERGY, MeV
JENDL-3
ENDF/B -VI
JEF-2
PRESENT

FIG.5.3

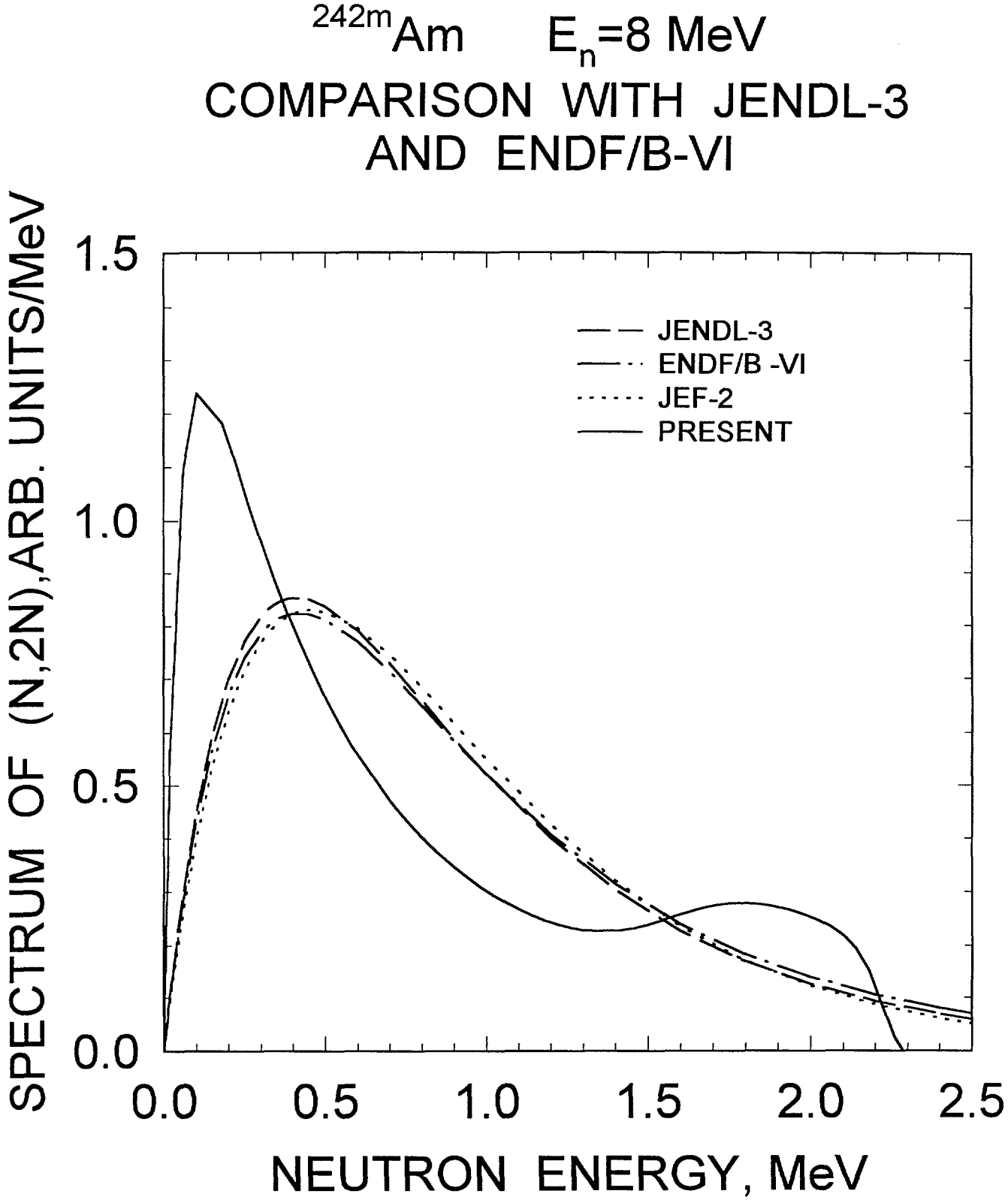
^{242m}Am E_n=8 MeV
COMPARISON WITH JENDL-3
AND ENDF/B-VI
SPECTRUM OF (N,2N),ARB. UNITS/MeV
1.5
1.0
0.5
0.0
JENDL-3
ENDF/B -VI
JEF-2
PRESENT
0.0
0.5
1.0
1.5
2.0
2.5
NEUTRON ENERGY, MeV

FIG.5.4

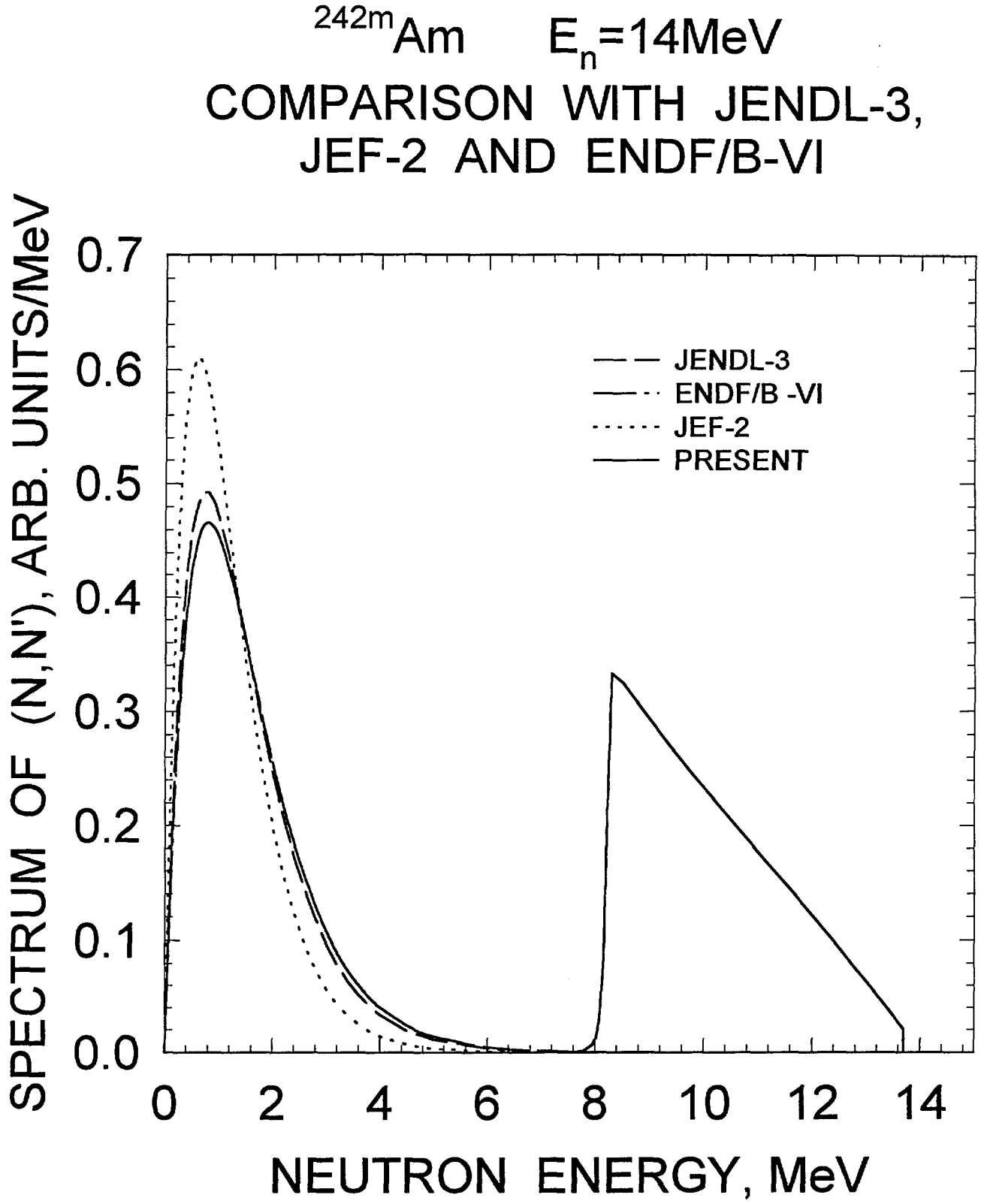
^{242m}Am E_n=14MeV
COMPARISON WITH JENDL-3, JEF-2 AND ENDF/B-VI
SPECTRUM OF (N,N'), ARB. UNITS/MeV
0.0
0.1
0.2
0.3
0.4
0.5
0.6
0.7
0
2
4
6
8
10
12
14
NEUTRON ENERGY, MeV
JENDL-3
ENDF/B -VI
JEF-2
PRESENT

FIG.5.5

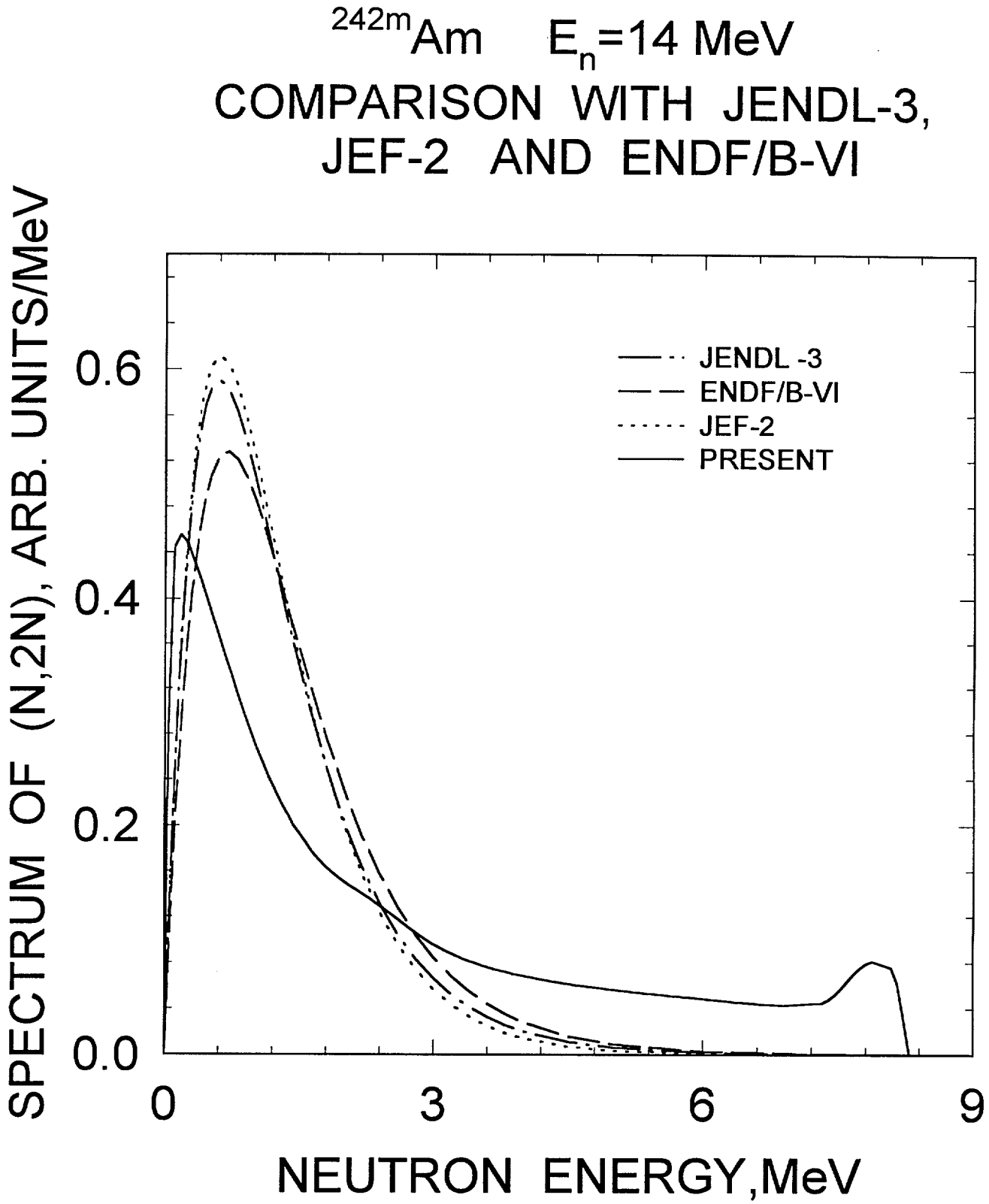
^{242m}Am E_n=14 MeV
COMPARISON WITH JENDL-3, JEF-2 AND ENDF/B-VI
SPECTRUM OF (N,2N), ARB. UNITS/MeV
0.0
0.2
0.4
0.6
0
3
6
9
NEUTRON ENERGY,MeV
JENDL -3
ENDF/B-VI
JEF-2
PRESENT

FIG.5.6

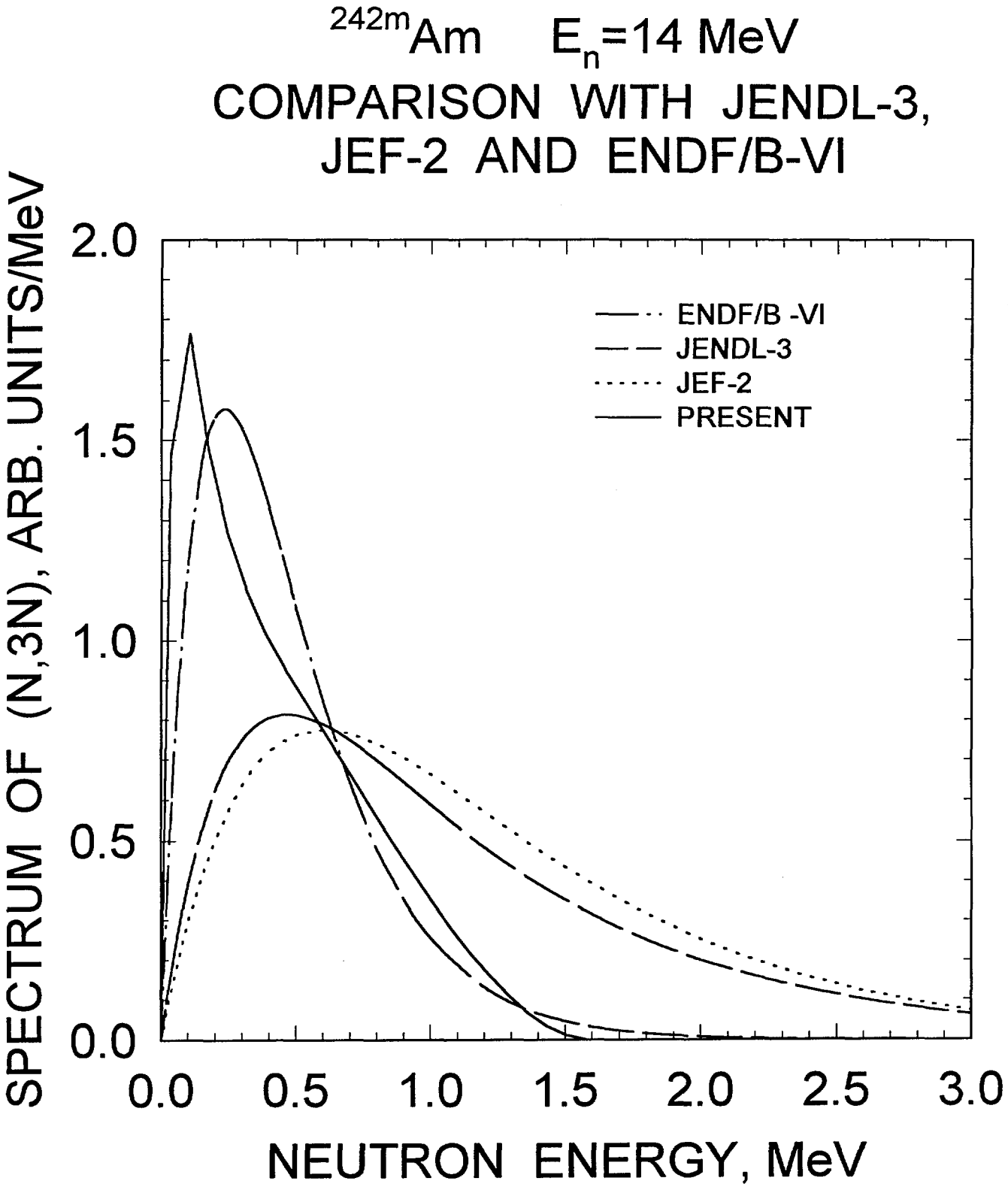
^{242m}Am E_n=14 MeV
COMPARISON WITH JENDL-3, JEF-2 AND ENDF/B-VI
SPECTRUM OF (N,3N), ARB. UNITS/MeV
2.0
1.5
1.0
0.5
0.0
ENDF/B -VI
JENDL-3
JEF-2
PRESENT
0.0
0.5
1.0
1.5
2.0
2.5
3.0
NEUTRON ENERGY, MeV

FIG.5.7

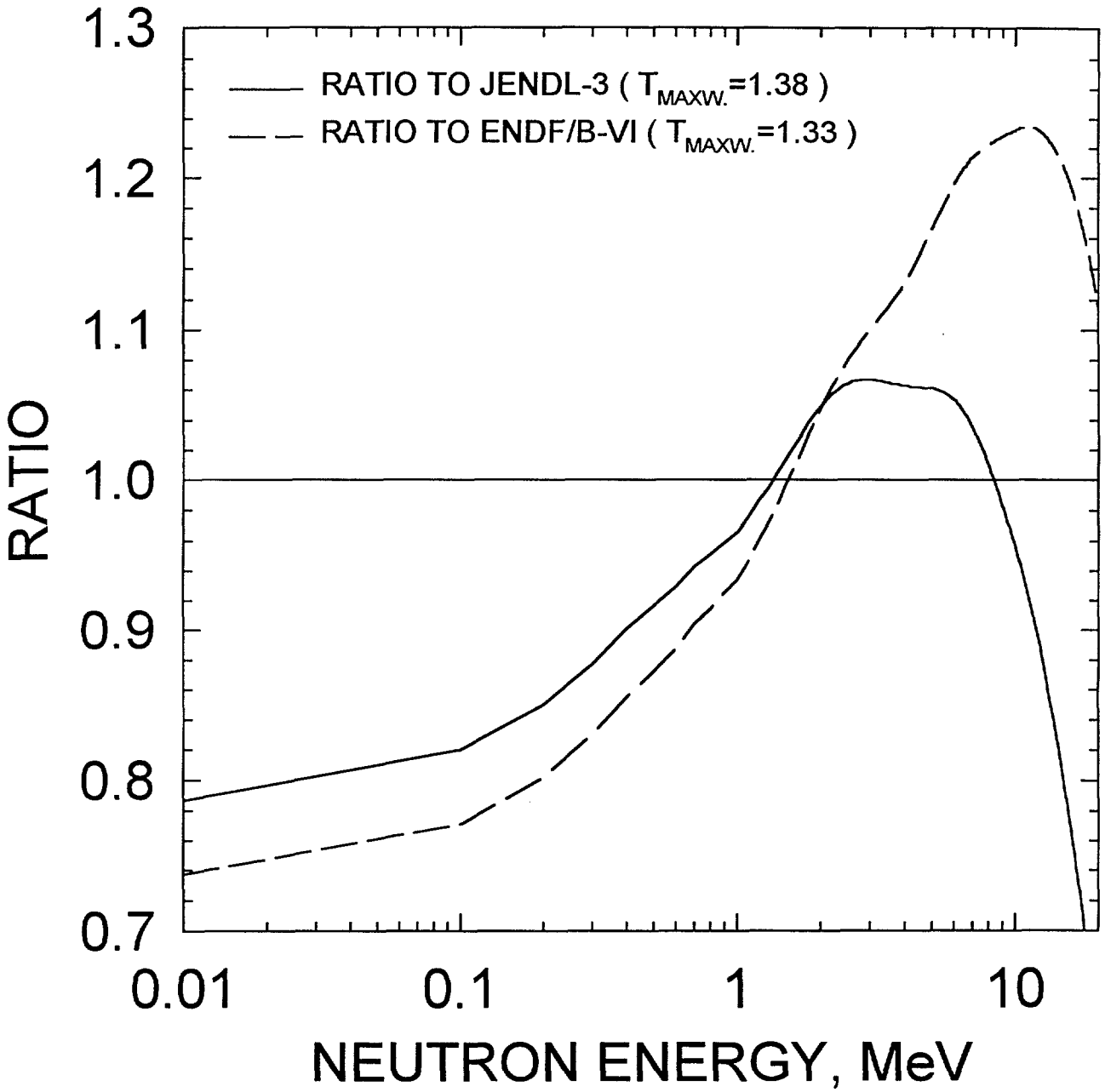
^{242m}Am THERMAL FISSION
PROMPT NEUTRON SPECTRA
RATIO TO JENDL-3 ($T_{MAXW.}$=1.38)
RATIO TO ENDF/B-VI ($T_{MAXW.}$=1.33)
RATIO
1.3
1.2
1.1
1.0
0.9
0.8
0.7
0.01
0.1
1
10
NEUTRON ENERGY, MeV

FIG.5.8

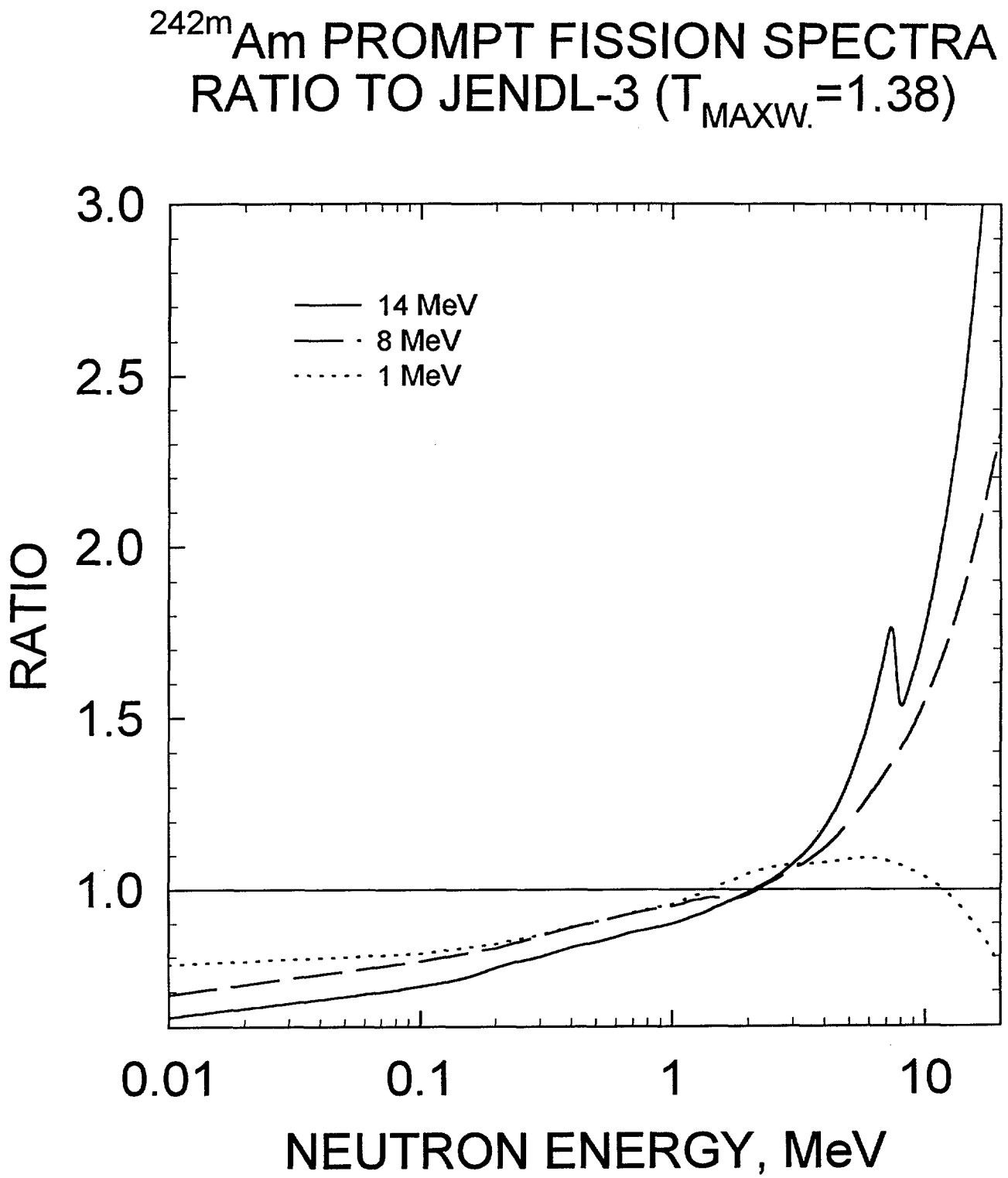
^{242m}Am PROMPT FISSION SPECTRA
RATIO TO JENDL-3 ($T_{MAXW.}$=1.38)
3.0
2.5
2.0
1.5
1.0
RATIO
14 MeV
8 MeV
1 MeV
0.01
0.1
1
10
NEUTRON ENERGY, MeV

FIG. 5.9

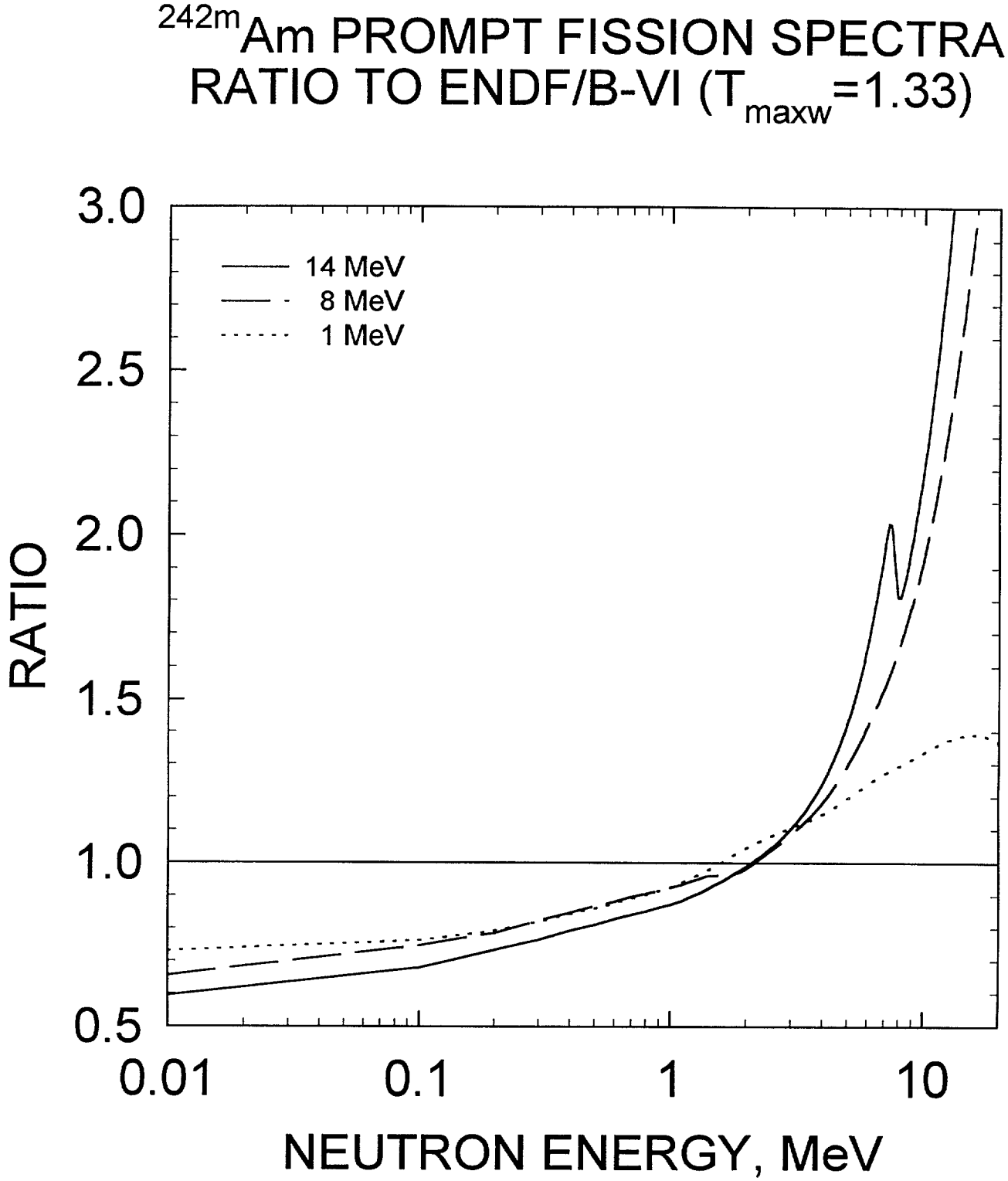
^{242m}Am PROMPT FISSION SPECTRA
RATIO TO ENDF/B-VI (T_{maxw}=1.33)
14 MeV
8 MeV
1 MeV
RATIO
3.0
2.5
2.0
1.5
1.0
0.5
0.01
0.1
1
10
NEUTRON ENERGY, MeV

FIG. 5.10

^{242m}Am FISSION NEUTRON SPECTRA RATIO TO MADLAND-NIX MODEL CALCULATION

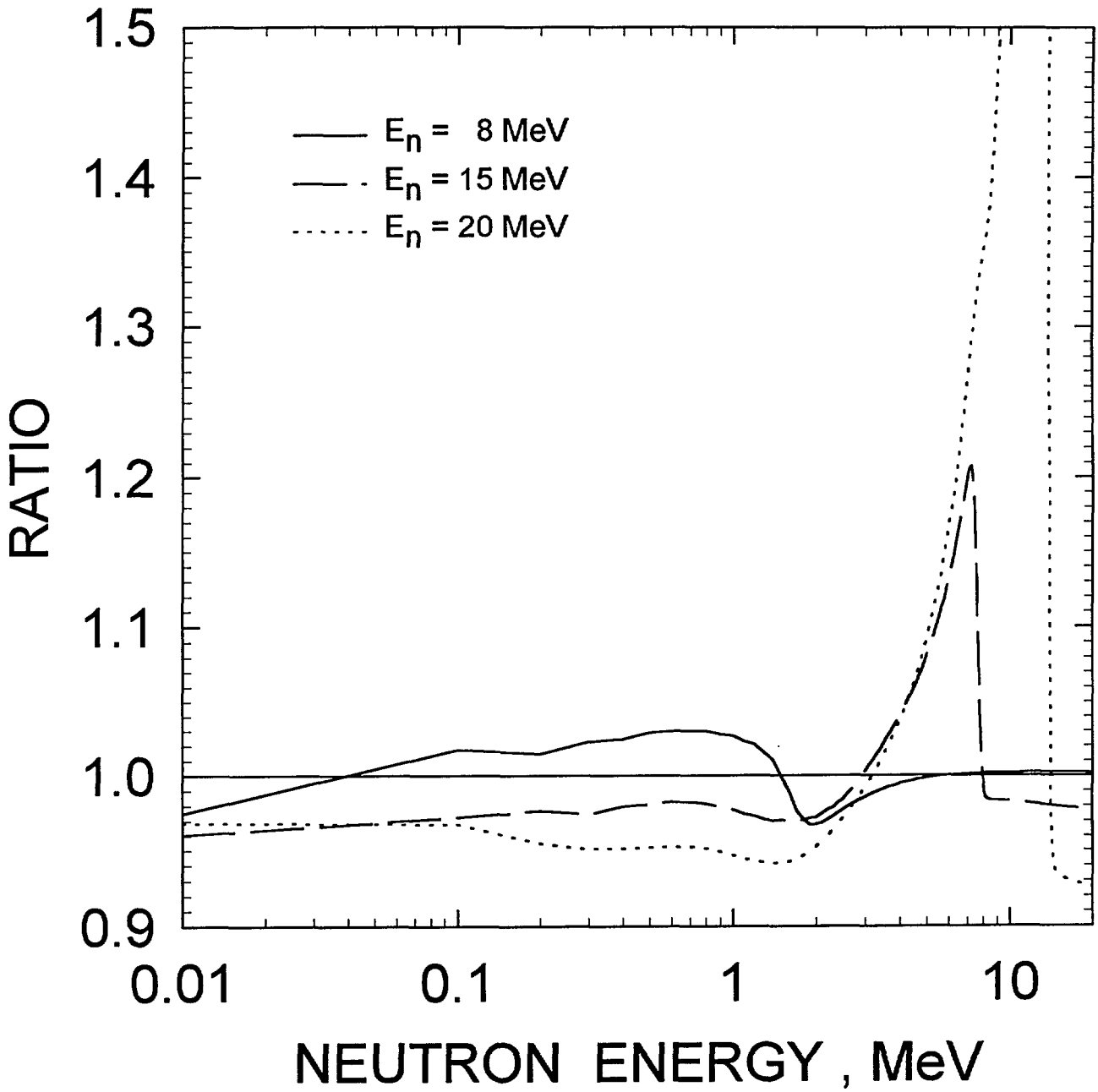

FIG.5.11

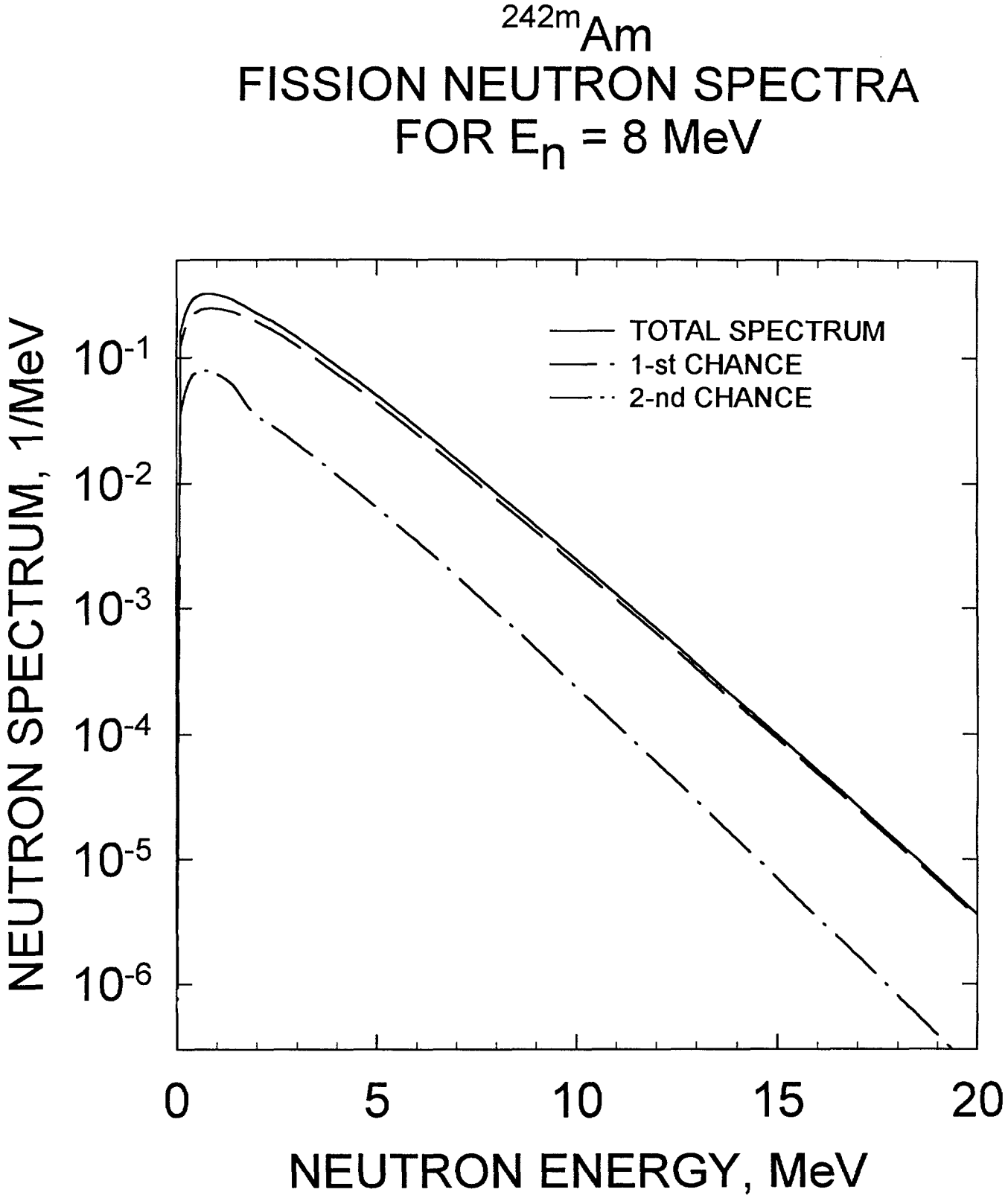
^{242m}Am
FISSION NEUTRON SPECTRA
FOR E_n = 8 MeV
TOTAL SPECTRUM
1-st CHANCE
2-nd CHANCE
NEUTRON SPECTRUM, 1/MeV
10^{-1}
10^{-2}
10^{-3}
10^{-4}
10^{-5}
10^{-6}
0
5
10
15
20
NEUTRON ENERGY, MeV

FIG.5.12

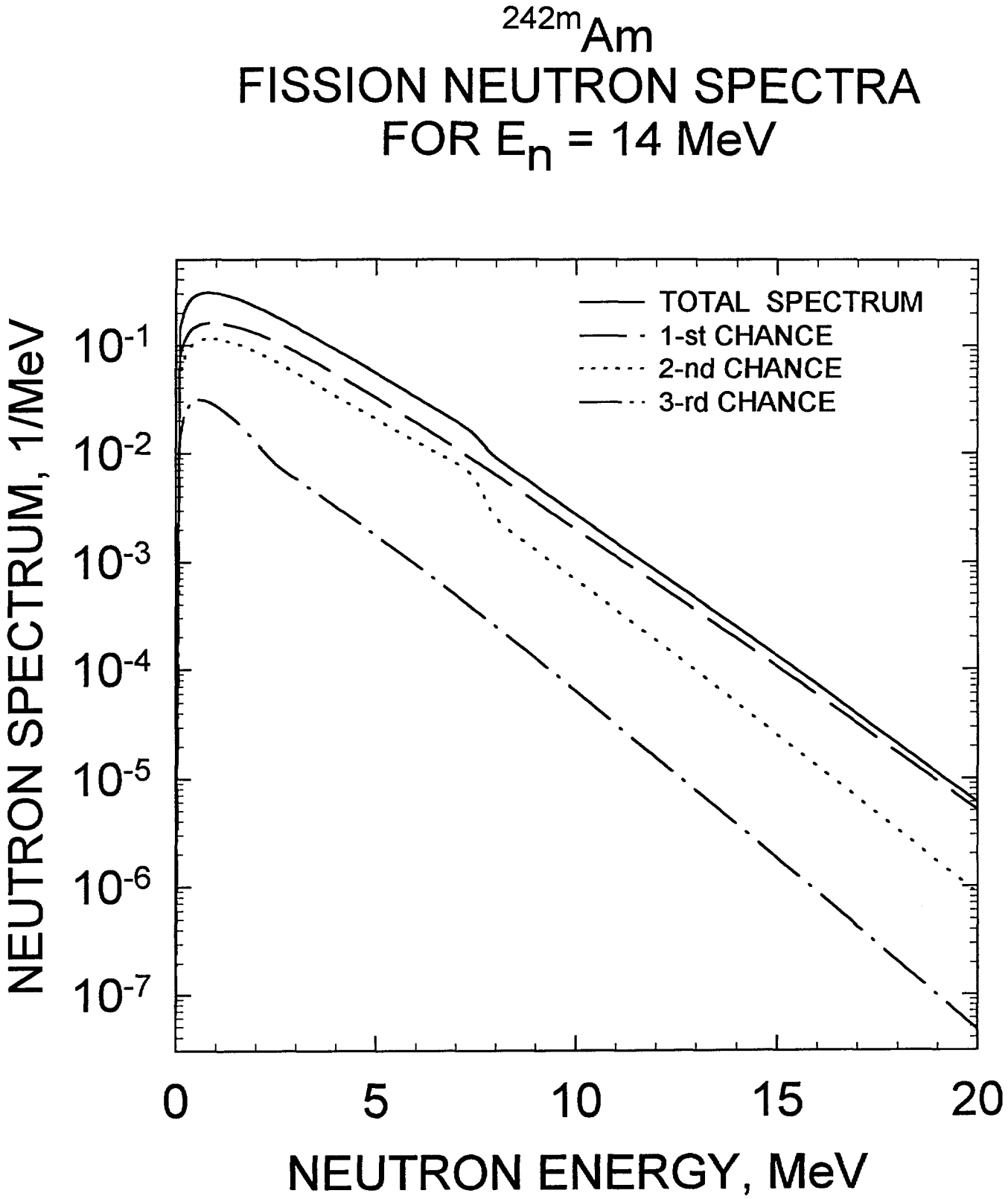
^{242m}Am
FISSION NEUTRON SPECTRA
FOR E_n = 14 MeV
TOTAL SPECTRUM
1-st CHANCE
2-nd CHANCE
3-rd CHANCE
NEUTRON SPECTRUM, 1/MeV
10^{-1}
10^{-2}
10^{-3}
10^{-4}
10^{-5}
10^{-6}
10^{-7}
0
5
10
15
20
NEUTRON ENERGY, MeV

FIG.5.13

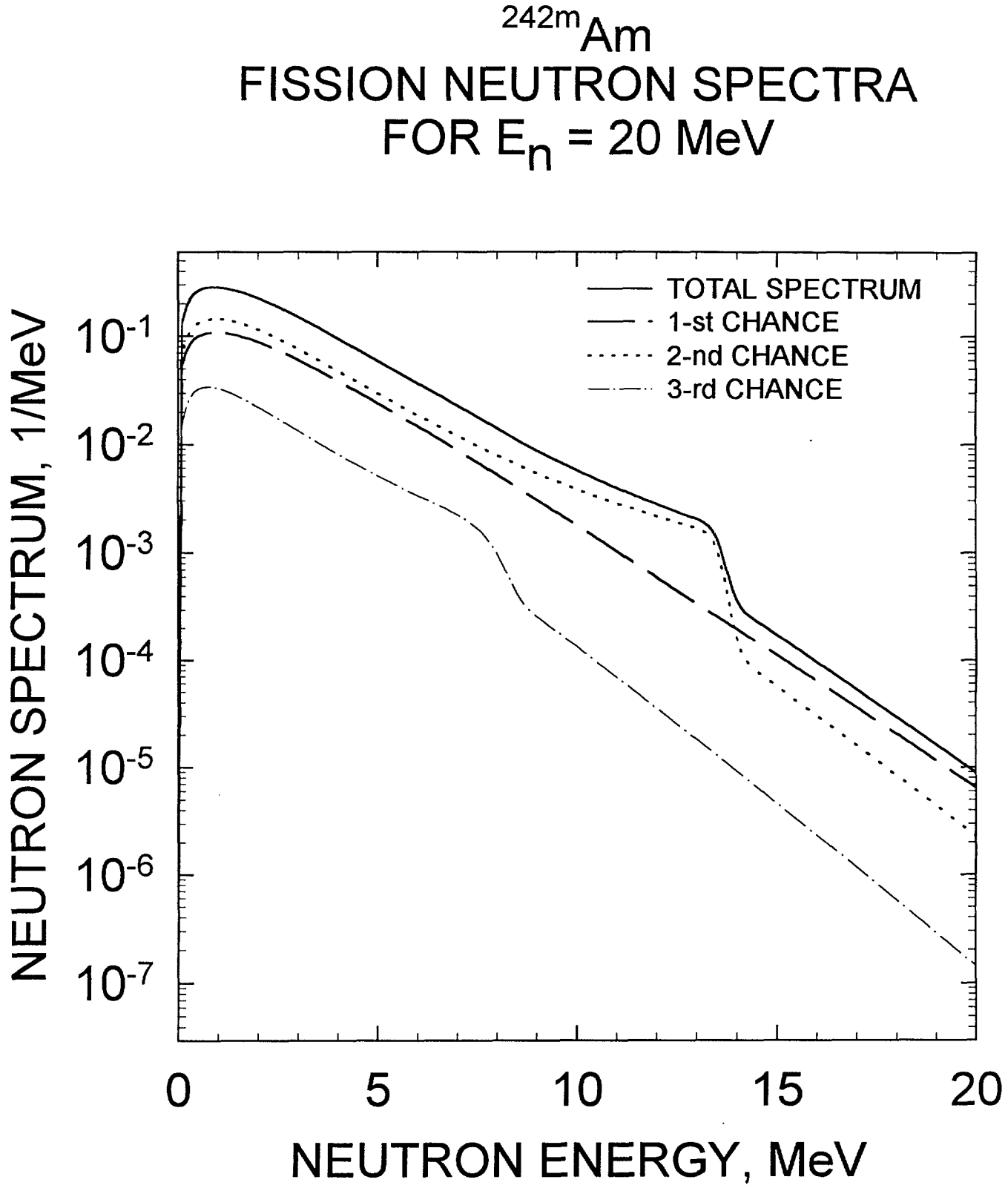
^{242m}Am
FISSION NEUTRON SPECTRA
FOR E_n = 20 MeV
TOTAL SPECTRUM
1-st CHANCE
2-nd CHANCE
3-rd CHANCE
NEUTRON SPECTRUM, 1/MeV
10^{-1}
10^{-2}
10^{-3}
10^{-4}
10^{-5}
10^{-6}
10^{-7}
0
5
10
15
20
NEUTRON ENERGY, MeV

FIG.5.14

^{242m}Am PROMPT NEUTRON MULTIPLICITY

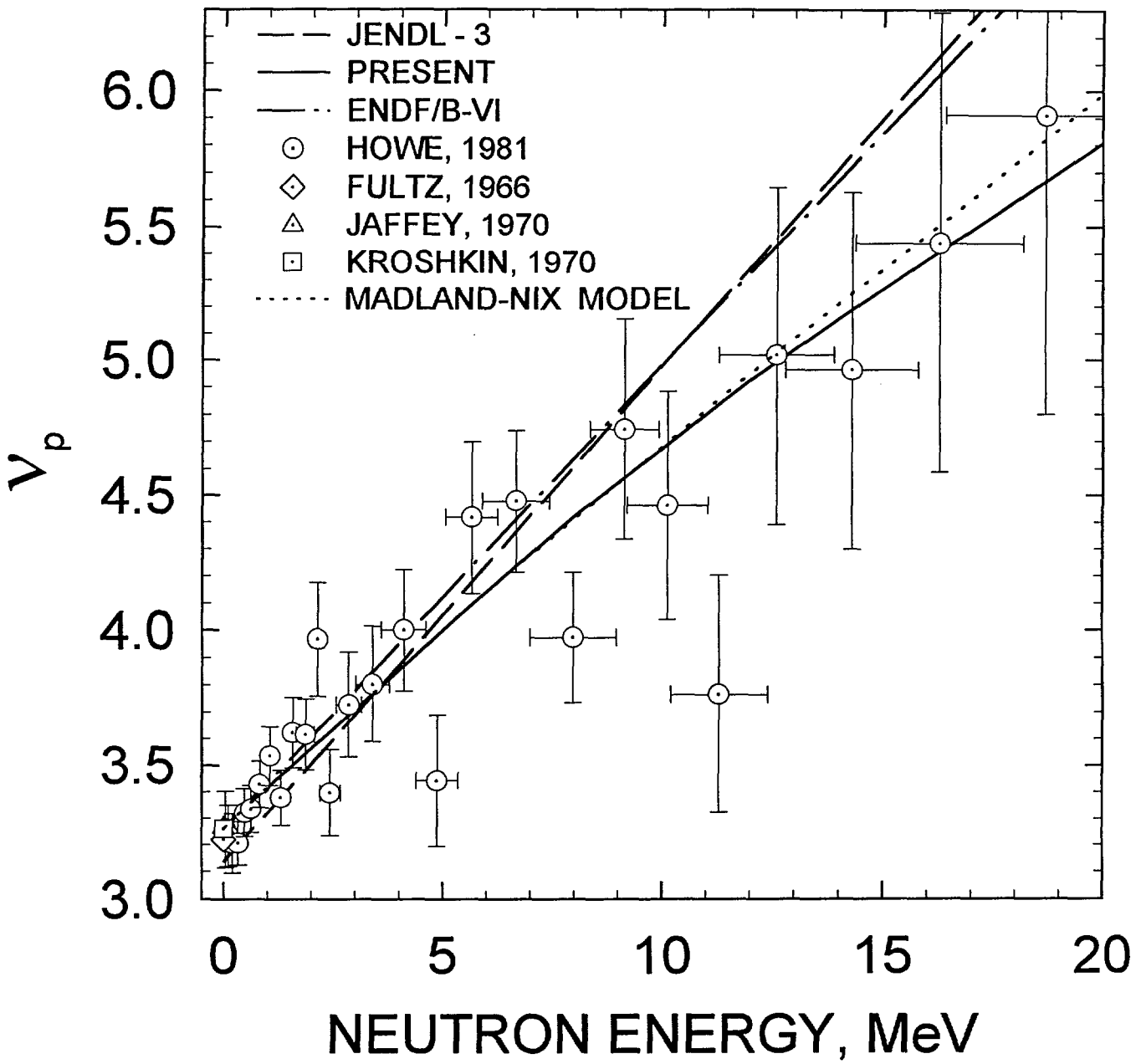

FIG.6.1

Nuclear Data Section
International Atomic Energy Agency
P.O. Box 100
A-1400 Vienna
Austria

e-mail, INTERNET: SERVICES@IAEAND.IAEA.OR.AT
fax: (43-1)20607
cable: INATOM VIENNA a
telex: 1-12645 atom a
telephone: (43-1)2060-21710

online: TELNET or FTP: IAEAND.IAEA.OR.AT
username: IAEANDS for interactive Nuclear Data Information System
username: ANONYMOUS for FTP file transfer
username: FENDL for FTP file transfer of FENDL files
For users with web-browsers: http://www.iaea.or.at